Infrared Studies of Novae

A Thesis

Submitted to

Gujarat University
Ahmedabad

for
The degree of
Doctor of Philosophy

in
Physics

by
Ramkrishna Das

Astronomy & Astrophysics Division
Physical Research Laboratory
Ahmedabad 380009
Gujarat, India

September 2009

Dedicated
to
my Parents
& *my beloved brother*

CERTIFICATE

I hereby declare that the work presented in this thesis entitled ”Infrared Studies of Novae” is original and has not formed the basis for the award of any degree or diploma by any University or Institution.

Ramkrishna Das
Astronomy & Astrophysics Division
Physical Research Laboratory
Ahmedabad - 380009
Gujarat, India

Certified by:

Prof. N. M. Ashok
Astronomy & Astrophysics Division
Physical Research Laboratory
Ahmedabad - 380009
Gujarat, India

Acknowledgements

This thesis is an outcome of my prolonged research that has been conducted over the years since I joined PRL five years back. In this long period of time I have interacted with a number of scholars, scientists, senior colleagues, friends and other people who have contributed in various ways to complete this research work in time. At the very outset of winding up my Doctoral thesis it is a great pleasure to me to convey my heartiest gratitude to all of them in my humble acknowledgment.

First and foremost I offer my sincerest gratitude to my supervisor, Dr. Dipankar . P. K. Banerjee, the pioneer of my life, who has introduced me to the observational universe, a world beyond the theoretical studies. The whole work presented in this thesis was brushed up and performed under the aegis of his guidance. No doubt, without his zeal and unstinted co-operation I would not have found the task so interesting and absorbing. I owe a great deal of gratitude to him for his eminent guidance, advice and supervision from the very early stage that have made the years working under him pleasant and memorable. His truly scientist intuition has made him as a constant oasis of ideas and passions in science that has always inspired me and enriched my growth as a student and a researcher. I express my deepest gratitude for all the knowledge that I have gained from him during the course of this work and also for his personal kindness at every stage. In addition, by being his first research student, I always have enjoyed the bonus of having greater concern and attention being paid not only to the progress of my work but also to my well-being. At this time I also convey my heartiest thanks to all his family members who always bestowed well-wishes upon me for every success, expressed their interest in my studies and deep concern for my well-being.

I take this opportunity to offer my profound gratitude to Prof. N.M. Ashok who has been my co-guide throughout this period. I am very much indebted to him for his valuable advice through astronomical discussion, supervision and furthermore, using his precious

times to go through this thesis and his critical comments on it. I also thank him for kindly granting me his valuable time even for answering some of my unintelligent questions. I acknowledge all kinds of helps he provided me time and again whenever I asked for it. In particular, I gratefully thank him for allotting additional observation times to acquire invaluable data on novae. His deep commitment and attitude towards science has always been a source of inspiration to me.

At this auspicious moment I intend to pay my tribute to other faculty members: Prof. B. G. Anandarao, Prof. T. Chandrasekhar, Prof. U. C. Joshi, Prof. P. Janardhan, Prof. K. S. Baliyan, Prof. H. O. vats, Dr. A. Singhal, Dr. A. Chakravorty and Dr.S. Naik, who always encouraged me during this period. In particular, I express profound gratitude to Prof. U. C. Joshi who taught the fundamentals of Astronomy during our course work. I could never have embarked and had a better start without his prior teachings in astrophysics.

I take this opportunity to thank to all other scientists and staff members of Astronomy division. I gratefully acknowledge the co-operation and support they extended to me.

I must express my appreciation for the co-operation and help extended ever-willingly by the library and its staff members. I would like to convey my thanks particularly to Mrs. Nishtha Anilkumar, Mrs. Uma Desai and Mr. Indrabadan Thakkar for their prompt response to supply all the books and references as and when I required.

My sincere thanks are due to the Physical Research Laboratory and the Department of Space, Govt. of India for funding my research and extending me all necessary facilities for carrying out my research work.

In this work I have used data from the international databases of AAVSO (American Association of Variable Star Observers), AFOEV (Association Francaise des Observateurs d'Etoiles Variables, France), VSNET (Variable Stars Network, Japan) and VSOLJ (Variable Star Observers League in Japan) provided by many unknown worldwide observers. I acknowledge and thank all of them.

It is needless to say that, a significant period of my Ph.D. tenure, I spent at Mount Abu for scientific observations. I always cherish every moment I spent at Mount Abu, a place that is so beautiful. I take this opportunity to express my heartfelt thanks to all the staff members at the Mount Abu Observatory who always were cooperative and extended their hands for all kinds of helps. In particular, I am grateful to Mr. Jinesh K. Jain and

Mr. G. S. Rajpurohit who taught me with utmost care how to handle the instruments and to take observations. I am very much thankful to Mr. Rajesh Shah for his continuous and unconditional efforts to keep the telescope and related softwares free from any trouble. Without their continuous efforts it would not be possible for me to make successful and smooth observations.

It is a pleasure to express my deepest gratitude to Mr. and Mrs. Jain and their family for their encouragement, affection and hospitality during my stay at Abu that always made me feel at home even through busy works. So to speak, I always recall the days at Abu with great pleasure also for having the nice company of Bulbul, the elder daughter of Jineshbhai. Her love and affections always offered immense pleasures which have made me happy, also refreshed my mind and never let me feel strenuous during long observational campaigns. Her fond memories will echo in my mind for ever. I also cherish the sweet times I spent with her sister Chinki who always kept me busy by asking thousands of questions.

Collective and individual acknowledgments are also owed to my colleagues cum friends: Venkat, Koshy, Lokesh, Sanjeev, Tapas, Ashish, Jayant and Vishal. I have learnt much from valuable discussions with them. I especially convey my heartiest thanks to Venkat for his spontaneous helps offered to me at several stages and in several ways. I recall the moments at the early stages when I was a novice, Venkat had kindly allowed me to ask for helps to solve the computer related problems and to learn IRAF. Beyond Physics (which sometimes seemed to be nothing more than a distant dream) Lokesh and Tapas had been a companionable lobby mates for many years as well as colleagues. Always they kept a careful watch on the health condition of this poor neighbor and provided all supports when needed.

This section of acknowledgements would remain incomplete if I do not mention about my close friends: Akhilesh, Rajesh, Ritesh, Rohit, Salman and Santosh, who has been an inseparable part of my life in this institute. I value my association and the golden moments spent with them. They have voluntarily done for me more than what one should expect. I do not know how to convey thanks to them adequately. It is said that "A friend is someone who knows all about you, and loves you just the same." I am bereft of words to acknowledge their love. I always feel extraordinarily fortunate for having such good friends.

During this period of my Ph. D. tenure I came to know few seniors viz. Sasadharda and Subhenduda who gradually became close friends of mine. I cherish the warm memories of many of the happy moments we spent together. I am also indebted to Sanatda whom I disturbed frequently asking hundreds of questions. It has been a memorable experience to

have spent nice time at Abu with him. I would like to express my thanks to all of them for making my life jovial during my stay at PRL.

In the conducive atmosphere of the student community, life at PRL hostel is always a memorable experience to me. I take this opportunity to thank all other Research Scholars, Post Doctorate Fellows and Project Associates who were important to the completion and successful realization of thesis, as well as express my apology that I could not mention personally one by one.

I always cherish the cheerful company of my friend Rajeshbhai (Mr. Rajesh Patel) who gradually introduced me to the local cultures and rituals. It is a pleasure to express my gratitude wholeheartedly to him and his family for their kind hospitality during my stay in Ahmedabad.

My deepest gratitude goes to my parents and uncles who have always supported my dreams and aspirations, for their unflagging love and support throughout my life. At this time of the successful realization of my Doctoral thesis, I specially recall and thank them for infusing a vigorous interest in astronomy into me in my childhood days. My beloved younger brothers Rana & Papai have also strikingly influenced and helped me by several ways. Simple thanks are not enough to express my feelings towards them. I offer my hearty and sincere love to them.

Before closing this section let me remember that "Our sweetest songs are those, That tell of saddest thoughts." Life does not go smoothly always. Occasionally, there are those moments of unutterable pain which is inexplicable by words. On the way to bear fruit in my long research I remember the most harmful year 2008 which I shall never forget. The year began well, I was working at a rapid pace. All of a sudden the progress of my work was stopped as I was attacked by viral hepatitis. On doctor's advice I went back home for recovery but bad days followed me. There my father suffered sudden acute heart attack and he had to undergo a cardiac surgery. Being his elder son I stayed back to take care of my family till the things were under control. The whole situations kept me away for about six months. The consecutive shocking events left me puzzled and hopeless, fatigued both mentally and physically, worried and feared also. I would have been lost in the darkness but my supervisor Dr. Banerjee stood by me and continuously encouraged me to fight back the hurdles. He did not lose his patience and waited for the moment to get the things settled down and gave me an opportunity to come back. No doubt, this thesis would not have seen the daylight without his unfailing inspiration, kind support and remarkable patience. Once and for all,

I take the opportunity to express my heart-felt gratitude and gratefulness to my supervisor Dr. Dipankar.P.K. Banerjee. I am indebted to him for everything that he has done for me.

R. K. Das
PRL, Ahmedabad.

Publications

Research Papers:

1. **Das R.K.**, Banerjee D.P.K., Ashok N.M., *A near-infrared shock wave in the 2006 outburst of recurrent nova RS Ophiuchi*, 2006, ApJ, 653, L141.

2. **Das R.K.**, Banerjee, D.P.K., Ashok N.M., Chesneau O., *Near-Infrared Studies of V1280 Sco (Nova Scorpii 2007)*, 2008, MNRAS, 391, 1874.

3. Chesneau O., Banerjee D.P.K.,..., **Das R.K.**, Ashok N.M. et al., *VLTI monitoring of the dust formation event of the Nova V1280 Scorpii*, 2008, A&A, 487, 223.

4. Banerjee D.P.K., **Das R.K.**, Ashok N.M., *Near-Infrared H and K band studies of the 2006 outburst of the recurrent nova RS Ophiuchi*, 2009, MNRAS, in press (arXiv.0903.3794).

5. **Das R.K.**, Banerjee D.P.K., Ashok N.M., *Detection and evolution of the CO (Δv = 2) emission nova V2615 Ophiuchi (2007)*, 2009, MNRAS, 398, 375.

6. Naik S., Ashok N.M., Banerjee D.P.K., **Das R.K.**, *Near-infrared Observations of Nova V574 Puppis*, 2009, submitted to MNRAS, under revision.

CBETs and IAUCs:

1. **Das R.K.**, Ashok N.M., Banerjee D.P.K., 2005, IAUC, 8617.
2. **Das R.K.**, Ashok N.M., Banerjee D.P.K., 2006, IAUC, 8673.
3. **Das R.K.**, Ashok N.M., Banerjee D.P.K., 2006, CBET, 730.
4. **Das R.K.**, Ashok N.M., Banerjee D.P.K., 2007, CBET, 866.
5. **Das R.K.**, Ashok N.M., Banerjee D.P.K., 2007, CBET, 864.
6. **Das R.K.**, Ashok N.M., Banerjee D.P.K., 2007, CBET, 925.

Statement

This thesis contains the results that emerged from extensive studies of three selected novae viz. V1280 Scorpii, RS Ophiuchi and V2615 Ophiuchi in infrared region (1 - 2.5 μm). The whole work has been carried out under the supervision of Dr. Dipankar P. K. Banerjee at Physical Research Laboratory, Ahmedabad. The observations of all the novae presented in this thesis have been made using the 1.2m telescope (+ NICMOS array) at the Mount Abu Infrared Observatory, Rajasthan operated by Physical Research Laboratory. The contents of the thesis have been divided in six chapters as follows.

- **Chapter 1: An Introduction to Novae**

  Chapter 1 presents an introductory review of novae. General properties and characteristics, classifications, physical processes viable for the eruption are explained. The astronomical significance and relevance of infrared studies are discussed and the aims and scope of the thesis are indicated.

- **Chapter 2: Observations and Data Analysis**

  Chapter 2 deals with the observation techniques and instruments that were used for the observations presented in the thesis. This is followed by discussions on the procedures for observations and data analysis.

- **Chapter 3: Studies of the Recurrent Nova RS Ophiuchi (Outburst 2006)**

  Chapter 3 documents the near-infrared (1 - 2.5 μm) evolution of the recent (2006) outburst of the recurrent nova RS Ophiuchi (RS Oph) in a detailed manner. The observations cover the period between 1 to 94 days after the eruption. An extensive set of spectra and the near infrared light curve is presented and an analysis and discussion are given of the emission lines seen therein (HI Paschen and Brackett recombination lines, coronal lines, Fe II lines etc.). The key result concerns the rare detection of an infrared shock wave. The evolution of the shock is traced through a free expansion stage to

a decelerative phase and the result is compared with current shock models. The author also discusses the behaviour and origin of the two *H* band Fe II lines at 1.6872 and 1.7414 μm that are prominently seen throughout the span of the observations. These *H* band Fe II lines are very uncommon in novae spectra. They appear to arise from a combination of Lyman alpha plus Lyman continuum fluorescence and collisional excitation. Based on the analysis of the Fe II lines and Case B recombination studies the site of origin of the near-infrared line emission is explored. An analysis of the temporal evolution of the [Si VI] 1.9641 μm coronal line and another coronal line at 2.0894 μm which is attributed to [Mn XIV] is made. Assuming collisional effects to dominate in the hot coronal gas, estimates are made of the ion temperature in the gas. The present observations also imply that the white dwarf in the RS Oph system has a high mass indicating that it could be a potential supernova (Type Ia) candidate.

- **Chapter 4: Study of the Dust Forming Nova V1280 Scorpii**

  Chapter 4 presents the near-infrared (1 - 2.5 μm) study of the dust forming nova V1280 Scorpii (V1280 Sco). V1280 Sco is one of few novae which was caught in outburst much earlier before it reached maximum. The results are based on the spectroscopic and photometric observations between 14 and 125 days after the discovery. A large number of spectra were recorded, sampling the nova's evolution at regular intervals, thereby leading to one of the most comprehensive studies of a classical nova in the near-infrared. The key result concerns the issue of predicting which novae will form dust. Diagnostic lines are identified which are shown to reliably aid in such a prediction. A synthetic spectrum is generated to qualitatively study different aspects of the observed spectral features and to give estimates of elemental abundances in V1280 Sco. The presence of a persisting absorption structure in the Br γ line is interpreted as the evidence for sustained mass-loss during the outburst and used to set a lower limit for the mass loss duration. Using the available photometric data during its prolonged rise to maximum, a study of the early fireball expansion in the nova has been made and values of parameters such as the angular size, distance to the nova have been determined and compared with the interferometric results.

- **Chapter 5: Study of V2615 Ophiuchi - A Nova with Prominent CO Emission**

  Chapter 5 describes near-infrared (1 - 2.5 μm) spectroscopic and photometric results, based on the observations between 9 and 82 days after outburst, of the dust forming nova V2615 Ophiuchi (V2615 Oph). The highlight of the observations is the detection of first overtone CO emission in this nova; earlier only in a few novae CO had been detected. In addition the current observations present the evolution of CO with time - observed for the first time in any nova. The CO bands have been recorded over several epochs thereby allowing a rare opportunity to study its evolution from a phase of constant strength through a stage when the CO is destroyed fairly rapidly. The observed CO bands are modeled to estimate the temperature and mass of the emitting CO gas and also to place limits on the $^{12}C/^{13}C$ ratio. The observed timescales involved in the evolution of the CO emission are compared and found in a good agreement with model predictions that investigate the chemistry in a nova outflow during the early stages. An observed line at 2.088 μm has been analyzed, it has been suggested that it could be due to FeII excited by Lyman α fluorescence.

- **Chapter 6: Summary and Future Work** Chapter 6, the last chapter, summarizes the important results obtained from the above studies and the scope for future in continuation to the present studies is also discussed.

The results presented in the above chapters have been published in journals and have been indicated in the list of publication. A list of references used in this thesis is presented at the end.

The manuscript of this thesis has been checked several times with extreme care to free it from all discrepancies and to convey the ideas properly. Even then the vigilant readers may find mistakes and several portions of this thesis which may seem intellectually unwarranted, mistaken and incorrect. The author takes the sole responsibility for these unwanted errors which have resulted from his inadequate knowledge in the subject and incomplete digestion of the relevant concepts or escaped his notice.

Contents

List of Figures

List of Tables

CHAPTER 1

An Introduction to Novae

Stellar explosions are gigantic cosmic events that take place very often in the Galaxies. The explosions can be so violent that within a very short period of time they emit a huge amount of energy comparable to that emitted by all other stars in the Galaxy; this makes the erupting system visible from far away. Each explosion may also thrust as much mass as that of the Sun into space. The mechanisms that cause the explosions are several e.g., gravitational collapse of the core of high mass stars, rapid nuclear burning, release of gravitational energy etc. Such explosions have great impact on the host galaxies. For example, they are the prime sources of heavier elements in the inter stellar medium. Sometimes, the expanding shock, driven by the explosion, can trigger new star formation inside cold molecular gas clouds.

The most violent stellar explosion is a supernova (*supernovae* in plural) outburst that occurs due to the sudden (on a time-scale of seconds) gravitational collapse of the core of a high mass star or the collapse of a white dwarf that has exceeded the Chandrasekhar limit of 1.4 $M_\odot$. The explosion tears apart the star completely and gives birth to a rotating neutron star or pulsar (if the core mass is less than 5 $M_\odot$) or a black hole (for the core mass more than 5 $M_\odot$). A supernova is the most luminous object in space, each explosion releases energy of about 10^{51} ergs, an amount comparable to the total energy radiated by the Sun in its whole life. From the cosmological point of view, supernovae (Type I) are of extreme importance. Since, a supernova explosion emits constant amount of energy, they work as a standard candle and are used to measure cosmological distances. Using the techniques involving supernovae, it has been possible to measure distances out to

around 1000 megaparsec (Mpc), which is a significant fraction of the radius of the visible Universe.

After a supernova, a nova (*novae* in plural) outburst is the second most violent explosion that occurs in a galaxy. In a nova explosion, the energy produced amounts to about 10^{45} erg. Though the eruption is relatively less energetic, novae occur more frequently than supernovae. A nova refers to a close binary stellar system consisting of a white dwarf and a companion star; the explosion occurs due to a thermonuclear runaway on the white dwarf surface (a detailed description is given in later subsections). Consequently, the system can brighten up by a factor of few millions in a few days and then fade gradually over months to years. The violence of the explosion throws a significant amount of mass in the form of a shell that may contain radioactive nuclei and form molecules and dust, into space; thus, novae play a significant role in the chemical evolution of Galaxy.

Novae have been the object of intense interest since long past. In ancient times also, quite a few have been observed by astronomers who interpreted them as *novae stella* (*new stars*) from which is derived the term *nova*. Following the modern taxonomy, novae belong to a general class of eruptive variable stars called *Cataclysmic Variables* (CVs). A brief description of CVs has been presented in a later section. However, the present thesis concentrates on the nova phenomenon in particular. Before describing the results proper on few selected novae, we discuss the general properties of novae in the rest of this chapter.

1.1 Early studies of novae and other eruptive variables

Our intention in studying the historical records is to find accounts of the new stars described in details. Though documented rather rarely, such descriptions may help us to know about the nature and characteristics of the outburst. The historical time period may be loosely divided into two epochs viz. the pre-1900 period and the post-1900 era that marks the beginning of the modern period.

We will briefly discuss them in the rest of this section. In this context, we must keep in mind that, in those time periods observers were generally unable to distinguish between a nova and a supernova. So, both were designated as new stars. Also, we must be cautious while we use those records, because many other events might have been mistaken as new stars.

1.1.1 Pre 1900 history

The principal sources of usable historical discoveries are (Clark & Stephenson 1977):

1. Far Eastern histories and diaries,
2. Arabic chronicles and astrological works,
3. Medieval European monastic chronicles and
4. Post renaissance European scientific writings.

The earliest discoveries of new stars were made in the Far East - China, Japan and Korea. Officials, employed by the rulers at the imperial Chinese court, maintained a systematic watch of the sky for any unusual celestial events from at least as early as 200 BC, although the purpose was purely astrological. The habit spread to Korea around the time of Christ and to Japan in the sixth century AD (Duerbeck 2008).

The historical records contain references to three main types of temporary stars: *xingbo* (bushy stars), *huixing* (broom stars) *kexing* (guest stars or visiting stars) and in addition *liuxing* (flowing stars). The first two almost invariably refer to comets, *liuxing* refers to meteors and *kexing* may be interpreted as encompassing novae and supernovae. The earliest compilation of reports of such temporary stars was prepared by the Chinese scholar Ma Dualin in the thirteenth century AD, he listed events from the Han dynasty (from 206 BC onward) to his own time. A detailed overview of Chinese, Korean and Japanese sources has been given by Stephenson and Green (2002). It appears that about 80 new stars were recorded up to about 1600, eight being supernovae and the rest being ordinary novae.

Two of those new stars are of extreme significance and deserve mention here. The first one was observed in 1006 AD, in the constellation of Lupus, is the only one known to be recorded in the Arabic history as well as in medieval Europe. It was also observed extensively by Chinese and Japanese astronomers. Several descriptions are found in favor of the extreme brilliance of the star (apparent magnitude being in the range of -6.5 to -9), probably it was the brightest stellar event in recorded history. As a result of a thorough search in several Arabic chronicles, Goldstein was able to bring out several detailed accounts about the star. He estimated the apparent magnitude to be -8 to -10. The remnant of the supernova associated with this event (SN 1006) has been detected in optical by van den Bergh (1976, IAU circular no. 2952) and in X-ray by Winkler and Laird (1976) (Clark & Stephenson

1977 and references therein).

Another such supernova took place in the constellation of Taurus. It was extensively observed only by the Chinese and Japanese in between July and November 1054 AD. Various reports reveal that the star reached a brightness of -6 or -7 magnitude and was visible even in the daylight for a total of 23 days. It was visible over a total period of time exceeding 22 months. The remnants of the event, presently known as the Crab Nebula, were rediscovered by Dr. John Bevis in 1731. Later Charles Messier placed it as the first object in his catalogue (1758) of deep-sky objects.

It appears that, few new stars were discovered in Roman times also. The famous historian Pliny reported a bright new star (possibly a nova) in July 134 BC in the constellation of Scorpius. Later, in February A.D. 78, one more new star was discovered. It is said that the discovery of another new star inspired the astronomer Hipparchus to produce the first star catalogue of the heavens.

The foundations of Western astronomy were laid by the Babylonians through their mathematics and systematic observations of the Sun, Moon, planets, and stars (mainly for astrological purposes). Later, Babylonian astronomy was absorbed into Greek culture, where it eventually led to models of the visible universe. Most popular was the model by Aristotle (384-322 BC) who wrote that the world was made of four elements: earth, water, air, and fire. Bodies beyond the sphere of the Moon were made of a fifth element or quintessence, which was ingenerable and incorruptible. There was no existence for the variable stars in Aristotle's universe.

The impact of the Aristotelian philosophy on the Western cultures was so profound that variable stars remained unacknowledged in their societies until the post-Copernican era. The sixteenth century brought a renaissance and revolution in scientific thought in the Western world. The occurrence of two supernovae opened the Western eye to the mutability of the stars. The first one was discovered by Tycho Brah*é* in November 1572, in the constellation of Cassiopeia. It reached a maximum of -4 magnitude, rivalling Venus in brightness. The second one was noticed just over three decades later, in October 1604, by Johannes Kepler. Though it was somewhat fainter than Tycho's star, but still at maximum brightness it rivalled Jupiter. However, these observations could not stimulate others towards observations of such events. The result is that a few bright new stars might have

escaped detection.

The first true nova, as opposed to a supernova, was discovered in 1670, at second magnitude in the constellation of Vulpecula, by the Carthusian monk Pere Dom Anthelme. No discovery was reported in the whole of the eighteenth century. In the first half of the nineteenth century, only one nova (nova Oph 1848) was discovered by John Russell Hind. Since the discovery of nova Vulpecula in 1670, this was the first such object to be observed publicly.

1.1.2 Modern history

The true modern history of variable stars began in the late 1800s with several developments of instruments and associated techniques in the late nineteenth century which had a profound effect on the study of variable stars; most important and significant was the introduction of instrumental photometry and use of the photoelectric photometer. By this time, also, the photographic emulsions became sensitive enough, and telescope drive systems became more accurate for astrophotography to make its full impact. The gradual improvements of electronic photometers, photomultiplier tubes, photo-sensitive diodes and charged couple devices (CCD) improved the accuracy and simplified the measurements that resulted in the discoveries of large number of novae. Further, developments of spectroscopes assisted in spectroscopic study that led to the understanding of the cause and nature of the nova outburst.

The beginning of systematic monitoring of the sky, by photographic means, started around 1892 with the discovery of T Aur. More discoveries of novae established the usefulness and importance of the observational studies of these types of stars. Consequently, more observatories came up like the stations of Harvard College Observatory, both in the northern and southern hemispheres followed by stations in Germany, Russia and elsewhere. After the cessation of systematic sky patrols by the Harvard Observatory in the early 1950s, quite a number of novae were found during objective prism surveys from the 1950s to the 1970s. Until the twentieth century, there was no discrimination between novae and supernovae. From 1917 onwards, serendipitous discoveries of novae in spiral nebulae mainly by G.W. Ritchey, H. D. Curtis and others, which were soon followed by systematic searches, indicated two distinct groups of objects.

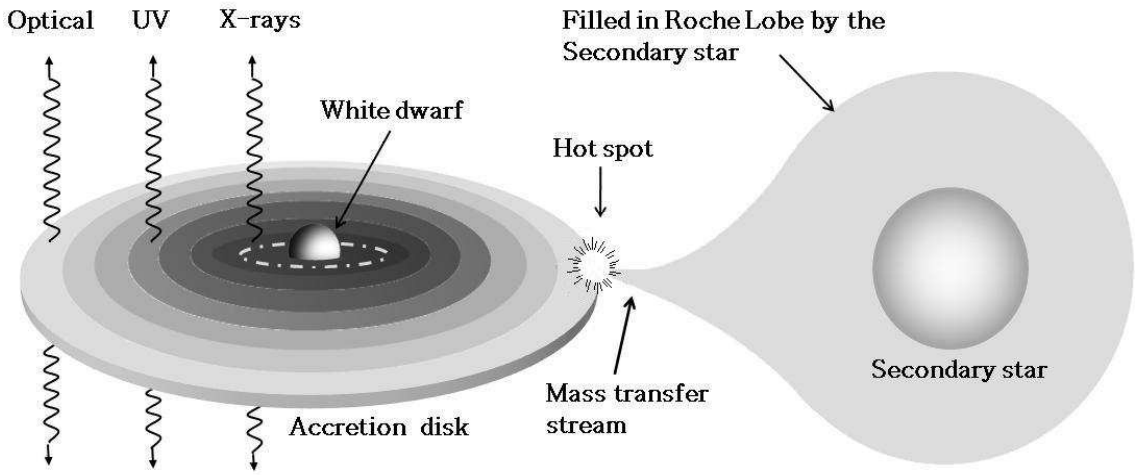

Figure 1.1: A schematic diagram of a cataclysmic variable (CV) star. A CV is a binary system consisting of a white dwarf (primary component) and a main sequence star or a late type giant (secondary component). More description is given in section 1.2.

The spectroscopic and photometric studies of novae, providing the breakthrough in our understanding of modern nova theory, came in the middle of the twentieth century. The beginning was made with observation of the dwarf novae RU Peg and SS Cyg by A. H. Joy. Both these novae showed composite spectra containing absorption features as well as emission features, which suggested binarity (Joy 1940, 1956). From the variation in the radial velocity he also determined an orbital period of 6 h 38 m for SS Cyg. Almost at the same time, Merle F. Walker discovered directly from the analysis of the lightcurve, that the nova DQ Her (Nova Her 1934) was also an eclipsing binary with a period of 4.6 h. Further work by Robert P. Kraft "led to the speculation that all cataclysmic variables might be binary systems" (Kraft 1962).

From about the mid 1970s, photographic and later CCD monitoring became common practice, so that most of the discoveries in recent times have been made on films and CCDs. Since the 1980s, discoveries of classical novae have almost totally become a domain of amateur astronomers. In the last few decades tremendous improvements in digital detectors and satellite-borne observations amplified the success in detecting novae and thereby added to our understanding the nova phenomena.

1.2 Physical structure

Since the photometric observations by Walker (1956) of the old nova DQ Her and the pioneering spectroscopic study by Kraft (1964) of ten old novae it is clear that nova explosions occur in close binary systems. It is now well established that novae in particular, and CVs in general, are **close binary systems** (separation $\approx 10^{11}$ cm) with short orbital periods (typically hours). The components of the binary systems are:

Primary component: The primary component of the binary system is a white dwarf, composed of carbon and oxygen (CO white dwarf) or of oxygen, neon and magnesium (ONeMg white dwarf). The masses of the white dwarfs can have a wide range up to the Chandrasekhar limit, but generally are found to be well above $\sim 0.5 M_\odot$ in novae.

Secondary component: The secondary component is usually a single main sequence star or a late type giant which fills its Roche lobe. The Roche lobe is the largest volume that a star can occupy in the neighborhood of a companion. Gravitational potential is equal everywhere on the surface of the Roche lobe. Further expansion of the secondary, or the shrinkage of the binary orbit, results in mass loss through the inner Lagrangian point (the common point where the Roche lobes of both the stars touch).

Accretion Disk: The hydrogen-rich matter ejected by the secondary passes through the inner Lagrangian point towards the primary and forms an accretion disk around the primary. The observed mass transfer rate is about 10^{-9} to 10^{-10} $M_\odot$ a year. The accreting material spirals inwards through an accretion disc and forms a layer of fuel on the white dwarf surface. Gradually, the bottom of the layer is heated and compressed by the strong surface gravity of the white dwarf and emits X-ray and extreme ultraviolet.

After the accretion disk has been formed, the stream of infalling matter from the secondary collides, at supersonic speeds, on the outer rim of the accretion disk. This impact creates a shock heated area called the 'hot spot' or 'bright spot'. The spot radiates huge amount of energy in optical that is equivalent to or more than the total energy emitted by the other components of the binary.

1.3 Masses and orbital period

The dimensions of a binary system are set by its orbital period (P_{orb}) and by the masses of its components. For Roche-lobe-filling main sequence secondaries the mass is uniquely determined by P_{orb} estimated from the equation:

$$P_{orb}^2 = \frac{4\pi^2 a^3}{G[M_{WD} + M_{sec}]} \tag{1.1}$$

where M_{WD} and M_{sec} represent the masses of the white dwarf and the secondary star; a is the separation between the two ($\approx 10^{11}$ cm). The orbital period of a CV is its most precisely known parameter.

One of the most important pieces of information about the structure and evolution of CVs is the observed distribution of orbital periods. Observational studies of several CVs show that P_{orb} lies in the range of few minutes to about 10 hr. It has been found that:

1. about 2/3 of the CVs have orbital periods in the range 3 h $\lesssim$ P $\lesssim$ 14 h.
2. about 1/3 of the systems have periods in the range 80 m $\lesssim$ P $\lesssim$ 2 h.
3. there is an almost total deficiency of CVs in the period range 2 h $\lesssim$ P $\lesssim$ 3 h. This is usually referred to as the *period gap* (explained in section 1.5).

1.4 Classification of cataclysmic variable stars

As mentioned earlier, novae belong to the general class of variable stars called *Cataclysmic Variables* (CVs). CVs include a broad range of eruptive variables, the largest outbursts are associated with the novae. All CVs are close binary stars consisting of a white dwarf and a companion star. The differences are due to the mechanism of the outburst.

1. **Classical novae (CN)**: By definition, classical novae show only one observed eruption. The CN eruptions are caused by a thermonuclear runaway in the hydrogen-rich material accreted by and on the white dwarf. The amplitude (difference of pre and post outburst magnitudes) of the outbursts range from 6 to greater than 19 and is strongly correlated with the rate of mass transfer. Fast novae, of very short durations, show the largest amplitude eruptions

while the slow novae show lower amplitude eruptions.

2. **Dwarf novae (DN)**: They show low-amplitude eruptions, typically of 2-5 magnitudes and upto 8 magnitudes in rare cases. Dwarf novae undergo eruptions frequently, every ~ 10 d to tens of years with a well-defined time scale for each object. The dwarf nova outburst is well understood as a release of gravitational energy, caused by large increase in rate of mass transfer through the accretion disc.

   Based on the morphology of the light curve DNs are further classified into three distinct subtypes:

   i. **Z Cam stars**: they are distinguished by random standstills. A standstill usually starts at the end of an outburst, about one magnitude below maximum light, and may last from a few days to 1,000 days. In this period the star maintains almost constant brightness. The average energy output in a standstill is larger than that during an outburst cycle. The prototype system, Z Camelopardalis, lies about 530 light years from Earth; it was the first dwarf nova to be detected. The orbital period for the system is 7h 21m; eruptions occur, on an average, every 20 days.

   ii. **SU UMa stars**: they are characterized by superoutbursts that take place very often. Generally, these occur once for every 3 to 10 normal outbursts, last for 10 to 18 days, and add one to two magnitudes in brightness over the normal maxima. While in super-outburst, a small periodic fluctuation of several tenths of a magnitude known as a super-hump is observed at maximum.

   iii. **U Gem stars**: they include all other dwarf novae. Most of the time, a U Gem star shows small, sometimes rapid variations in light. U Gem stars blaze up at semiregular intervals: the longer the interval, the greater the increase in brightness. The prototype, U Geminorum itself, remains at magnitude 13.5 for periods varying between 40 and 130 days, and rises to 9.5 or brighter in the course of a day or two, before returning to its usual state over the next couple of weeks; it also experiences a minor minimum every 4h 11m as its larger, secondary component passes in front of the white dwarf primary.

3. **Recurrent novae (RN)**: Recurrent novae are defined as the previously recognized classical novae that are found to repeat their eruptions. The eruptions occur due to thermonuclear runway on the white dwarf surface. Till date, about nine have been recognized as recurrent novae with a few others considered as potential candidates. They group themselves in three subgroups (Warner 2008):

   i. **The T CrB type**: they have giant secondaries. Due to high mass transfer rate they erupt more frequently. The definite members of this class are T CrB, V745 Sco, V3890 Sgr and RS Oph.

   ii. **The U Sco type**: they also have evolved secondaries. The subgroup includes U Sco, V394 CrA, CI Aql and LMC-RN. They are among the fastest novae observed. Unlike normal novae, in quiescence, their spectra are dominated by He lines. U Sco and CI Aql with their periods ~1 d are typical of the class.

   iii. **The T Pyx type**: it has been a class with only one member, T Pyx itself. T Pyx shows a relatively slow decay (t_3 = 88 d) with oscillations in the transition region. Its short P_{orb} (1.83 h) also put it in a class by itself, but the recently recognized recurrent nova IM Nor, with P_{orb} = 2.46 h and t_3 = 50 d allies it to T Pyx. T Pyx has a quiescent bolometric luminosity greater than expected by an order of magnitude, and is suspected of being in a rapid and possibly terminal phase of evolution.

4. **Novae like variables (NL)**: They include other CVs, for example, pre-nova, post-nova and perhaps Z Cam stars. Most NLs have emission line spectra, but a subgroup called UX UMa stars show additional absorption lines.

5. **Magnetic CVs**: They have an intense magnetic field that is strong enough to disrupt the accretion disk; either partially or totally. The two popular subclasses are:

   i. **Polars**: they have the strongest magnetic field (B $\gtrsim 10^7$ G). The field lines connect to the inter-star stream and prevent the formation of any accretion disc.

   ii. **Intermediate Polars** (IPs): they have relatively weaker fields ($10^6 \lesssim$ B $\lesssim 10^7$ G), e.g., DQ Her. In case of IPs, a disc forms but the inner parts are

truncated where the primary's magnetosphere controls the flow.

Symbiotic novae:

Besides the above classification, one more class of novae called *symbiotic novae* has been defined. They differ from CVs by their spectra and structure. Symbiotic novae are slowly eruptive variables and are suspected to be wide binary systems (separation $\sim 10^{14}$-10^{15} cm) with long orbital period ($200 \lesssim P_{orb} \lesssim 1000$ days) with few exceptions. Spectra of symbiotic novae show simultaneously the absorption features of a late type giant and emission features of HI, HeI and other ions of high ionization potential (≥ 20 eV). The spectra evolve to an A or F type continuum with additional HI, HeI absorption lines or to pure nebular spectra during eruption (Warner 1995 and references therein).

So far about ten variable stars have been recognized as symbiotic novae (Warner 1995). It is believed that the white dwarfs in symbiotic novae accumulate matter directly from the wind ejected by the secondary and do not form any accretion disk. They are classified in two groups depending on the nature of the secondary:

1. **S-type**: contains normal M giants and
2. **D-type**: contains heavily dust-reddened Mira variables.

1.5 Origin and evolution of CVs

The precursors of CVs are thought to be binaries consisting of a low mass secondary and a high mass primary that evolves faster than the secondary. Initially, the separation must have been large so that the primary (progenitor of the white dwarf) could form a well-developed core-envelope structure. During the red giant phase, the primary fills its Roche lobe after developing an electron-degenerate core composed of carbon and oxygen or of oxygen, neon and a modest abundance of heavier elements. A common envelope is formed when the primary overflows its Roche lobe. If the mass of the secondary is much smaller than the initial mass of the primary, most of the mass ejected by the primary into the common envelope leaves the system. After expulsion of the common envelope and some short-lived residual burning of hydrogen or helium, or both, the remnant becomes a cooling white dwarf.

The common envelope phase plays a crucial role in the life history of these binaries and finally leads them towards the formation of CVs. Inside the common envelope, both the components orbit in a resistive medium; the friction causes orbital decay and transfers angular momentum to the steadily expanding envelope. The details of this common envelope phase are very complicated and not fully understood (see Iben et al. 1993 for a review), but it is generally believed that the overall effect is that the lower-mass star and the degenerate core (soon to become a white dwarf) spiral inwards until the envelope has been driven off and the frictional angular momentum loss stops. The predicted end result is a planetary nebula with a close binary at its center. A significant number of planetary nebulae do have binary central stars. If the orbital shrinkage during the preceding common envelope phase has been sufficient, tidal torques exerted by the white dwarf component keeps the secondary spinning at a frequency nearly equal to the orbital frequency. The spin angular momentum of the secondary is maintained at the expense of orbital angular momentum and the orbital separation therefore decreases.

The gradual reduction of orbital separation continues until the secondary fills its Roche lobe, and the mass transfer begins to produce CVs with periods of an initial value P_{orb} ~10 h, then slowly down to ~3 h. Steady mass transfer is maintained by the systemic loss of orbital angular momentum. Viable mechanisms for the gradual loss of angular momentum are gravitational radiation and/or a magnetically coupled stellar wind from the secondary (*magnetic braking*). In the framework of the period gap model, mass transfer in systems above the gap, i.e. with P > 3 h, is driven by the combined action of magnetic braking and gravitational radiation,while in systems below the gap, i.e.with P < 2 h, it is essentially driven only by gravitational radiation.

The period gap has been interpreted in the way that, at $P_{orb} \sim 3$ h the efficacy of the magnetic stellar wind declines sharply. A possible explanation for the decline is that the secondary becomes completely convective which leads to a re-arrangement in the geometry of the magnetic field which considerably reduces the torquing action between anchored magnetic field and ionized wind particles. As a result the angular momentum loss rate drops suddenly. This, in turn, causes the secondary to detach from its Roche lobe and to stop transferring mass. Thus the systems cross the gap as detached binaries and, therefore, are virtually invisible during this phase. By the time the period is as small as 3 h, gravitational wave radiation (GWR) becomes an effective way of decreasing the orbital angular momentum. After ~5 -

8×10^8 yrs of GWR, the orbital period decreases to ~2 h; the secondary once again comes into contact with its Roche lobe and mass transfer resumes.

The ultimate fate of novae systems is open to some doubt. There are two possibilities.

1. These systems could just fizzle out. There is direct observational evidence that CO novae explosions expel an excess of carbon and other heavy elements. This strongly suggests that a nova explosion expels not just the outer layer of accumulated hydrogen but also some matter dredged up from the white dwarf interior itself. This would mean that the CO white dwarf loses mass in nova explosions (Starrfield et al. 2008 and references therein). If this is the case, the white dwarf primary will remain in the binary system until the secondary star evolves and forms a white dwarf of its own.

   The two white dwarfs will spiral together until the separation and hence the Roche lobes become small enough so that one of the white dwarfs fills its lobe. The smaller mass white dwarf will fill its lobe first and begin to lose mass to the larger-mass dwarf. The only outcome can be the disappearance of the small-mass dwarf. The larger-mass dwarf will simply gobble up the smaller-mass one. As the larger-mass white dwarf consumes the smaller-mass one, the larger-mass white dwarf becomes more massive. If the total mass exceeds the Chandrasekhar limit, the white dwarf will collapse and give birth of a Type I supernova.

2. Alternatively, novae could end in a cataclysmic implosion or explosion. In case of recurrent novae the primary is a high mass ONeMg (or ONe) novae. Comparison between observations and theoretical modeling show that about 10% of the accreted matter settles down on the white dwarf. So, the mass of the white dwarf increases gradually and approaches Chandrasekhar limit. Therefore, only the white dwarfs in recurrent novae offer the possibility of producing supernovae (MacDonald 1984, Livio & Truran 1992). Livio & Truran (1992) estimate a supernovae production rate $\sim 1 \times 10^{-4}$ yr^{-1} from the above evolution. It is also possible that, the white dwarf may collapse rather than explode. This process will leave a neutron star in orbit around the main-sequence star. This collapse may result in the ejection of little or no mass. The energy of the collapse might come out almost entirely in the form

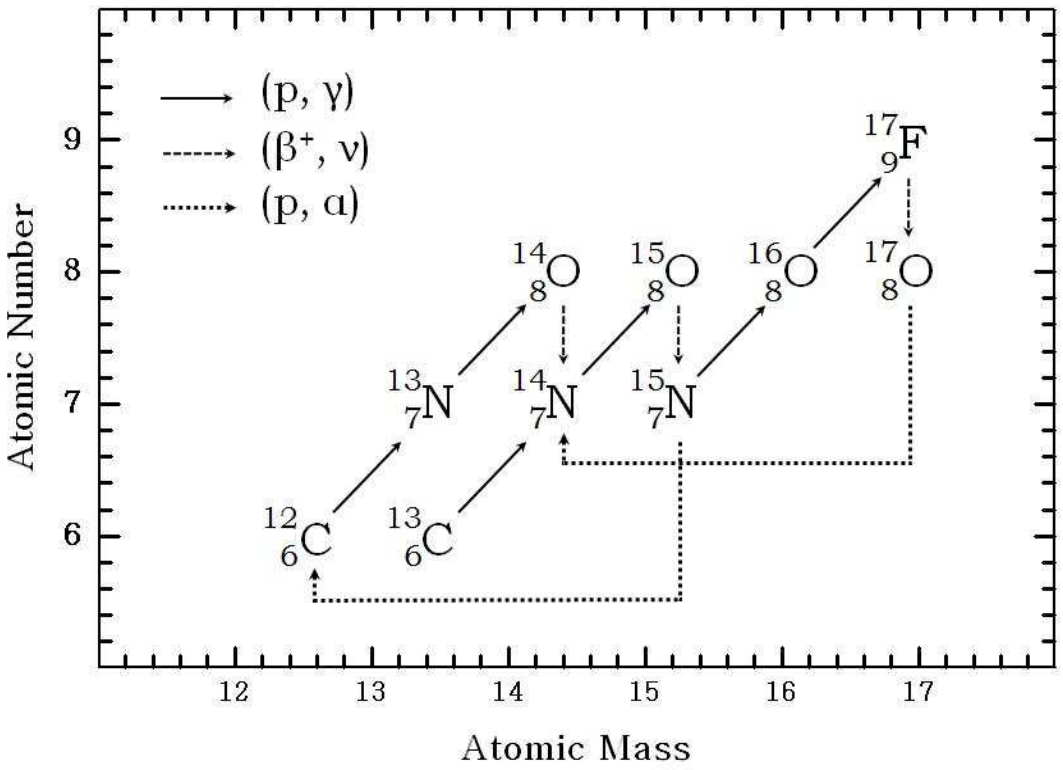

Figure 1.2: CNO nuclei and the nuclear reactions of CNO cycle.

of neutrinos.

1.6 Outburst mechanism: thermonuclear runway

Essentially, a nova explosion is a gigantic thermonuclear explosion on the white dwarf surface. Preparation for the explosion goes on over a long period of time. Due to the continued accretion of hydrogen-rich material, the pressure at the bottom of the accreted layer gradually increases. The result is that the bottom layer is compressed and heated by the strong surface gravity of the white dwarf. When a critical pressure P_{crit} is achieved, the temperature at the bottom layer rises to few times 10^6 K and hydrogen burning begins. This pressure is dependent on the mass of the white dwarf as well as the mass of accreted matter by the relation (Gehrz et al. 1998):

$$P_{crit} \quad (\text{in dynes cm}^{-2}) = \frac{GM_{WD}M_{envl}}{4\pi R_{WD}^4} \tag{1.2}$$

where, $G = 6.67 \times 10^{-8}$ dynes cm^{-2}, M_{WD} and M_{envl} are in grams, and R_{WD} in cm. The presently accepted value of $P_{crit} = 2 \times 10^{19}$ dynes cm^{-2} consistent with numerical hydrostatic models of nova explosion. This value is achieved for a critical value of the accreted envelope mass $M_{envl} = 10^{-4}$ - 10^{-5} $M_\odot$.

The hydrogen burning starts first through proton-proton (p-p) chain:

$$\left.\begin{array}{rcl} {}^1_1\mathrm{H} + {}^1_1\mathrm{H} & \rightarrow & {}^2_1\mathrm{H} + e^+ + \nu_e \\ {}^2_1\mathrm{H} + {}^1_1\mathrm{H} & \rightarrow & {}^3_2\mathrm{He} + \gamma \\ {}^3_2\mathrm{He} + {}^3_2\mathrm{He} & \rightarrow & {}^4_2\mathrm{He} + 2{}^1_1\mathrm{H} \end{array}\right\} \quad (1.3)$$

The energy production of the p-p chain is very sensitive to the temperature ($\propto T^4$). Now, at the base of this enriched layer of hydrogen, the material is supported by electron degeneracy pressure. For highly degenerate matter the pressure $P = \rho^\gamma$ is independent of the temperature, so the shell source cannot dampen the reaction rate by expanding and cooling like the stars. Consequently, any small increase in temperature, leading to enhanced energy production but no increase in pressure, is amplified in exponential runaway which is commonly known as *thermonuclear runaway* (TNR). This explosive burning of hydrogen is commonly termed as a 'nova explosion'.

After a short lived phase when the temperature at the base of the envelope reaches about 2×10^7 K, the carbon-nitrogen-oxygen (CNO) cycle (Figure 1.2) begins. The energy production of the CNO cycle is highly dependent on temperature ($\propto T^{18}$) (Warner 1995). While the p-p chain is important in the initial phase, it is the CNO cycle reactions that power the final stages of the TNR and the evolution to the peak. This tremendous amount of energy generated, cannot be carried out by radiation alone, and so the envelope becomes convective. At T = 8×10^7 K the envelope becomes fully convective. Convection transports fresh CNO into the high temperature region and takes a significant number of β^+ unstable nuclei (^{13}N, ^{14}O, ^{15}O, ^{17}F with half-lives of 598 s, 71 s, 122 s, 92 s respectively) are brought to the surface before they decay. The convection turnover time scale is ~100 s. The abundance of β^+ unstable nuclei increases when temperature reaches to 10^8 K. The decay of these nuclei deposits huge amount of energy. Consequently, the thermal pressure becomes exceeds the electron degeneracy pressure and the envelope expands to reduce the overpressure. This is also the principal cause of most of the total luminosity of the eruption.

Table 1.1: Typical parameters for novae outburst.

Outburst energy (L_o)	=	10^{45} ergs
Bolometric luminosity	=	2x10^4 $L_\odot$ (constant)
Outburst amplitude	=	6-15 magnitudes
Time to decline by 2 magnitudes below visual maximum (t_2)	=	7-250 days
Time to decline by 3 magnitudes below visual maximum (t_3)	=	5-1000 days
Dust formation time (t_d)	=	7-100 days
Dust temperature (T_d)	=	1200 K
Grain size (a)	=	0.1 to 3 micron
Velocity of the ejecta (V_{ej})	=	few 100 to few 1000 km/s
Absolute magnitude (M_V)	=	-7 to -9
Mass of the ejected gas (M_{ej})	=	10^{-5} - 10^{-4} $M_\odot$
Ejecta particle density	=	5×10^{11} cm^{-3} (at t=5 days)
Composition		Metals (C, N, O, Fe, Na, Mg etc.) enhanced over cosmic by 10-100 times, grains, molecules, radioactive nuclei

1.7 Post-outburst development of novae

In the initial expansion phase, only about 10-50% of the hydrogen layer is ejected by the nova explosion and the rest of the accreted mass settles down on the white dwarf surface. Following this initial hydrodynamic ejection phase which dominates for fast novae, hydrostatic equilibrium is established and the hydrostatic burning phase begins. During this prolonged stage of hydrogen burning, which is most important for slow novae, energy is produced at a constant bolometric luminosity.

The modern understanding of nova eruptions is that they have bolometric luminosities that are all at or somewhat above the Eddington luminosity (the maximum luminosity, which a star of a given mass can have before the outward radiation pressure exceeds the inward gravitational force) given by the equation:

$$L_{Edd} = \frac{4\pi GcM_{WD}}{\kappa_T} \tag{1.4}$$

where c = 2.9979×10^{10} cm s^{-1}, κ_T is the Thomson opacity for scattering by free

electrons and equal to 0.3975 cm^2 g^{-1} for hydrogen (Gehrz 1998).

The continuous mass loss through a wind at this stage steadily decreases the remaining mass on the white dwarf. Deprived of fuel, the hydrostatic burning phase ends slowly, and the white dwarf begins to cool. Eventually the binary system reverts to its quiescent configuration and the accretion process begins anew and prepares for the next outburst. Following the eruption, the recurrence would be expected after a time

$$T_R = M_{crit} / < \dot{M}_{accr} > \tag{1.5}$$

If we assume the accretion rate $\dot{M}_{accr}$ to be 10^{-8} to 10^{-9} $M_\odot$ yr^{-1} , it will take some 10^4 to 10^5 years to build up another surface layer of critical mass $M_{crit} = 10^{-4}$ $M_\odot$.

The physical character of the ejected gas generally passes through a few distinct phases as a consequence of the nova explosion.

Fireball phase During the initial expansion phase, the ejecta is very thick and behaves like a "fireball" that radiates as a hot blackbody of temperature 6000 - 10,000 K. The observed light originates in this "pseudophotosphere" of the expanding fireball; at this point the spectrum of the nova resembles an A to F spectral type.

Optically thin expansion phase The optically thick fireball phase generally ends in a few days, at or close to the point of maximum visual brightness. Then, as the shell of gas thrown off by the nova continues to expand, it becomes less and less dense, the shell becomes transparent and the optically thin phase begins. The central white dwarf, swollen by its hydrostatic burning phase, now has the appearance of a blue horizontal-branch object located just blueward of the RR Lyrae stars on the HR diagram. The white dwarf envelope may burn irregularly, resulting in the substantial fluctuations in brightness observed in some novae.

Dust formation phase After a few months (or less; see Table 1.1), when the temperature of the expanding envelope of gases has fallen to about $\sim$ 1200 K, carbon and other elements in the ejecta can condense to form dust. The resulting dust shell becomes optically thick in roughly 50% of all dust forming

novae. The visible light from a nova is undiminished by an optically thin shell, but the formation of an optically thick cocoon of dust obscures or completely hides the central white dwarf. In the latter case, the output of visible light suddenly plunges. The light from the white dwarf is absorbed and re-emitted by the dust grains, so the optically thick dust shell radiates as a ~1200 K blackbody at infrared (IR) wavelengths. About 25-30% of all novae pass through dust formation phase; novae with a carbon-oxygen core white dwarf generally tend to form dust. In other novae, in which dust does not form, the optically thin ejecta is ionized and excited by the hot central remnant and shows nebular and coronal lines.

1.8 Observational properties of novae

The several stages of the progress of a nova following its outburst is reflected in its observational properties. As the nova passes through different stages, the observed light curve and spectra evolve accordingly following the outburst.

1.8.1 Evolution of the optical light curve

Our present understanding of novae light curves is largely based on the descriptions introduced by McLaughlin. From a study of several novae he found that, if the time-scales are compressed properly, all nova optical light curves could be made to resemble each other, and also at the same time the spectral evolution could be brought into better accord (McLaughlin 1939, 1960). The idealized light curve is shown in Figure 1.3. A nova light curve generally passes through the following stages during its evolution.

1. Pre-nova: This refers to the undisturbed system before outburst has taken place. The brightness generally shows weak variations and the spectrum resembles that of a hot star.

2. Initial Rise: Following the eruption, the light curve rises steeply towards maximum. Only a few novae have been caught on the initial rise (e.g., V1500 Cyg and PW Vul (Gehrz 1988 and references therein), nova LMC 1991 (Della Valle 1991), V1280 Sco (Das et al. 2008)). All indicate that the duration of this phase is generally of the order of a week or less.

3. Pre-maximum halt: In many novae there is a pause about 2 magnitudes below maximum. This ranges from a few hours in fast novae to a few days in slow novae.

4. Final Rise: The nova then brightens to maximum, taking 1-2 days for fast novae and several weeks for the slowest novae.

5. Principal maximum: The maximum phase itself is relatively short-lived, being only hours for very fast novae and only a few days for slow novae. Maximum bolometric luminosity is reached at the peak of the thermonuclear runaway, typically on a time scale of hours. Visual maximum is reached when the photosphere of the expanding envelope reaches its largest radius $\sim 10^{12}$-10^{13} cm.

6. Early Decline: The initial fall from maximum is usually smooth, except for slow novae, which have brightness variations on time-scales of 1-20 days with amplitudes up to 2 mag. This phase is marked by the fall in brightness of the observable continuum, the relative increase of the emission spectrum, and the appearance of multiple absorptions at the photospheric level.

7. Transition phase: At 3 to 4 magnitudes below maximum, the light curve shows either of the three distinct possibilities:

   i. there may be a deep minimum due to the formation of dust in the gas ejected, about 7 to 10 mag below the maximum. This lasts for months or even years, after which the nova recovers and follows an extrapolated decline.

   ii. there could be large amplitude oscillations with quasi-periods of ~5-15 days and amplitudes of up to 1.5 mag.

   iii. the light curve declines smoothly. About one-third of the fast and very fast systems plus a few of the slower ones, pass through this transition region without any noticeable peculiarities.

8. Final Decline: During this phase, the absorption features disappear, the nebular spectrum develops again, and often gives evidence of high and rising

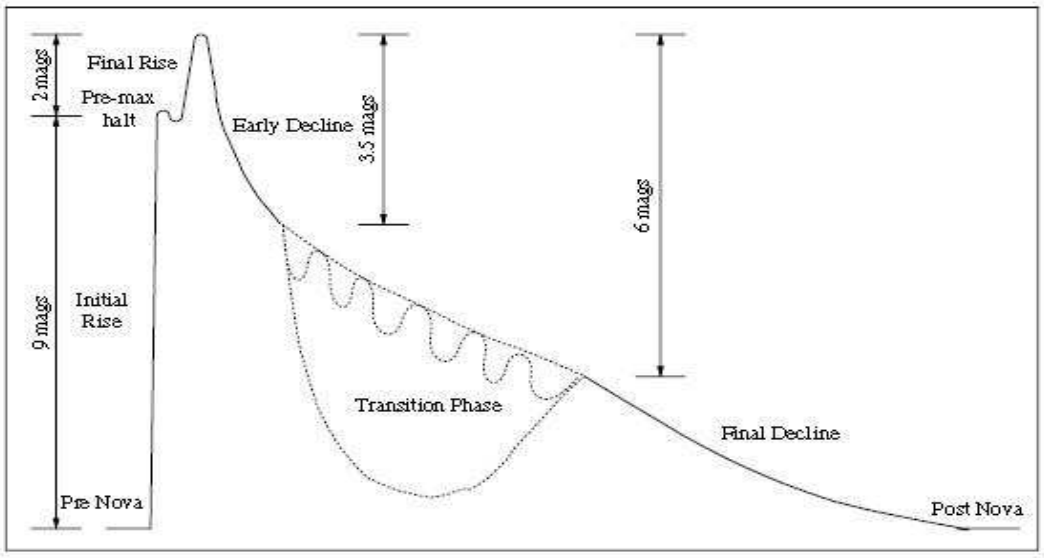

Figure 1.3: A typical light curve of a nova (taken from Bode & Evans 2008). Different stages have been described in subsection 1.8.2.

ionization and excitation.

9. Post-nova: It sees the star gradually returning to that of the pre-nova stage in a process that may be a very long one.

1.8.2 Evolution of the optical spectra - general characteristics:

Each nova shows a unique and spectacular pattern of spectroscopic variability. The spectra develop from absorption line spectra to pure emission line spectra, from permitted to forbidden transitions, from neutral lines and low ionization to high ionization stages, and subsequent return to intermediate ionization.

1. **Pre-Maximum Spectra:**
The pre-maximum spectra, on the rising branch of the light curve, are dominated by broad, blue-shifted absorption lines, resembling those of early type stars. The spectral lines generally display P Cygni absorption features. At maximum, novae usually show B5 to F5 type of spectra; later type is generally associated with slower novae. The large widths of the lines imply a high expansion velocity. Pre-maximum spectra are characteristic of a uniformly expanding optically thick envelope.

2. **Principal Spectrum:**
The principal spectrum, that appears at the visual maximum, has stronger and more blueshifted absorption lines than those at pre-maximum phase and resembles that of an A or F type supergiant spectrum with enhancements of the lines of C, N or O. The absorption lines often show multiple substructure, the velocity evolutions of which vary greatly from component to component and also from nova to nova; these components gradually evolve into the emission lines of the nebular shell. The average velocities of the absorption lines correlate with speed class, being up to 1000 km s^{-1} for the fastest novae and down to 150 km s^{-1} for the slowest.

As the nova declines from the maximum, the absorption components disappear and the spectrum becomes a pure emission one by the end of early decline. UV spectrum contains strong emission lines of He, C, N, O, Mg, Al and Si; in the IR, lines of HI, HeI, CI, NI, OI, NaI, MgI become stronger. Generally, the emission lines have complex profiles, indicative of non-uniformity of the ejected gas.

3. **The Diffuse Enhanced Spectrum:**
The diffuse enhanced system appears shortly after maximum light (typically from 1 to 20 days, according to speed class). It also shows the P Cyg profiles similar to that of the principal spectrum but about twice as broad and blue-shifted, and lasts for about two weeks in very fast novae to three or four months in typical slow novae. In the later stages, the broad absorptions often show multiple narrow structures.

4. **The Orion spectrum:**
The Orion spectrum, named for its similarity to the stellar wind lines in luminous OB stars, appears after novae have declined by one to two magnitudes from maximum. Its absorption lines are usually single, diffuse and blue-shifted by at least as much as the diffuse enhanced system, from -2700 to -1000 km s^{-1}. These velocities become steadily larger until the Orion spectrum disappears (about 2 mag down from maximum for slow novae and 4 mag down for fast novae). The lines in the optical are at first generally from He I, C II, NII and OII, and then from NIII and NV in later stage. There are occasional dramatic changes in line strengths, both in absorption and emission components. Particular species can become very strong; for example, enhancement of the NIII multiplet near 4640 Å due to 'nitrogen flaring'.

5. **The Nebular Spetrum**
This is the final recognized distinctive stage; the spectrum is an entirely emission spectrum and it steadily evolves towards the appearance of the spectrum of a planetary nebula. The significant lines are from [O I], [N II], [O III] and [Ne III]. Eventually, the coronal lines develop if the ionizing radiation reaches temperatures over 10^6 K, with lines from successive ionization states up to [Fe XIV] and other high ions from abundant elements. Such lines are also seen in the ultraviolet. Few novae show extremely strong lines of neon, especially [Ne III] and [Ne V] lines, particularly prominently in the nebular phase, which has led to a class known as 'neon novae'. These come predominantly from the fast and very fast novae.

It should be emphasized that the spectrum can be complex indeed. Several of these stages may be present simultaneously and each stage may have multiple components.

1.9 General properties of novae obtained from lightcurves and spectra

It is true that no two novae show exactly the same kind of lightcurves or spectra during eruption. However, from the systematic studies of lightcurves and spectra of a large number novae it has been possible to obtain several properties common to all novae. Here we discuss few of such general properties with necessary mathematical relations. Some of these properties are of immense value in other areas also.

1.9.1 Distribution and frequency of novae in the Galaxy

The apparent Galactic distribution of novae shows a strong concentration towards the plane and bulge. Therefore, some of their global properties have only been revealed recently from studies of novae in nearby galaxies. Novae are generally associated with an older stellar population in galaxies. Studies by Della Valle et al. (1992) show that more massive ONe novae are concentrated more tightly to the Galactic plane than are the lower mass carbon-oxygen (CO) novae.

There are many factors (seasonal, weather, biasing of sky coverage towards the Galactic bulge, missed fast novae) that lead to incompleteness in nova searches. Considering all of them, selection effects and interstellar extinction produces esti-

mates for a total Galactic nova rate of 73 ± 24 yr^{-1} (Liller & Mayer, 1987), 29 ± 17 yr^{-1} (Ciardullo et al., 1990), 30 ± 10 yr^{-1} (Shafter, 2002) and 34^{+15}_{-12} yr^{-1} (Darnley et al., 2006).

1.9.2 Characteristic times

In order to quantify very different rates of decline of the light curve, two characteristic time scales have been defined as follows:

1. t_2: time to decline by 2 magnitudes from the visual maximum.
2. t_3: time to decline by 3 magnitudes from the visual maximum.

The observed values of these time scales vary widely from nova to nova (see Table 1.1 and 1.2). From the studies of several novae Warner (1995) finds that $t_3 = 2.75{t_2}^{0.88}$.

1.9.3 Speed class

The rate at which the visual lightcurve decays after maximum defines the most readily observable property of a nova, the *speed class*. Novae could be almost uniquely identified on the basis of their speed classes. Depending on the characteristic time t_n (n = 2 or 3), novae are termed "fast" or "slow" . For the first time, Gerasimovic (1936) started to divide novae into several groups. However, this first attempt did not appear to be well designed. Refinement was made by McLaughlin (1939). He introduced the speed classes: fast, average, slow etc. as derived from their lightcurve decay times t_2 and t_3 (see Table 1.2). This was again redefined by Payne-Gaposchkin (1957) on the basis of their t_2 times (see Table 1.2). Modern studies of nova light curves still depend largely on those descriptions.

Generally, a slow nova occurs on a CO white dwarf and a fast nova occurs on a ONe white dwarf. However, there are many other factors such as mass and composition of the white dwarf, mass transfer rate etc., that affect the outburst. The visual lightcurves of the fastest novae have the most rapid rise to maximum (~ 1-2 days) and have a smooth decay with only small deviations. In slow novae, the lightcurves can take weeks or months to reach maximum and typically take on a more erratic decline with strong fluctuations or a "dip" that is associated with dust formation.

Table 1.2: Speed class of novae

Author	Speed class	t_2 (in days)	t_3 (in days)
McLaughlin (1945)	Very fast	7	15
	Fast	8-24	15-45
	Average	25-49	50-84
	Slow	50-250	85-449
	RT Ser	≥300	≥500
Payne-Gaposchkin (1957)	Very fast	<10	<20
	Fast	11-25	21-49
	Moderately fast	26-80	50-140
	Slow	81-150	141-264
	Very slow	151-250	265-440

1.9.4 Maximum magnitude vs. rate of decline (MMRD) relation

Novae are potential candidates as extragalactic distance indicators since they radiate almost at constant bolometric luminosity during their outburst (-7 ≤ M_V ≤ -9) and also because they occur frequently. Hubble was the first to notice that the brightest novae exhibited the fastest decline while observing novae in M31 (Hubble 1929). The real breakthrough came when McLaughlin (1945) calibrated a relationship between a nova's luminosity and its rate of decline, which he referred to as the 'life-luminosity relation'. This relation, which became widely known in subsequent years as the 'maximum magnitude versus rate of decline' or MMRD relation is usually cast in a form with the absolute magnitude given as a linear function of log t_n, where, as usual, t_n is the time in days a nova takes to decline n magnitudes from maximum light (usually n = 2 or 3).

The importance of the maximum magnitude-rate of decline (MMRD) relationship as an extragalactic distance indicator is immense and has resulted in continued discussion and updating. The observational MMRD results given by DellaValle and Livio (1995) are considered to be the most comprehensive to date. Generally, the linear MMRD relationship is usually expressed in the form:

$$M = b_n log(t_n) + a_n \tag{1.6}$$

where, M is the absolute magnitude and t_n is the characteristic time in days. Typical values of the parameters a_n and b_n are given in Table 1.3. The MMRD relation by

Table 1.3: Typical values of MMRD constants (Warner 2008).

M	n	a_n	b_n	References
pg	3	-11.3	2.4	de Vaucouleurs (1978)
B	3	-10.67 (± 0.30)	1.80 (± 0.20)	Pfau (1976)
V	2	-10.70 (± 0.30)	2.41 (± 0.23)	Cohen (1985)
V	2	-11.32 (± 0.44)	2.55 (± 0.32)	Downes & Duerbeck (2000)
V	3	-11.99 (± 0.56)	2.54 (± 0.35)	Downes & Duerbeck (2000)

Della Valle & Livio (1995) is given by:

$$M_V = -7.92 - 0.81 arctan \frac{1.32 - log t_2}{0.23} \tag{1.7}$$

where M_V is the absolute magnitude of the nova.

1.9.5 Modern spectral classification

The modern spectral classification of novae is based on the scheme for the emission lines, caused by the photoionization of the ejected material from novae, proposed by Williams (1992). Based on the appearance of permitted lines in the spectra near maximum novae are classified in two categories:

I. FeII type: The "Fe II" class of novae, constituting about 60% of the total, exhibit low ionization lines with "Fe II" lines as the strongest non-Balmer lines. 'FeII' spectra are formed in the optically thick wind from the white dwarf. Their spectra develop slowly, over a time-scale of few weeks and generally show the P Cygni type absorption features. In the early phase, low-ionization lines such as the lines of NaI, MgI, CaII etc. are seen in the spectrum. The expansion velocity lies in the range of $1000 \leq V_{ej}$ (km s^{-1}) ≤ 3500. They in general, evolve into either 'standard' novae (45% of all novae) or 'neon' novae.

II. He/N type: The "He/N" novae spectra are dominated by strongest non-Balmer lines of HeI, HeII or NII, NIII. The He/N lines originate in the discrete shell of gas ejected during the time of eruption. The emission lines are of higher excitation than in the "Fe II" class. In case of the He/N novae V_{ej} generally is more than 2500 km s^{-1}. In contrast to the "Fe II" novae, the emission lines in "He/N" novae are broader and evolve fast. The "He/N" novae show a

tendency to concentrate towards the Galactic plane.

All novae with $V_{ej} \gtrsim 2500$ km s^{-1} tend to evolve into either neon novae (30% of all novae), or into the 'coronal' class (15% of the total). The remaining 10% fall into a class that has no forbidden lines.

Apart from the above classification, on the basis of infrared observations novae may again be divided into two groups, depending on the type white dwarf:

I. CO novae: They are the explosions that occur on the low-mass carbon-oxygen (CO) white dwarfs. They show slow post-outburst evolution with low expansion velocity. They are known to form copious amount of dust, either optically thick or thin. The abundances are enhanced in CNO but not generally heavier elements and the He/H ratio is near the solar abundance.

II. OMgNe novae: The white dwarf is a oxygen-magnesium-neon (ONeMg) massive ($M_{WD} \geq 1.2\ M_{\odot}$) white dwarf. They evolve fast with a high expansion velocity. ONe novae generally do not form dust. They are principally distinguished by their infrared spectra marked by the early emission of [Ne II] 12.8 μm in greater strength, which has led to their popular characterization as 'neon novae'. The abundances for these novae vary but usually show some evidence of carbon depletion relative to solar, with associated enhancements of oxygen and neon.

1.10 Determination of physical parameters

Photometric and spectroscopic observations of novae in outburst are useful for characterizing the nova event. Particularly, from analysis of the optical/infrared SEDs formulae for evaluating specific physical parameters may be derived. Summaries of such results on bright novae have been discussed by several authors (Gehrz 2008 and references therein). In this section methods of deriving few important parameters are discussed.

1.10.1 Angular radius and distance to nova

Initially after the outburst, in the 'fireball' phase, nova ejecta behaves like hot blackbodies (6000 - 10000 K). If T_{BB} be the temperature of the blackbody, the bolometric apparent flux is expressed by the relation:

$$F = \sigma {T_{BB}}^4 = 1.3586(\lambda f_\lambda)_{max} \tag{1.8}$$

where $(\lambda f_\lambda)_{max}$ is peak apparent flux density of the spectral energy distribution in W cm^{-2} and $\sigma = 5.6696 \times 10^{-5}$ erg s^{-1} cm^{-2} K^{-4} is the Stefan-Boltzmann constant. Using the above relation, the angular diameter θ_{BB} (in milliarcsecond) can be calculated from the equation:

$$\theta_{\rm BB} = 2.0 \times 10^{14} {(\lambda F_\lambda)_{\rm max}}^{1/2} {T_{\rm bb}}^{-2} \tag{1.9}$$

This angular size of the thick "fireball" that is expanding at constant velocity, increases linearly with time. A plot of $\theta_{\rm BB}$ versus time t can be extrapolated back to $\theta_{\rm BB} = 0$ to find the exact time when the ejection started. The same technique can be used to determine the angular size and expansion rate ($d\theta/dt$) of a optically thick dust shell around a nova.

The angular expansion rate combined with the Doppler expansion velocities can be used to determine the distance D (in kiloparsec) to the nova through the following equation:

$$\left.\begin{aligned} D &= 1.15 \times 10^{-3} \frac{V_{ej}}{d\theta/dt} \\ &= 1.15 \times 10^{-3} \frac{V_{ej} t}{\theta(t)} \\ &= 5.69 \times 10^{-18} \frac{T_{BB}^2 V_{ej} t}{{(\lambda f_\lambda)_{max}}^{1/2}} \end{aligned}\right\} \tag{1.10}$$

The expansion velocity V_{ej} (in km s^{-1}) can be determined from optical/infrared spectral lines, the expansion rate $d\theta_{\rm BB}/dt$ (in milliarcsec day^{-1}) can be obtained from the blackbody fits of blackbody energy distribution.

1.10.2 Velocity and geometry of the ejecta

The expansion velocity is measured from the width of the spectral lines using the Doppler shift relation:

$$\frac{V_{ej}}{c} = \frac{HWHM}{\lambda} \tag{1.11}$$

where, c is the velocity of light = $3{\times}10^{10}$ cm s^{-1}, HWHM is the half width at half maxima of the spectral line at wavelength λ. However, the velocity is not uniform everywhere in the ejecta and generally the ejecta is non-spherical.

The geometry of the ejecta may be interpreted by studying the multiple absorption and emission features, width and shapes of the spectral lines. Few examples related to the present work may be presented here to explain this. The trace of the absorption feature, which is due to P Cygni profile, on the wings of the Brγ in V1280 Sco (see chapter 4) confirmed that mass ejection is a sustained process. The presence of wings on the spectral lines of RS Oph were due to the non-spherical shape of the ejecta. In few cases the interaction of novae ejecta with the pre-existing stellar wind from the secondary produces shock wave. Such an infrared shock, which is extremely rare, was detected in the recurrent nova RS Oph (2006) (see chapter 3).

Mass of the ejected gas

Infrared observations of novae provide several independent methods to calculate the mass of the ejected gas M_{gas}. It is a crucial parameter for constraining the TNR models and to calculate the abundance in the ejecta. A common method to find M_{gas} is to observe the expanding photosphere of nova to establish the time t_T when the SED starts to deviate from blackbody energy distribution and becomes optically thin at infrared wavelengths. At this stage the the gas temperature T is still high enough that Thomson scattering dominates, and the envelope mass is given by (Gehrz 2008):

$$\frac{M_{env}}{M_{\odot}} = \frac{\pi {R_{env}}^2}{\kappa_T} = 3.3 \times 10^{-13} (V_{ej} t_T)^2 \tag{1.12}$$

where, κ_T is the Thomson's scattering opacity, and R_{env} is the radius of the envelope = $V_{ej} t_T$ is the expansion velocity in km s^{-1}.

Ejecta abundances

At the different stages of outburst, different techniques are used to determine the abundances in novae ejecta. Different techniques of the abundance analysis were discussed earlier by several authors viz. Boyarchuk & Antipova (1990), Snijders (1990), Andreä (1992). However, in most cases compositions and the physical conditions of the nova ejecta are derived from the spectral lines, for example by modeling the ultraviolet, optical, and infrared spectra observed in the early phases

of the nova outburst and/or by modeling optically thin nebular spectra in the coronal stage. Several computer codes, such as PHOENIX and CLOUDY, are used to model the spectra. Abundances may also be derived from spatially resolved nova shells. Whichever technique is used, all the derivations show that novae ejecta are highly abundant in metals, about 10 -100 times the cosmic abundances (Jose & Hernanz 1998). In the present work, an attempt has been made to model the early spectra of V1280 Sco from which an estimation of abundances in the ejecta has been made (see Chapter 4).

1.11 Astronomical significance of novae

Over the past few years, new observations have shed more light on the understanding of novae. It has now been realized that they have much to offer. They claim importance for their relevance to other exciting areas of astrophysics. For example:

1. Accretion disks are very commonly occurring structures not only in stars but also in galaxies. In CVs, all kinds of accretion disks are formed and hence offer the richest opportunities to study them. Observational studies of the accretion process and accretion disks could be carried out more effectively in novae those are closer to us.

2. Being in binaries they are capable of providing important constraints upon the theory of stellar evolution in binary systems.

3. Novae ejecta enrich the metal abundances of the galactic 'ecosystem' as they possess very high metal abundance. Observations confirm that the metal abundance in novae ejecta could be as much as 100 times of the metal abundance in the Sun.

4. A nova is one of the places where dust and molecules (e.g., CO, H_2, PAH) form and eventually merge with the inter stellar medium. Though they produce only about 0.1 percent of the dust in the galaxy, CVs are the only objects in which it has been possible to observe directly all aspects of the temporal development of circumstellar grain formation events on a frequent basis.

5. Several radioactive nuclei like ^{26}Al, ^{22}Na, ^{7}Li are expected to be synthesized during novae explosions which contribute significantly to the galactic budget of these elements. The actual sources (supernovae, novae, WR stars, AGB

stars etc.) which contribute to the production of the nuclei ^{26}Al is still an unresolved problem.

6. The overabundance in C, N, O, Ne, Mg, Al, and Si in some novae are high enough to suggest that novae are potential contributors to some chemical anomalies on local and Galactic scales. Novae explosions may efficiently produce some of the chemical anomalies that characterized the primitive Solar System.

7. Recurrent novae are believed to be the progenitors of Type Ia supernovae. A Type Ia supernova explosion takes place when the white dwarf mass exceeds the Chandrasekhar limit. So recurrent novae provide the opportunity to study the physics of Type Ia supernovae.

8. Novae are some of the most luminous sources (absolute magnitude $\sim$ -7 to -9) in the sky. This provides the mean for measuring intergalactic distances.

Thus observational studies of novae provide test beds for theories which then may be applied to understand other relevant astrophysical events.

1.12 Observations of novae in different regimes: Radio, IR, UV, X-rays, γ-rays

Novae both in outburst and quiescence emit their the energy over the entire electromagnetic spectrum in such a diverse way, that they are required to be observed at all wavelengths, from Gamma rays to radio, using all the modern techniques in order to understand the nova phenomena completely. Earlier observations were concentrated on the optical only because of two reasons: lack of proper instrumentations and non-uniformity of atmospheric transformations. That is why, a bulk amount of observations of novae in the optical have been recorded in last two centuries. On the basis of those observations, several classifications and definitions were made which are still in use.

After it has been realized that, novae radiate significantly at other wavelengths viz. X-rays, UV, IR and radio, regular attempts have been made to observe them in those bands too using sophisticated equipment. However, such observations really blossomed with the use of digital detectors on satellites in space. These satellite

data along with the data from ground-based observatories aided us in understanding novae better. Here, we briefly discuss the several aspects of these observations.

Radio observations

The radio emission from novae is caused by thermal bremsstrahlung. The benefit of radio observations over the observations in the other wavelength regions is that radio emission does not suffer external and/or internal extinction by dust. Radio observations are especially useful for resolved images which permit an estimate of the optically thick radio surface brightness and hence the electron temperature. We can make estimation of the distances to novae by comparing the angular expansion rates derived from the radio with the absorption line velocities. Another important aspect of radio observations is that it provides a mean to probe the large scale structure of the binaries on the scale of $\gtrsim 10^{11}$ cm that is comparable to the orbital separations of CVs.

The first classical novae to be detected at radio wavelengths were HR Del and FH Ser by Hjellming and Wade (1970). They were observed using the three-element interferometer of the National Radio Astronomy Observatory (NRAO) at 2.7 and 8.1 GHz. The early studies of novae at radio wavelength are summarized by Hjellming (1974). Till date, most of the radio observations have been made with the three-element interferometer at Green Bank, West Virginia, the Westerbork Synthesis Radio Telescope (WSRT), the Very Large Array (VLA) in New Mexico, or the MERLIN network of telescopes (Seaquist & Bode 2008). With the availability of the modern telescopes having high resolving power it has been possible to resolve the expanding shell in many novae and recurrent novae and to detect a few dwarf novae and magnetic CVs. So far, more than 20 novae have been observed in radio.

IR observations

Novae radiate a significant amount of energy in infrared (IR) during the several stages of evolution. The prime sources of infrared emission are:

- optically thick ejecta in the fireball phase.
- thermal bremstrahlung in the free expansion phase.
- dust formed in the ejecta. The 'isothermal dust phase' has been observed in a number of novae and analysis of this phase has provided valuable information, especially on the properties of the emitting dust.
- emission from X-ray heated grains.

- fine-structure line emission from a cold phase of the nova nebula and
- cooling of grains heated by the shocked gas at the interface between the nova ejecta and the interstellar medium.

Infrared photometric and spectroscopic observations of novae in outburst are particularly useful to quantify several parameters describing the outburst, to investigate the phenomena of dust formation and to determine metal abundances in their ejecta. Derivations of formulae for evaluating specific physical parameters from analysis of infrared data, and summaries of results on recent bright novae have been discussed in detail by a number of authors (Gehrz 1988, 1998, 2002; Gehrz, Truran & Williams, 1993 and references therein).

Most of our observational knowledge of the infrared properties of novae is based on pioneering and sustained observational studies by a few groups around the world. To name a few they are Robert Gehrz (with predecessors and coworkers) at the University of Minnesota, U.S.; Aneurin Evans and coworkers at Keele University, U.K.; and David Lynch, Richard Rudy and coworkers at the Aerospace Cooperation, U.S.

UV observations

The UV radiation from novae is generated combinedly by nebular emission and emission from the pseudo-photosphere. UV data are particularly useful to determine, with unprecedented accuracy, the chemical abundances in the ejecta (see e.g., Stickland et al. 1981; Williams et al. 1985; Snijders et al. 1987). Precise abundance determinations is necessary to provide crucial constraints on nucleosynthesis during TNR as well as on the efficiency of diffusion and mixing processes. Since, the white dwarf radiates much in UV, observations in UV are important tools to gain insight on the nature of the white dwarf components. In addition, the UV observations provide effective means to determine the value of the reddening from the strength of the 2200 Å dust feature or from the emission line ratios; an accurate determination of this parameter from the UV is essential, for example, to determine the energy budget of novae and the temperature of the remnants.

Several CVs had been observed in UV by the satellites such as Orbiting Astronomical Observatory 2 in 1968, Orbiting Astronomical Observatory 3 (Copernicus) and the European Space Research Organization's TDI in 1972, the International Ultraviolet Explorer (IUE) in 1978. Out of these, IUE provided the largest body of observations in its long and productive life. One of the major achievements of UV

observations is the determination of the bolometric light of Nova Serpentis (1970). From the observations on 53 days, it was concluded that as the nova faded visually, the flux distribution shifted towards the UV, thereby maintaining almost constant luminosity (Gallagher and Code 1974). Later, such bolometric light curves were achieved also for V1668 Cyg 1978 (Stickland et al. 1981), V1370 Aql 1982 (Snijders et al. 1984) and RS Oph (Snijders 1987). Another major result of UV observations is the discovery of a new class of novae, the ONe novae (Starrfield, Sparks and Truran 1986), in which very large overabundance of intermediate mass nuclei like Ne, Mg, O and Al have been found (see Snijders et al. 1984, 1987 for V1370 Aql 1982 and Williams et al. 1985 for V693 CrA 1981).

X-ray observations

In principle, there are four different mechanisms which might lead to X-ray emission from novae in outburst (Krautter 2008 and references therein):

- thermal emission from the hot white dwarf during the initial and later phases of the outburst.
- interaction of the expanding nova shell and/or a nova wind with the surrounding medium of the nova system or the pre-existing material.
- re-establishment of accretion process via an accretion disk or magnetic accretion.
- Compton downgradation (scattering leading to a reduction in energy) of γ -rays produced by the radioactive decay of ^{22}Na though no evidence for X-rays originating by this mechanism has yet been found.

X-ray observations offer a wide variety of opportunities of studying the outbursts of classical novae. They allow us to study the hot white dwarfs and shocks in the expanding envelope, and to derive physical parameters such as the effective temperature and luminosity, the duration of the hydrogen burning phase on top of the white dwarf and chemical abundances. In addition, X-ray observations of the scattered light from bright super-soft sources provide an opportunity to study the interstellar medium.

X-ray astronomy has been revolutionized by the launch of satellites, particularly UHURU in 1970 and the High Energy Astrophysical Observatory B ('Einstein') in 1978 and ROSAT in 1990, Chandra and XMM-Newton in 1999 and SWIFT in 2004.

Reviews on X-ray observations of novae in outburst have been given by Ögelman (1990); Ögelman and Orio (1995); Orio (1999); Krautter (2002); and Orio (2004). GQ Mus was the first classical nova from which X-ray emission was detected during the outburst (Ögelman, Beuermann & Krautter, 1984). So far the most completely covered X-ray light curve of a classical nova is that of V1974 Cygni, where X-ray observations have been obtained on 18 occasions over a period of ≤2 yr, i.e. with reasonably spaced observing epochs from early rise to decline (Krautter et al. 1996). In the recent years SWIFT has obtained pointed observations of more than ten classical novae in outburst (Ness et al. 2007).

γ-ray observations

The launch of the satellite INTEGRAL (INTErnational Gamma-Ray Astrophysics Laboratory) by the European Space Agency in 2002 has opened new perspectives for the detection of γ-rays, the most energetic (> 10 kev) photons in the whole electromagnetic spectrum, from nuclear radioactivity in explosive events like novae and supernovae. The prime source of γ-rays in novae is electron-positron annihilation; positrons come from the decay of ^{13}N, ^{14}O, ^{15}O, ^{22}Na, ^{14}O and ^{22}Na (Clayton and Hoyle, 1974) and transformation of ^{7}Be (through an electron capture) to an excited state of ^{7}Li (Clayton 1981).

Thus, γ-rays are capable to give a direct insight into the nucleosynthesis during the nova explosions and also into the global properties, like the density, temperature, chemical composition and velocity profiles of the expanding envelope. Gamma-ray observations can directly trace isotopes and thus should trace the Galactic distribution of classical novae. However, more sophisticated calculations show that possibility of the production of γ-rays from the above reaction is very less. That is why γ-rays are yet to be detected, till date, from any nova. If detected, γ-rays would give invaluable information that are very difficult to obtain from observations at other wavelengths.

1.13 Significance of IR observations of novae

Infrared observations are of great importance, especially because they carry information from low temperature zones. They are thus a very powerful tool to study novae phenomena corresponding to low temperature. Novae are known to produce prolific amount of dust and every known type of astrophysical grain. IR observations become the sole instrument to study all physical and chemical

properties related to the dust and associated dust grains. IR photometry at longer wavelengths can be used to distinguish the temporal development of extreme CO and ONe novae, presenting the possibility that IR photometry can be used for determining their occurrence rates and global influence in nearby galaxies.

In addition, the near-IR spectrum is rich with many emission lines that strongly supplement data from the optical. As an example, while the Balmer series lines of Hydrogen are seen in the optical, in the near-IR a greater number of additional H lines of the Paschen, Brackett and Pfund series are present. Though relatively fewer near-infrared observations are available, these observations when combined with optical measurements can provide quantitative measurements of the primary physical parameters that characterize the outburst and the nature of the ejecta.

IR observations of quiescent nova emphasize the cooler components of their structure. The two dominant contributors are the atmosphere of the secondary and the cool outer regions of the accretion disk. Thus, IR observations may be used to bring out the nature of these components. Apart from that the infrared observations are the best tracers of the true fireball stage since the principal opacity source at these long wavelengths is due to thermal bremsstrahlung which depends only on the change in the column density.

1.14 Motivation and scope of the present work

While surveying the literature, it was noted that optical studies of novae were quite extensive. In comparison, studies in the IR were relatively less. Meaningful astrophysical observations in the near-IR were started late, only after the development of red-sensitive CCDs in 1970s and 1980s. Since then, we have made serious progress in understanding novae outburst due to those observations using digital detectors and satellites in space. In spite of that, there are still many unsolved problems and intriguing puzzles that make our understanding of the nova theory incomplete. Because our process of understanding is largely dependent on observational data, more observations are required in order to learn as much as possible about the characteristics of the outburst.

The prime objectives of the present investigation were to study and understand the infrared characteristics of novae in details. We were interested in several aspects

viz. understanding the process of dust formation in these objects; studying the evolution of novae spectra in the IR in details; identifying and understanding the different lines that are seen in the near-IR spectra (their strengths, temporal variations, excitation mechanisms etc.) through modeling if possible. We also hoped to observe a statistically large number of novae to enable a infrared classification scheme based on their near-IR spectra (along similar lines as that proposed by Williams; 1992 based on optical spectra). Though progress has been made in this last topic and a significant observational database accumulated, the analysis/results are deferred to the future and does not constitute a part of this thesis. During the course of my observations, the recurrent nova RS Oph underwent its sixth recorded outburst in 2006. Being a rare event, it was observed extensively to get a better understanding of the recurrent nova phenomenon.

To achieve the above objectives photometric and spectroscopic observations were done by me of several novae using our Institutes 1.2m telescope at Mount Abu. The advantage of having a captive, home telescope is that accessibility to telescope time becomes easier and flexibility in scheduling is possible for targets of opportunity such as novae. This advantage made us realize that bright novae can be extensively observed over a large number of epochs thereby giving a good coverage of their temporal evolution. It was noted that such extensive observations documenting the infrared evolution of novae had rarely been done. This realization thus served as one of the motivational drivers of the present work. Observations from Mt. Abu were made of more than ten novae (a list of the observed novae is presented in Chapter 2), out of which a few were observed relatively more extensively than the others. Due to the considerable time involved in making the observations and completing the subsequent analysis, it was possible to accommodate in the present thesis detailed results of three of the observed objects viz. RS Ophiuchi, V1280 Scorpii and V2615 Ophiuchi - a brief description of them are given below:

- **RS Ophiuchi (RS Oph):** RS Oph is a well known recurrent nova, recurrence time being ~ 22 years. RS Oph underwent its sixth recorded outburst recently on 2006 February 12, the previous being in 1985. Our observations cover a period of 94 days - from 2006 February 13.9 UT to May 17.8 UT.

- **V1280 Scorpii (V1280 Sco):** Nova V1280 Sco was discovered on 2007 February 4.8 UT. The nova brightened quickly to its maximum in visual light on Feb. 16.19 (m_{vmax}= 3.79) to become one of the brightest novae in recent times. V1280

Sco belongs to the class of 'classical nova'. This nova formed thick dust in the later stages. Following the outburst the near IR observations commenced on 2007 February 18.9 and continued till 2007 June 08.8.

- **V2615 Ophiuchi (V2615 Oph):** V2615 Oph is also a classical nova. It was discovered on 2007 March 19.812 UT. The highlight of the observations was the rare detection of the first-overtone CO emission (2.29 - 2.4 μm) in the nova - similar emission has been recorded previously only in a few novae. It also formed dust in the later stages. The near-IR observations of V2615 Oph, presented in the thesis, were started on 2007 March 28.8 UT while the nova was around maximum brightness. The nova was followed till 2007 June 09.7 UT - after the nova had formed dust.

In collating material for this chapter several sources of information were referred to. In particular, I acknowledge substantial help from material drawn from various articles in the books, *Classical Novae* edited and compiled by Bode and Evans (2008), *Cataclysmic Variables* by Warner (1995), *Physics of Classical Novae* edited and compiled by Cassatella & Viotti (1990) and *The Historical Supernovae* by Clark & Stephenson (1977).

CHAPTER 2

Observations and Data Analysis

The near-Infrared spectroscopic and photometric observations of novae, presented in this thesis, were made using the 1.2 m telescope at the Mount Abu Infrared Observatory (Latitude: 24° 39′ 10″ N, Longitude: 72° 46′ 47″ E, altitude 1680 m), Mount Abu, Rajasthan, India. The observatory is operated by the Physical Research Laboratory (PRL), Ahmedabad, India.

The low amount of precipitable water vapor and about 200 cloud free nights per year make it a good site for scientific observations. Observations run throughout the year except during the monsoon season (June to September). Every year, the new observation session starts in early October after the withdrawal of the South-West monsoons. The best observation time is in winter, from December to February when the precipitable water vapor content is very low (1-2 mm) and seeing condition is extremely good (~ 1 arcsec; Ashok & Banerjee 2002). In the later part, from the month of April, the seeing condition gets affected by the dust storms from the desert of Thar situated to the north of the observatory. Pre-monsoon showers hit the region in late May and the observatory is generally closed from June.

In this chapter, we discuss about the Mt. Abu telescope and the detectors attached to the telescope. This is followed by a detailed description of the observational procedures and the data analysis process in later sections.

2.1 Mount Abu telescope

The Mount Abu telescope provides the first major facility in India, specially designed for ground based observations in the near-Infrared region (J, H, and K bands). The telescope structure uses an equatorial mount. The optical system of the telescope consists of a 1.2 m paraboloid primary mirror (focal ratio of f/3) and three hyperboloid secondary mirrors that can direct the light to three foci (two Cassegrain and one Coude).

The system can be used both in conventional Cassegrain and Coude configurations, however, at present only the Cassegrain configuration is in use. The Cassegrain configuration uses a non-vibrating secondary mirror with an effective focal ratio of f/13. Greater details of the optical parameters of the telescope system are given in Banerjee et al. (1997). The f/13 beam, emerging through the Cassegrain focus is directed to the NICMOS detector by a gold coated 45° mirror. A schematic diagram of the optical system is shown in Figure 2.3. The peak to valley surface accuracy of the telescope mirrors is one tenth lambda at 589 nm so that the telescope can be effectively used for imaging in visible as well as in infrared region. The mirrors were figured and polished by the Sinden Optical Company, U.K.

Presently, the following instruments are used with the telescope for different kind of observations:
I. NICMOS Camera cum Grating spectrometer (PRLNIC)
II. High Speed Two Channel IR Photometer
III. Optical Polarimeter
IV. Imaging Fabry-Perot Spectrometer
V. Fibre Fed Optical Spectrometer

Except for the PRLNIC, the other instruments were designed and fabricated at the Physical Research Laboratory. In the present work, the required spectroscopic and photometric observations of novae have been made using the PRLNIC. The basic design of the PRLNIC system is described in the next section.

2.2 PRLNIC

The NICMOS (Near-Infrared Camera and Multi-Object Spectrograph) system at the 1.2m Mt. Abu telescope (PRLNIC) utilizes the 256×256 NICMOS3 HgCdTe detec-

Figure 2.1: Front view of the Mount Abu Infrared Observatory, Rajasthan, India.

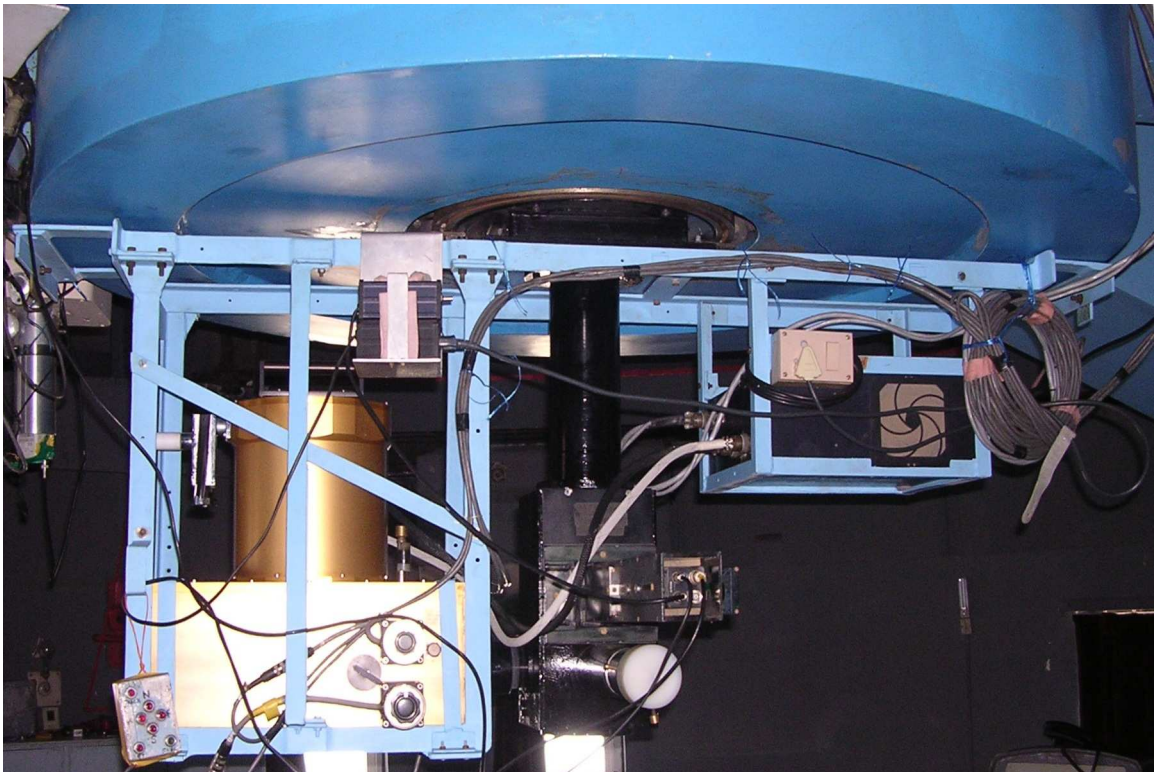

Figure 2.2: Photograph of the NICMOS system (golden colored box on the left side) attached to the telescope Cassegrain focus.

Table 2.1: Characteristics of the detector array

Detector	256x256 HgCdTe
Pixel size	40 μm
Readnoise	53 e^-
Darknoise	$\leq$0.7 e^-/s
ADC	32 bit
Bad Pixels	46
Total yield (Usable Pixels)	99.9 %
System Quantum Efficiencies	
J band	32.75 %
H band	18.30 %
K band	28.91 %

tor arrays cooled to liquid nitrogen temperature (77 K). It was fabricated for PRL by Infrared Labs Inc., USA. The characteristics of the detector are given in Table 2.1.

A schematic diagram of PRLNIC is shown in Figure 2.4. The f/13 beam enters the system through the 50 mm entrance aperture after being reflected by the 45° gold coated mirror. This beam can be compressed by a focal reducer lens that compresses the focal ratio to f/6.5 beam. The focal reducer also changes the camera field of view (FOV) from $2' \times 2'$ to $4' \times 4'$. Correspondingly, the plate scale changes from 0.5″/pixel to 1″/pixel for the two FOVs respectively. The focal reducer lens is a cooled plano convex doublet that has BaF_2 and Fused Silica components. The beam then passes through the filter wheels and is focussed on the cold Lyot stop (aperture). The system has two circular filter wheels; the first one contains broad band filters (*JHKK'*) and the second one contains narrow band filters. The descriptions of these filters are presented in Tables 2.2 and 2.3 respectively. The rotation of the filter wheels is controlled by stepper motors.

Three types of Lyot stops are available - the circular and the square apertures are used for imaging and the slit (width = 75 μm i.e. $\sim$ 2 pixels) is used for spectroscopy. The optical beam emerging out of the Lyot stop is collimated by a section of a parabolic mirror that sends the collimated parallel beam on to a mirror/grating assembly. This assembly can be rotated to switch between a plane mirror and grating for imaging or spectroscopic observations respectively. The spectrometer set-up follows the Ebert-Fastie configuration. The telescope beam passing through the entrance slit is reflected from the collimator to form a parallel beam that is

Table 2.2: Description of broad-band filters

Band	Central wavelength (μm)	Bandwidth (μm)	Lower cut-off (μm)	Upper cut-off (μm)	Transmission at peak wavelength (%)
J	1.253	0.296	1.105	1.401	93.23
H	1.659	0.288	1.514	1.803	91.96
K	2.185	0.408	1.981	2.389	85.39
K'	2.120	0.360	1.940	2.300	> 80

Table 2.3: Description of narrow-band filters

Band	Central wavelength (μm)	Bandwidth (μm)	Lower cut-off (μm)	Upper cut-off (μm)	Transmission at peak wavelength (%)
[Fe II]	1.645	0.0375	1.6262	1.6638	> 80
$H_2S(1)$	2.1175	0.0429	2.0961	2.1390	74.1
NB* 1	2.1352	0.0428	2.1138	2.1566	78.0
Br γ	2.164	0.0443	2.1427	2.1870	59.1
CO band	2.3726	0.1013	2.3220	2.4232	83.0
NB* 2	2.2169	0.0831	2.1754	2.2585	74.0

* NBs stand for *narrow band* filters; these are used for continuum measurement.

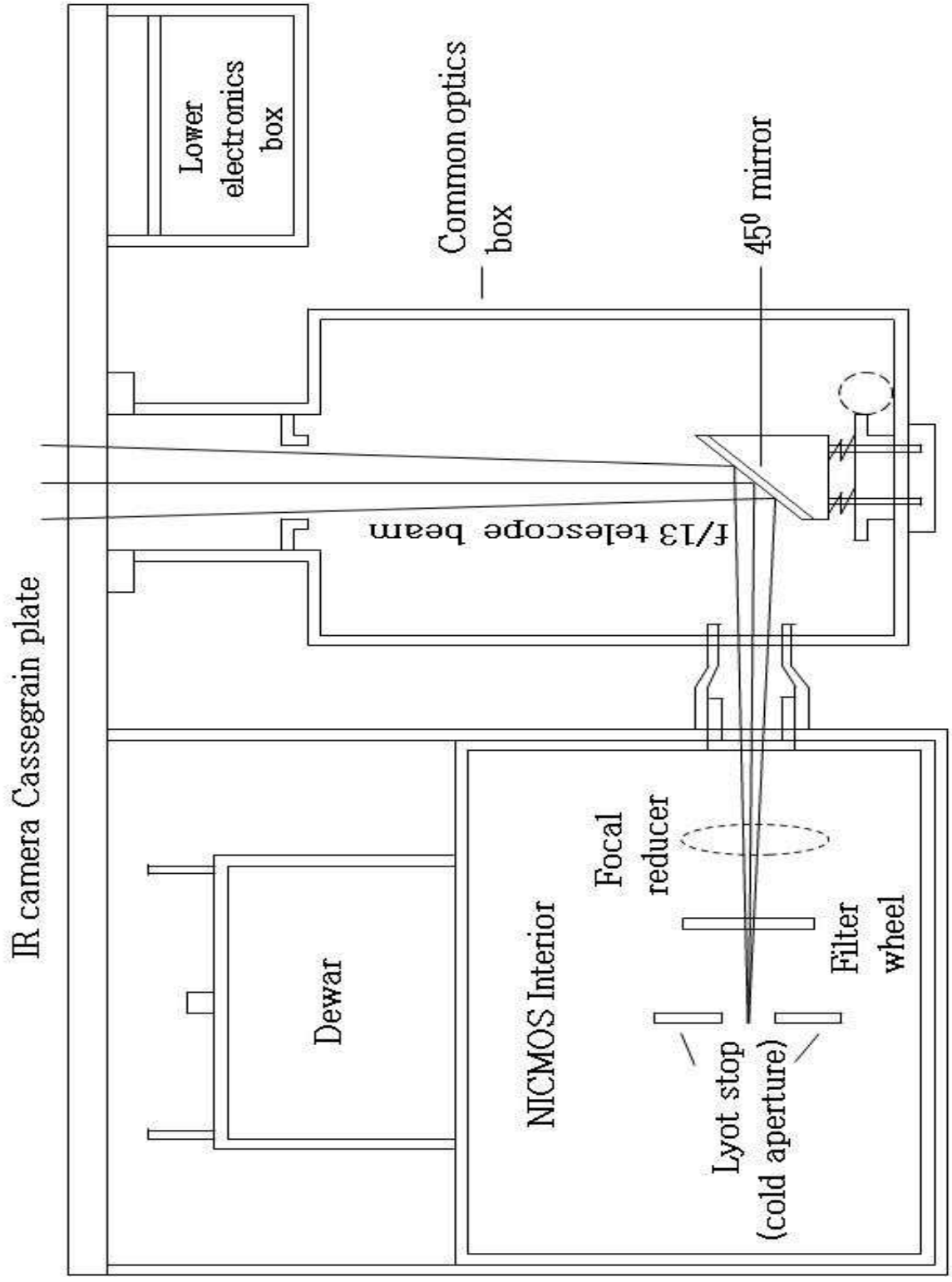

Figure 2.3: Schematic diagram of the optical system coupled with the 1.2 m telescope at Mt. Abu Observatory.

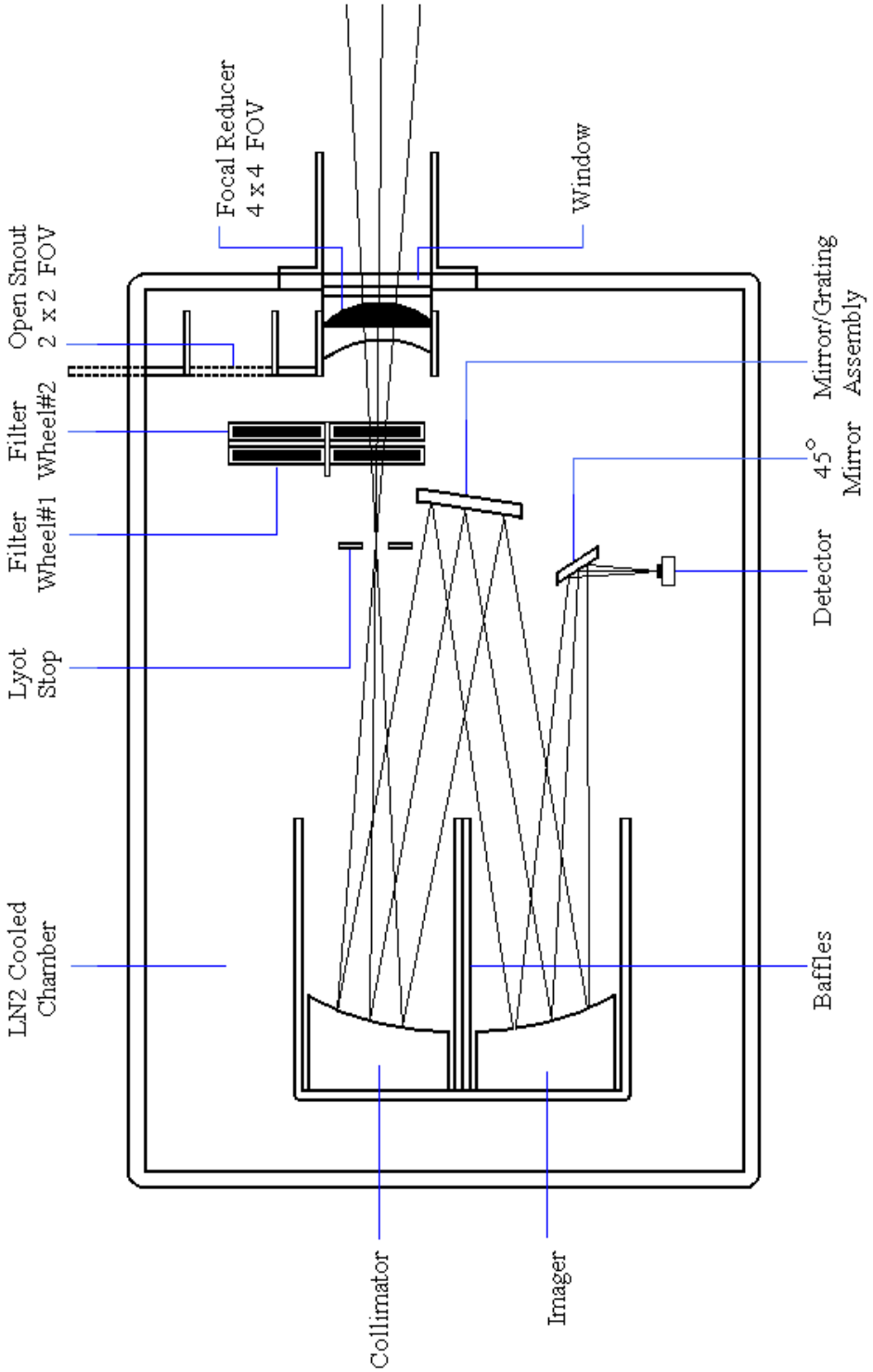

Figure 2.4: The schematic diagram of the NICMOS camera system at the 1.2 m telescope at Mt. Abu Observatory.

directed towards mirror/grating assembly. The parallel beam emerging from the mirror/grating assembly is directed to another section of the parabolic mirror. This section of the parabolic mirror converges the beam; the converged beam ultimately falls on the detector after being reflected by a small adjustable plane mirror.

2.3 General procedure of observations

In addition to the desired image (i.e. the true or intrinsic image), the raw observed image contains unwanted background emission from the telescope and the atmosphere, a number of instrumental effects such as bad pixels, different kinds of noise, effects of cosmic rays etc. Also, the infrared radiation from the source, on its way to the observer, suffers scattering and absorption by both the inter stellar medium and the Earth's atmosphere; the atmospheric transmission is not uniform and varies with wavelengths. All these effects must be removed from the acquired image to get the proper spectrum or image of the source. In order to achieve this, certain procedures are followed during observations that aid in the reduction and analysis of the data.

2.3.1 Procedure for spectroscopic observations

1. Each time, a set of at least two spectra of the nova were taken with the object dithered to two positions (offset by 20-30 arcseconds) along the slit; the exposure time was same for both the spectra. The purpose of taking two spectra at two different locations is to remove the background contribution (sky + dark counts) by subtracting the images from each other.

2. Following the same procedure mentioned above, two spectra of a standard star were obtained along with the nova spectra. The spectra of the standard star are used to correct for atmospheric absorptions and transmission effects. Since the intensity of the atmospheric transmission varies with airmass, we have always tried to choose a standard star near the nova so that the airmasses do not differ too much. Generally a standard star of spectral type A was chosen/preferred because the spectra of A type stars have a featureless continuum except for the presence of prominent absorption lines of HI which can be easily identified and removed.

3. The dispersion in each of the JHK bands exceeds the array size. Hence, the spectra were observed, in each band, in two parts - first the initial part of the wavelength region and then the later part. In both images the middle part of the spectra was kept common, so that the intensities of the spectral features in the middle part could be matched and the two parts could be spliced together to form the complete spectra.

2.3.2 Procedure for photometric observations

1. In each of the *JHK* bands, generally images of the nova were obtained at five dithered positions, offset typically by 20 arcsec. At each position, a large number of frames of short integration time were obtained. The integration time was decided depending on the brightness of the nova.

2. Following the same method, several frames of a standard star were acquired at five dithered locations. The standard star was chosen in such a way that the differences between the magnitudes of the target nova and the standard star were small (generally $\sim$ 2 - 3 magnitudes).

3. The detector array is a combination of four individual quadrants. Since, the response of these parts are not same, the dithered images of the nova during photometry, were preferably taken in the same (first) quadrant of the array. The reason for choosing the first quadrant is that, it contains less number of bad pixels relative to the others.

2.4 Data analysis

Spectroscopic observations of novae were made using the grating spectrometer based on HgCdTe 256 $\times$ 256 focal plane array (resolving power $\lambda/\delta\lambda$ = 1000; dispersion of $\sim$ 10 Angstroms per pixel) whereas photometric observations were performed under photometric sky conditions using the imaging mode of the NICMOS3 array. Observed data were analyzed using several tasks under IRAF. IRAF (Image Reduction and Analysis Facility) is an image processing and astronomical data analysis software developed at the National Optical Astronomy Observatories (NOAO), USA. The different steps of the data analysis process and the principal tasks used are presented in Table 2.4.

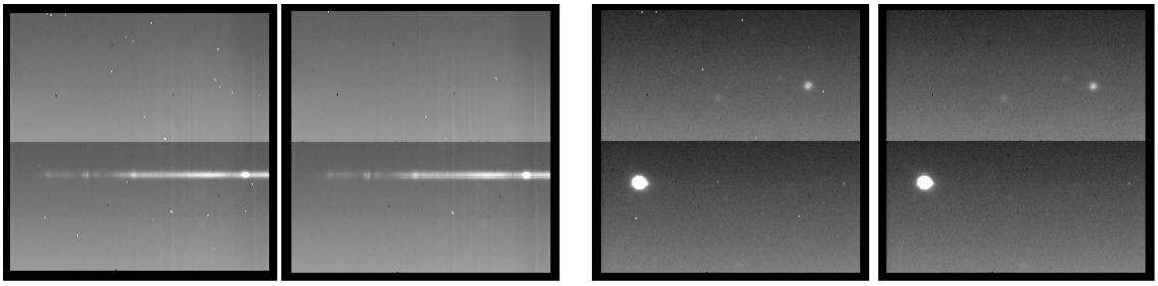

Figure 2.5: The figures show the effect of cosmic rays on the observed images. In both the figures (*a* - images of spectra and *b* - images of the star) the first image is the raw observed image. The randomly scattered white spots are due to cosmic ray hits. In the second image, the spurious signals caused by cosmic rays have been cleaned.

2.4.1 Extracting spectra

The spectra were extracted using the APEXTRACT task in IRAF. The spectral analysis process follows the steps described below and shown in Figure 2.6.

Removal of cosmic rays The first task, in the data reduction process, deals with the removal of the effects of cosmic rays. Cosmic ray events appear as high count signals randomly scattered over the observed frames (see Figure 2.5) caused by ionizing radiation. The cosmic ray hits are usually confined to one or two pixels. These are removed using the IRAF task *cosmicrays*.

Sky and dark subtraction In order to remove the sky background and dark counts, the frames of two spectra, observed in the same wavelength region but with the star shifted along the slit, were subtracted from each other (see figure 2.6).

Extraction of spectra After the subtraction, a image contains two spectra of the star viz. one spectrum with positive counts and the second one with negative counts. Generally, the width of a spectrum spreads over about ten pixels. The positive spectrum is converted to a 1D spectra using the task *apall*. The extracted spectrum is a plot of the number of counts against the pixel number.

Wavelength calibration Wavelength calibration (conversion of pixel number to wavelength) was done using a combination of OH sky lines and telluric lines that register with the stellar spectra. Generally, the sky lines in a particular frame is calibrated first, then this frame is used as a reference for calibrating the other spectra in the same wavelength region.

Table 2.4: List of major IRAF tasks used for data reduction.

Steps	IRAF tasks
Cosmicrays removal	*cosmicrays*
Subtraction of images	*imarith*
Defining the dispersion axis	*hedit*
Extracting spectra	*apall*
Wavelength calibration	*identify*
Defining the reference spectra	*refspectra*, *dispcor*
Making blackbody curve	*mk*1*dspec*
Arithmetic of spectra	*sarith*
Plotting spectra	*splot*, *specplot*
Combining images	*imcombine*
Aperture photometry	tasks under APPHOT

Removal of telluric effects To remove the telluric absorption features, the nova spectra were divided by the spectra of the standard star. Prior to this, the hydrogen Paschen and Brackett absorption lines are manually removed from the spectra of the standard star.

Blackbody correction The ratioed spectrum provides the relative strength of the nova. At a particular wavelength, the relative intensity is given by $F_{nova}/F_{standard}$, where F represents the flux of the respective object at that wavelength. To recover the nova spectrum, the ratioed spectra are multiplied with a blackbody curve corresponding to the effective temperature of the standard star; this yields the final spectra.

2.4.2 Photometric data reduction

Photometric data were reduced to derive *JHK* magnitudes of the nova using the IRAF aperture photometry task APPHOT. The process is described below (also see Figure 2.7).

Removal of cosmic rays: As in the case of spectroscopic data reduction process, the spurious signal caused by cosmic rays are removed using the task *cosmicrays*.

Generating an average frame: From each set of the images of star observed at a particular position, an average frame is generated. This process improves the signal to noise ratio in the average frames.

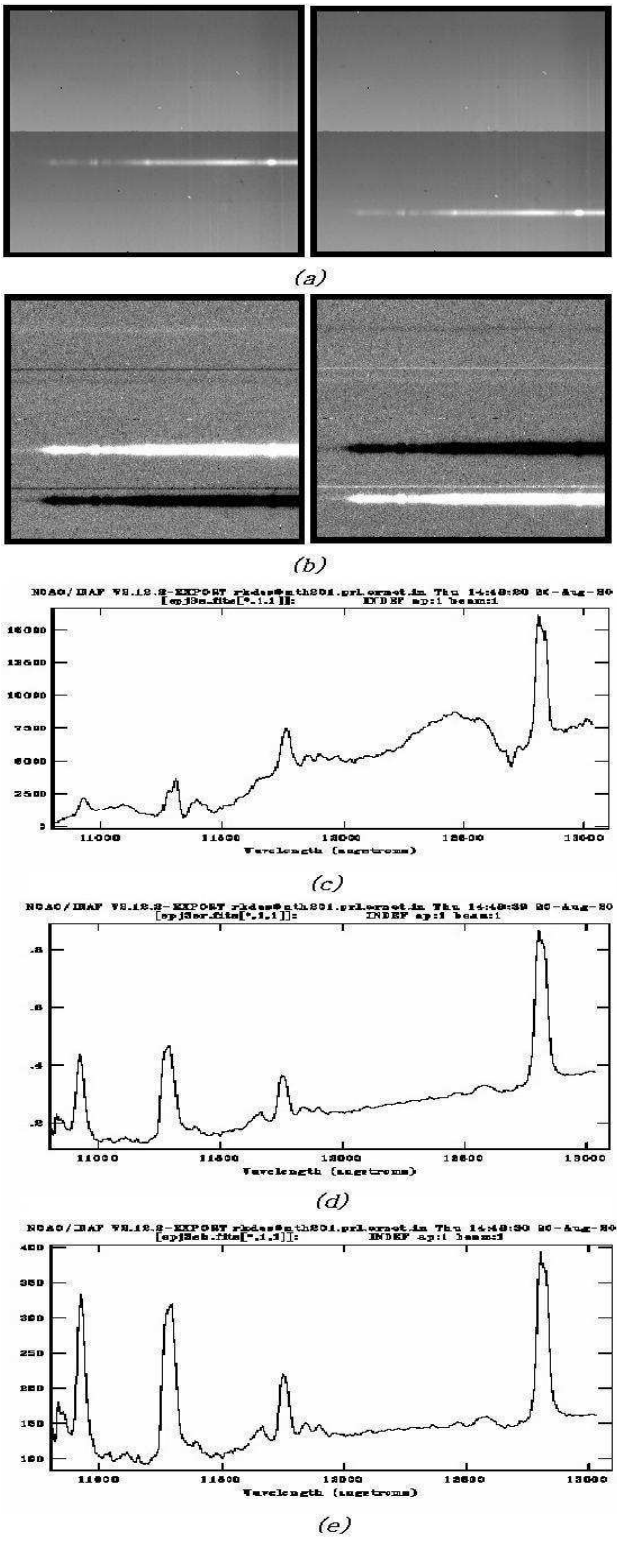

Figure 2.6: The images correspond to the several steps of the spectra analysis process (see subsection 2.4.1 for more details).
(a) A set of two images of the nova spectra (corrected for cosmic rays), observed in the same wavelength region with the star off-set to 2 positions along the slit.
(b) Subtracted images - each of the observed images has been subtracted from each other to remove the sky background and dark counts.
(c) An example of a spectrum extracted from one of the subtracted images. The observed intensity is a function of atmospheric and filter transmission properties.
(d) An example of the ratioed spectrum after dividing by the standard star spectrum. This process removes telluric and filter effects from the nova spectrum.
(e) The blackbody corrected spectrum. The intrinsic nova spectrum is recovered by multiplying the ratioed spectra by a black body curve corresponding to the temperature of the standard star.

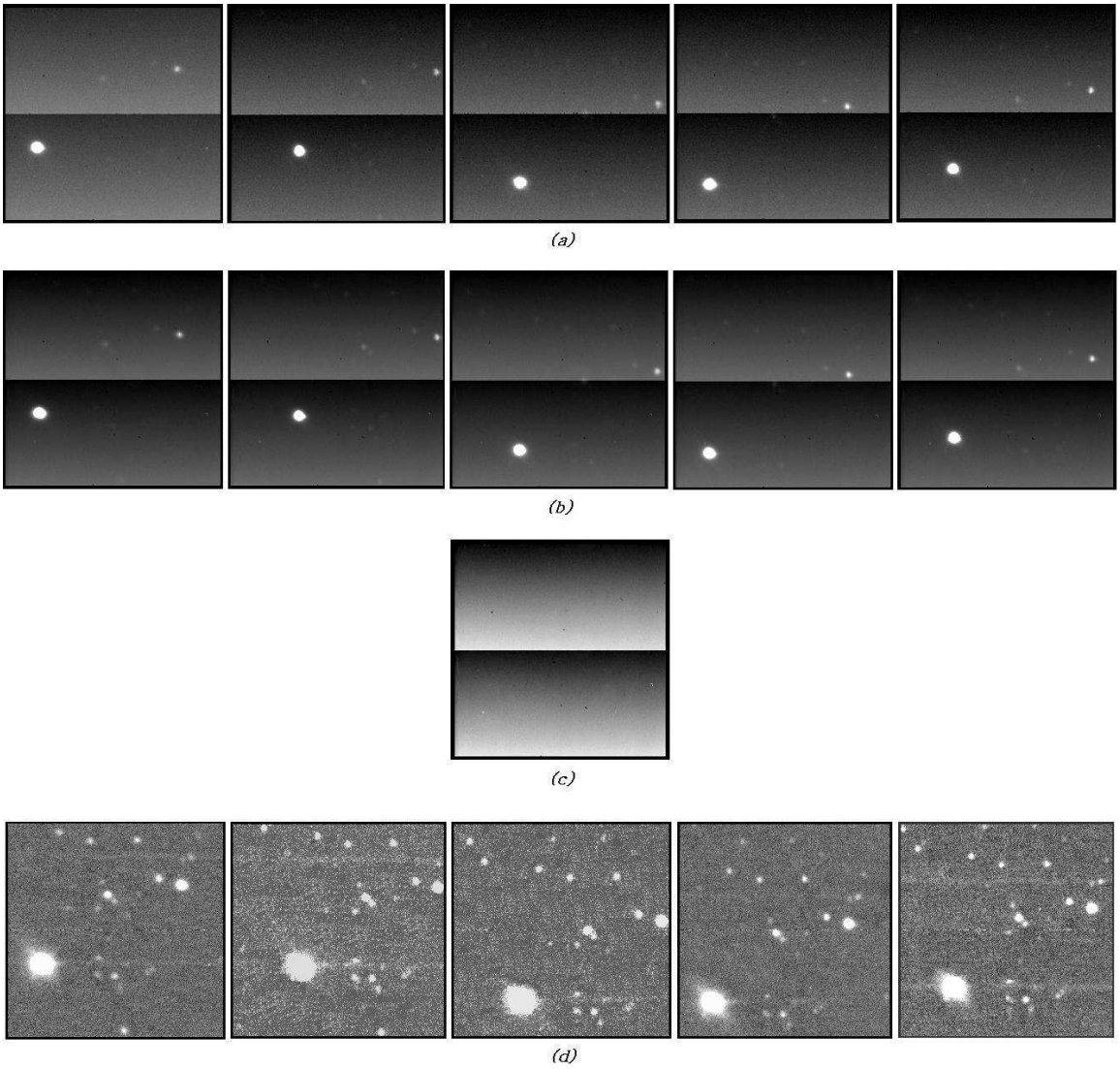

Figure 2.7: The images explains a few of the basic steps of photometric data analysis process (see the subsection 2.4.2 for details).
(a) The raw images (corrected for cosmic rays) of nova observed at five dithered positions. Several frames are acquired at each position.
(b) Average frames. An average frame is generated from the set of the frames observed at a particular position. Five such average frames are generated for each dithered position.
(c) The median averaged sky frame generated from the average frames.
(d) Background removed images. These are achieved by subtracting the sky frame from the average frames.

Removal of background: To determine the background we followed the method of median averaging and an "empty" sky frame of equal exposure time is generated by median averaging the average frames. The median average of a set of measurements yields a value that has equal quantities of individual values above and below it. The background is removed by subtracting the sky frame from each of the average frames. The sky frame is also used for flat fielding.

Calculating magnitudes: After the removal of the sky and dark current background, a subtracted frame contains the signal from the star only. From the subtracted images the instrumental magnitude of the nova ($m_{nova_{instrumental}}$) is obtained using aperture photometry.

Following the same procedure described above, the instrumental magnitude of the observed standard star ($m_{std_{instrumental}}$) is also derived. The apparent magnitude of the nova (m_{nova}) is then calculated from the following relation:

$$m_{nova} = m_{nova_{instrumental}} + (m_{std} - m_{std_{instrumental}}) \tag{2.1}$$

where, m_{std} is the apparent magnitude of the standard star. Minor corrections to the nova's magnitude, due to airmass differences between the standard star and the nova, are applied.

Interstellar extinction correction: Inter stellar extinction refers to the loss of radiation from the star by scattering and absorbtion by the inter stellar medium. Though its effect is smaller in the infrared than in the visible, the derived magnitude of a nova must be corrected for extinction to find the true radiation flux. The necessary corrections can be made by using the extinction coefficients. In the present work, we have calculated the extinction corrections using Koorneef's relations (1983):

$$\left.\begin{aligned} A_V &= 3.1 \times E(B-V) \\ A_J &= 0.265 \times A_V \\ A_H &= 0.155 \times A_V \\ A_K &= 0.09 \times A_V \end{aligned}\right\} \tag{2.2}$$

where $E(B-V)$ is the color excess and the A's are the extinction coefficients

Table 2.5: The flux densities for a *zero-magnitude* star (Bessell et al. 1998).

Near-IR bands	λ_{eff} (μm)	F_λ W cm^{-2} μm^{-1}	F_ν W m^{-2} Hz^{-1}
J	1.22	3.15×10^{-13}	1.59×10^{-23}
H	1.63	1.14×10^{-13}	1.02×10^{-23}
K	2.19	3.96×10^{-14}	6.40×10^{-24}

in the respective bands. Hence, the corrected magnitudes will be

$$m_{JHK} = m_{nova} - A_{JHK} \tag{2.3}$$

2.4.3 Flux Calibration

The flux from the nova, F, is derived using the basic equation

$$m = -2.5log\frac{F}{F_0} \tag{2.4}$$

where m is the corrected magnitude of the nova, F_0 is the flux of a *zero magnitude* star. The flux densities for a *zero magnitude* star are known. In the present work, we have used the *JHK* calibrations (see Table 2.5) from the work of Bessel, Castelli and Plez (1998).

2.5 Observations of novae

To achieve the science objectives mentioned in the previous chapter, spectroscopic and photometric observations were made by me of several novae from Mt. Abu. A total of fourteen novae were observed, the details are presented in Table 2.6 outlining the number of separate epochs on which they could be studied spectroscopically and photometrically. Out of those novae a few were observed more extensively than the others. As mentioned earlier, constraints of time did not allow a complete analysis of all the objects observed. Thus the present thesis incorporates results of the three best-observed objects viz. RS Ophiuchi, V1280 Scorpii and V2615 Ophiuchi. Of these RS Ophiuchi is a recurrent nova and V1280 Scorpii & V2615 Ophiuchi are classical novae.

Table 2.6: List of observed novae in the *JHK* bands.

Observed novae	Discovery date	Epochs	
		Spectroscopy	Photometry
V574 Pup	Nov. 20.67 UT, 2004	5	12
V5115 Sgr	Mar. 28.78 UT, 2005	3	3
V476 Scu	Sep. 30.52 UT, 2005	11	12
V477 Scu	Oct. 13.42 UT, 2005	7	3
V2575 Oph	Feb. 10.83 UT, 2006	15	8
RS Oph	Feb. 12.82 UT, 2006	34	13
V5117 Sgr	Feb. 17.37 UT, 2006	4	3
V2467 Cyg	Mar. 15.79 UT, 2006	8	7
V2362 Cyg	Apr. 02.81 UT, 2006	2	2
V2576 Oph	Apr. 06.57 UT, 2006	1	-
V1280 Sco	Feb. 04.85 UT, 2007	26	34
V1281 Sco	Feb. 19.85 UT, 2007	2	1
V2615 Oph	Mar. 19.81 UT, 2007	15	14
V5558 Sgr	Apr. 14.78 UT, 2007	11	5

CHAPTER 3

Study of the Recurrent Nova RS Ophiuchi (2006 outburst)

3.1 Introduction

RS Ophiuchi (RS Oph), the well known recurrent nova (RN), underwent its sixth recorded outburst recently on 2006 February 12. It was discovered at $V = 4.5$ near the optical peak (Hirosawa 2006). The five previous known eruptions of the object occurred in 1898, 1933, 1958, 1967 and 1985. The RS Oph binary system comprises of a white dwarf primary accompanied by a red giant secondary - the orbital period of the system being 455.72 ± 0.83 days (Fekel et al. 2000). A more recent study by Brandi et al. (2009) finds a closely similar value of 453.6 ± 0.4 days for the orbital period. The outburst occurs due to thermonuclear runaway on the very massive white dwarf surface which has accreted matter from a companion star. There is some uncertainty regarding the exact classification of the secondary companion - suggested classifications range from K0 III to M4 III with M2 III being the most likely (Worters et al. 2008 and references therein).

The special nature of RS Oph system stems from two reasons. Firstly, the high velocity ejecta in the nova outburst is immediately impeded by the surrounding wind of the red giant companion. This leads to the generation of a shock wave that propagates into the red giant wind. The temporal evolution of the shock and associated physical parameters like the shock velocity have been predicted theoretically but an astrophysical environment where such predictions can be rigorously tested are extremely rare to come by. Recurrent novae provide such an opportunity

for testing and therefore have special significance. Another class of objects where similar shock waves are open to study are young supernova remnants, but here the evolution of the shock occurs on the timescale of a few hundreds of years (vis-a-vis a few days for an analogous development to occur in a RN) making it difficult to follow the evolution in supernova remnants.

Second, the mass of the white dwarf in recurrent novae are believed to be very high, because the amount of hydrogen needed to trigger an outburst decreases dramatically as the white dwarf mass increases and consequently the time of recurrence decreases. If the mass of the white dwarfs in recurrent novae is assumed to increase, they should eventually explode as Type Ia supernovae (SNe Ia), one of the most luminous explosive events in stars, when they reach the Chandrasekhar mass limit of about 1.38 $M_{\odot}$. But there has been intense debates on this hypothesis (Starrfield et al. 2004, Wood-Vasey & Sokoloski 2006). One of the greatest problems, by far, for the SN Ia theorists is the lack of a progenitor where the theories can be tested (see, e.g., Livio 2000 for a recent review). SNe Ia explosions have special significance, because they have been used as good distance indicators and provide a promising tool for determining cosmological parameters because of their almost uniform maximum luminosities (Riess et al. 1998; Perlmutter et al. 1999). Both Riess et al. and Perlmutter et al. derived the maximum luminosities (L_{max}) of nearby SNe Ia empirically from the shape of their light curves (LCS) and assumed that the same L_{max} - LCS relation also holds for high-redshift SNe Ia. To be sure of any systematic biases, it is necessary to understand the physics of SNe Ia completely.

From the theoretical modeling of the light curve of the previous outburst in 1985, it has been calculated that the white dwarf in the RS Oph system is very massive and likely extremely close (within 1%) to the Chandrasekhar limit of 1.38 $M_{\odot}$ (Hachisu & Kato 2000, 2001). More detailed calculations indicate that in the outburst about 90% of the accreted mass is blown off and the remaining 10% mass is left and added to the helium layer of the white dwarf. The net effect is increase of the white dwarf mass at a rate of 1.2×10^{-8} $M_{\odot}$ yr^{-1}. Thus, RS Oph is certainly a strong candidate for a Type Ia supernova progenitor.

The recent outburst of RS Oph has been studied in great details at several wavelength regimes viz. in X-rays (e.g. Sokoloski et al. 2006, Bode et al. 2006), in the optical (Iijima 2006, Skopal et al. 2008; Buil 2006, Fujii 2006), in the infrared (e.g. Das et al. 2006, Evans et al. 2007a, Monnier et al. 2006) and in the radio (e.g. O'Brien et

al. 2006; Kantharia et al. 2007; Rupen et al. 2008). The prime result, that come out from these studies, is the detection of a shock wave. The X-ray results clearly detect a X-ray blast wave that expands into the red giant wind. The XRT observations from the Swift satellite (Bode et al. 2006) trace the temporal change in the shock velocity based on a set of 8 observations between 3.16 to 26 days after the outburst. Similarly the Rossi X-ray Timing Explorer (RXTE) observations (Sokoloski et al. 2006) cover the shock wave evolution based on 6 epochs of observations between 3 days to 21 days after the eruption.

In the present work, we study the general near-IR characteristics of the present eruption in greater detail. We present new and extensive *J*, *H* and *K* spectroscopic and photometric observations of RS Oph upto 94 days after its outburst. The major new result lies in our detection of an infrared shock wave which manifests itself through the narrowing of emission lines observed in the spectra. The detection of such a shock wave in the infrared has not been made earlier in a RN. The present data, also have significantly better sampling, especially in the ~ first 20 days after outburst when fairly fast changes are seen in the shock evolution. Additionally, the data cover a much more extended period. Thus this appears to be the most comprehensive data set available for analyzing the shock evolution in RS Oph-like systems and for validating related theoretical models. While we make such an analysis, based on the theoretical shock model of Bode & Kahn (1985), some deviations that are seen between model and observations suggest the data set could be invaluable for testing alternative models that may be proposed subsequently or for introducing refinements/modifications in presently available ones.

3.2 Observations

Since its outburst in February 2006, RS Oph was observed regularly in near-IR *JHK* bands. Both spectroscopic and photometric observations in the near-IR *JHK* bands were obtained at the Mt. Abu 1.2m telescope. The general procedure of observations and data reduction have been described in section 2.3 and 2.4 respectively. In order to observe temporal evolution, spectra of RS Oph have been taken extensively using Near Infrared Imager/Spectrometer with a 256×256 HgCdTe NICMOS3 arrays. An early set of spectra, taken soon after the outburst, is described in Das, Ashok & Banerjee (2006). The log of spectroscopic observations is presented in Table 3.1. In order to remove telluric features in the object spectra, the star SAO

122754 (spectral type A0V) was observed as the standard star. In this context, a few words would be appropriate here. Following the standard reduction procedure, while the absorption lines of Hydrogen Paschen and Brackett removed by manual extrapolation from the spectra of the comparison star, it is estimated that residuals amounting to 5 percent of the line strength may still remain. In addition, the ratioing process (dividing the spectra of the nova by the spectra of the standard star), while removing telluric features sufficiently well, leaves some residuals in the wavelength regions where telluric absorption is strong. This applies significantly to the region around 2.0 μm in the *K* band which is strongly affected by atmospheric carbon-dioxide.

The *JHK* photometry of RS Oph was done under photometric sky conditions using the imaging mode of the NICMOS3 array. Following the general procedure the nova and a selected standard star SAO 159963 (V = 4.29, J = 2.89, H = 2.47, K = 2.33) and SAO 141886 (V = 7.75, J = 7.15, H = 7.10, K = 7.03) was observed at five dithered positions. The derived *JHK* magnitudes, with typical errors in the range of 0.01 to 0.03 magnitudes, along with the log of the photometric observations are given in Table 3.2.

3.3 Results

3.3.1 Photometry: The *JHK* Lightcurve

We present in Figure 3.1 the *JHK* lightcurves of RS Oph using photometric data obtained between 11 to 94 days after outburst. Although we would have liked to have sampled the lightcurve more frequently, our efforts were focused more on the spectroscopy. Also superimposed in Figure 3.1 is the near-IR lightcurve of the 1985 outburst which was obtained by Evans et al. (1988). While it is known that the visual lightcurve behaves similarly from outburst to outburst (Rosino & Iijima 1987), an equivalent comparison for the near-IR lightcurve had not been possible earlier for lack of data. The present data shows that the IR decline is quite similar to that of the 1985 outburst. However, some caution is needed while comparing the near-IR light curves because of the effect of emission lines on the measured continuum flux in the photometric bands. The JHK spectra of RS Oph has prominent emission lines, some of which lie at the edge of the photometric bands. Filter transmissions in these regions can vary significantly in different photometric systems thereby contributing different amounts of the line flux to the measured continuum. For

Table 3.1: A log of the spectroscopic observations of RS Ophiuchi. The date of outburst is taken to be 2006 Feb 12.83 UT.

Date 2006 (UT)	Days since Outburst	Integration time (sec) J	H	K
Feb. 13.9929	1.1629	10	10	10
Feb. 14.9915	2.1615	10	10	10
Feb. 15.9898	3.1598	10	10	10
Feb. 16.9866	4.1566	10	10	10
Feb. 19.9759	7.1459	10	8	10
Feb. 20.9721	8.1421	5	8	10
Feb. 21.9463	9.1163	10	10	15
Feb. 22.9505	10.1205	10	10	10
Feb. 24.9705	12.1405	10	10	10
Feb. 26.9926	14.1626	10	10	10
Feb. 28.9542	16.1242	15	10	10
Mar. 02.9465	18.1165	20	20	20
Mar. 16.9465	32.1165	20	30	30
Mar. 17.8866	33.0566	30	30	30
Mar. 18.9372	34.1072	30	30	30
Mar. 19.8833	35.0533	30	30	30
Mar. 20.8733	36.0433	45	30	30
Mar. 22.8682	38.0382	45	45	45
Mar. 26.8778	42.0478	60	60	60
Mar. 27.8644	43.0344	60	60	60
Mar. 29.8462	45.0162	75	90	90
Mar. 30.8629	46.0329	75	90	90
Mar. 31.8701	47.0401	90	90	90
Apr. 02.8736	49.0436	90	120	120
Apr. 03.9691	50.1391	90	120	120
Apr. 05.9607	52.1307	90	90	90
Apr. 10.8936	57.0636	90	120	90
Apr. 12.8454	59.0154	90	120	90
Apr. 22.9392	69.1092	90	90	90
Apr. 29.8355	76.0055	120	120	120
May. 01.8149	77.9849	120	180	180
May. 03.810	79.980	180	180	180
May. 11.8353	88.0053	270	270	270
May. 17.8103	93.9803	270	270	270

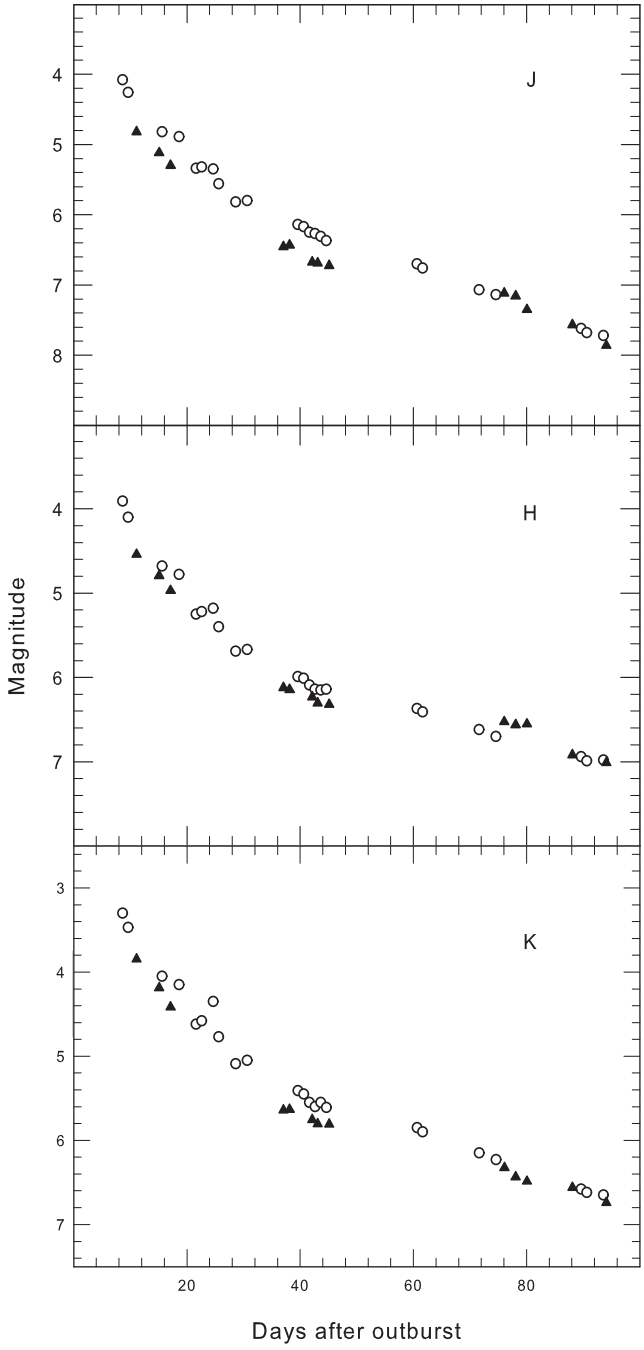

Figure 3.1: The J, H, K lightcurves for RS Oph, based on data from Table 3.2, is shown with filled triangles. To show the similarity of the lightcurve behaviour from different outbursts, the data from the 1985 outburst (Evans et al. 1988) are also shown with open circles.

Table 3.2: A log of the photometric observations of RS Oph. The date of outburst is taken to be 2006 February 12.83 UT.

Date 2006 (UT)	Days since Outburst	Magnitudes		
		J	*H*	*K*
Feb. 23.9518	11.1218	4.82	4.54	3.85
Feb. 27.9259	15.0959	5.12	4.79	4.19
Mar. 01.9485	17.1185	5.30	4.97	4.42
Mar. 21.8986	37.0686	6.46	6.12	5.64
Mar. 22.9645	38.1545	6.43	6.14	5.63
Mar. 26.9534	42.1234	6.67	6.23	5.75
Mar. 27.9189	43.0889	6.69	6.30	5.81
Mar. 29.9696	45.1396	6.73	6.32	5.81
Apr. 29.9037	76.0737	7.12	6.53	6.33
May. 01.8913	78.0613	7.16	6.56	6.43
May. 03.8845	80.0545	7.35	6.55	6.49
May. 11.9199	88.0899	7.57	6.92	6.56
May. 17.9127	94.0827	7.86	7.01	6.74

example, Whitelock et al. (1984) point out the significant effect of the HeI 1.083 μm line on the measured *J* magnitudes in emission line stars (the HeI line lies at the edge of the *J* band and can be strong).

A compilation of several observations of the pre-outburst or quiescent photometry of RS Oph shows that it has a mean pre-outburst values of $J = 7.72$; $H = 6.945$; $K = 6.66$ (Evans et al. 1988; Table 1 therein). From our data we see that in each of the *JHK* bands the magnitude returned to its pre-outburst value by ~ 88 days. Our last observation on day 94 suggests that the decline appears to continue below this level - such a trend was clearly seen by Evans et al. (1988) for the 1985 outburst.

3.3.2 Spectroscopy: General characteristics of the *JHK* spectra and line identification

Although spectra of RS Oph were obtained on several days, we present in Figures 3.2, 3.3 and 3.4 selected *J*, *H* and *K* band spectra respectively that suffice to give the general trend of the spectral evolution of the object. However, the mosaic of *J* spectra covers a period of first 47 days after the eruption - the aim is to show more spectra in that period of time so that the fast change in the shock behavior can be visualized from the changes in the spectral lines. To facilitate studying the overall

evolution of the object in the *J*, *H* and *K* bands, we show three representative *J* band spectra in Figure 3.5 and also expanded views of selected *H* and *K* band spectra. These spectra in Figure 3.5 enable a proper line identification to be made and to also bring out the weaker lines which are not easily discernible in Figures 3.2, 3.3 and 3.4. The line identification is given in Table 3.3 and certain related aspects are discussed in more details below.

Over the span of our observations, the HI recombination lines remain prominent in the *JHK* spectra - these include Brackett γ in the *K* band, Br 10 to 21 in the *H* band, and Paschen β and Paschen γ in the *J* band. Among the HeI lines, those at 1.0830, 1.7002 and 2.0581 μm are prominent. The other weaker lines of HeI detected are those at 1.1969, 1.2527, 1.2968, 2.1120 and 2.1132 μm. The other prominent lines in the spectra are the Ly β fluoresced 1.1287 μm and continuum fluoresced 1.3164 μm OI lines respectively and two lines at 1.6872 and 1.7414 μm which we attribute to Fe II. A more detailed discussion on these Fe II lines is made in a following subsection. Nitrogen is detected as a broad feature centered around 1.245 μm which is seen conspicuously in the spectrum soon after outburst (top panel of Figure 3.5). This feature, which could be a blend of NI lines at 1.2461 and 1.2469 μm, weakens with time but can still be readily discerned in the later spectra (second and third panel from top of Figure 3.5) on the blue wing of the HeI 1.2527 μm line. An additional NI feature, a blend of the NI 1.2074 and 1.2096 μm lines, also appears to be detected (however see Evans et al. 2007 who attribute this feature to OII 1.2084 μm). Weak features of carbon are also possibly being detected. Immediately after outburst (top panel of Figure 3.5), a broad conspicuous bump is seen centered around 1.175 μm. This feature could be a blend of several carbon lines that lie between 1.1653 and 1.1886 μm (the strongest of these are the 1.1748, 1.1753 and 1.1755 μm lines - the blended feature of these lines appears to persist weakly at 1.1748 μm for quite some time after outburst). These carbon lines which are weak here, can be extremely strong in novae which have less massive central white dwarfs (CO novae) e.g. in V1280 Sco (Das et al. 2008) and V2274 Cyg (Rudy et al. 2003). In this context it is noted that the analysis of optical and X-ray spectra indicate the ejecta to be enriched in nitrogen and depleted in carbon (Ness et al. 2008 and references therein).

Among the coronal lines, we detect [Si VI] 1.9641 μm, [S IX] 1.2520 μm, [Al IX] 2.0444 μm and a line at $\sim$ 2.09 μm which could possibly be [Mn XIV] 2.0887 μm. The [Si VI] 1.9641 μm line appears at the edge of our instrument spectral window

i.e. in a region of low instrument and atmospheric transmission. The spectrum in this region is noisy making it difficult to accurately estimate the strength of the line. However we can state, with a fair level of confidence, that the line begins to be clearly detected in the spectrum of 26.88 March 2006. This sets an upper limit on when the line began to be seen in the *K* band. On the other hand, it is difficult to be definitive about when the [S IX] 1.2520 μm line first begins to appear because it is severely blended with the HeI 1.2527 μm line. But from an examination of all our *J* band spectra (Das et al. 2006), we see a significant strengthening of the 1.2527 HeI plus [S IX] feature between 20-29 March. It is likely that this strengthening is due to the emergence of the [S IX] 1.2520 μm line at around this time. Though the identification is uncertain, we attribute the observed line at $\sim$ 2.09 μm to [Mn XIV] 2.0894 μm. The [Mn XIV] 2.0894 μm line is not one among the commonly observed coronal lines in novae. Wagner & Depoy (1996) did observe a line at 2.092 μm in nova V1974 Cyg during its coronal phase and tentatively assigned it to [Mn XIV] 2.0894 μm. An analysis of the temporal evolution of the coronal lines is given in subsection 3.3.9.

There is no evidence for dust formation in the ejecta till the end of our observations. Neither the *JHK* magnitudes show a development of an infrared excess nor do the slope of the continua in the spectra show an upturn towards longer wavelengths indicative of dust formation. It may be noted that Spitzer observations obtained over the period 208-430 days after the eruption revealed evidence for silicate dust features at 9.7 and 18 μm (Evans et al. 2007b). But this silicate dust appears not to have formed in the nova ejecta; rather it has been interpreted as being a part of the red giant wind that existed prior to the 2006 eruption and has survived the outburst (Evans et al. 2007b).

3.3.3 Detection of shock wave and its behavior

The *J* band spectra are shown in Figure 3.2. All the emission lines strikingly show a narrowing with time - a phenomenon also seen during in the UV during the 1985 outburst (Shore et al. 1996). Such a behavior implies a reduction in expansion velocity best explained by associating the line emitting matter with a decelerating shock wave. The propagation of the shock wave in RS Oph-like systems, assuming a spherical geometry, has been studied earlier and can be divided into three phases (Bode & Kahn 1985).

Table 3.3: List of observed lines in the *JHK* spectra.

Wavelength (μm)	Species	Other contributing lines & remarks
1.0830	He I	
1.0938	Pa γ	
1.1126	Fe II	
1.1287	O I	
1.1626	He II	
1.1748	C I	Possible blend of several CI lines between 1.1653 & 1.1886
1.1969	He I	
1.2074	N I	blended with N I 1.2096
1.2470	N I	blended with N I 1.2461
1.2527	He I	
1.2520	[S IX]	
1.2818	Pa β	
1.2968	He I?	
1.3164	O I	
1.5133	Br21	
1.5184	Br20	
1.5256	Br19	
1.5341	Br18	
1.5439	Br17	
1.5557	Br16	
1.5685	Br15	
1.5753	u.i.	unidentified
1.5881	Br14	
1.6109	Br13	
1.6407	Br12	
1.6806	Br11	
1.6872	Fe II	
1.7002	He I	
1.7362	Br10	
1.7413	Fe II	
1.9446	Br8	
1.9641	[Si VI]	
2.0444	[Al IX]	
2.0581	He I	
2.0894	[Mn XIV]	uncertain identification
2.1120	He I	blended with He I 2.1132
2.1369	u.i	unidentified
2.1655	Br γ	

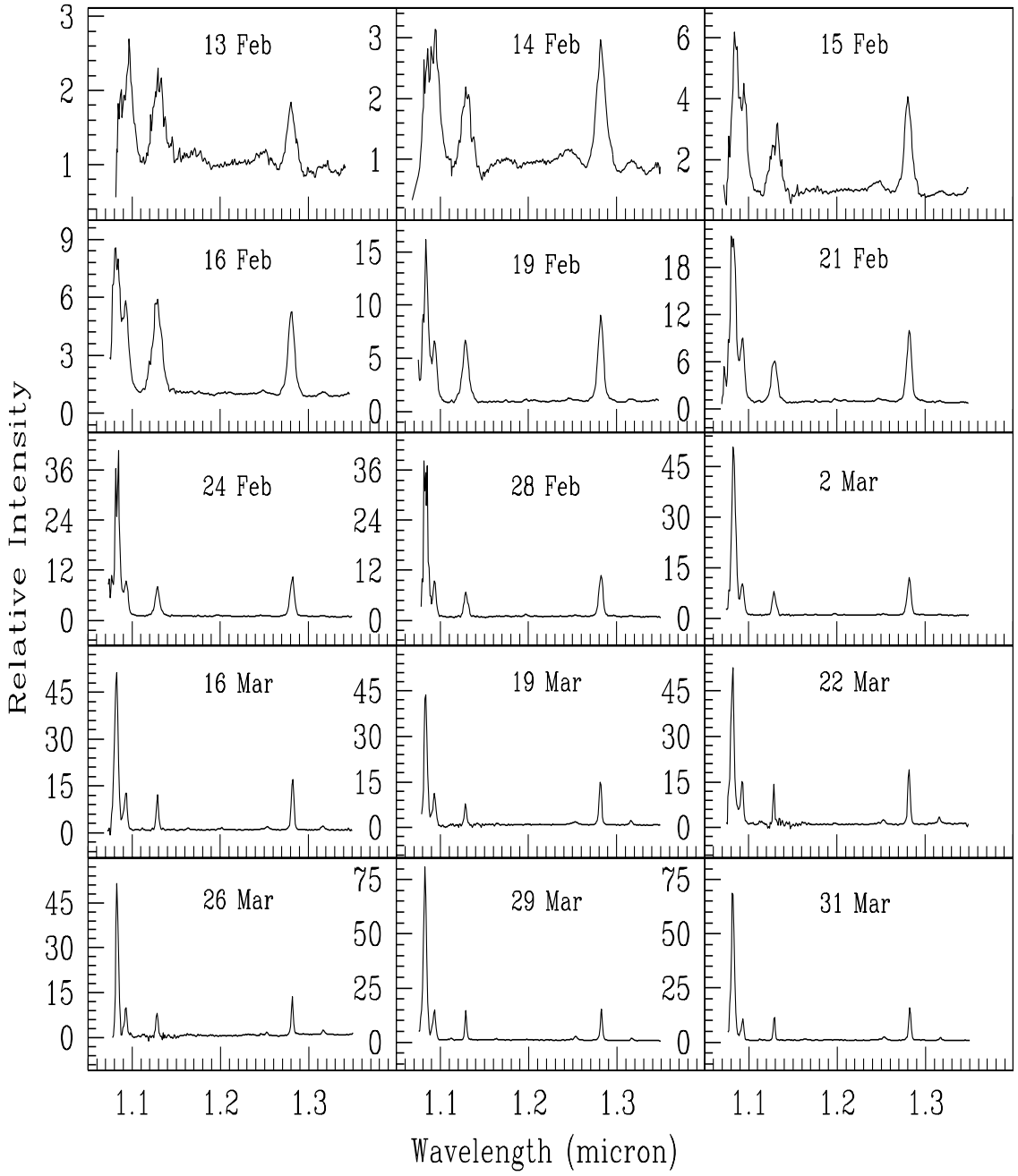

Figure 3.2: The *J* band spectra of RS Ophiuchi on different days with the flux normalized to unity at 1.25 μm.

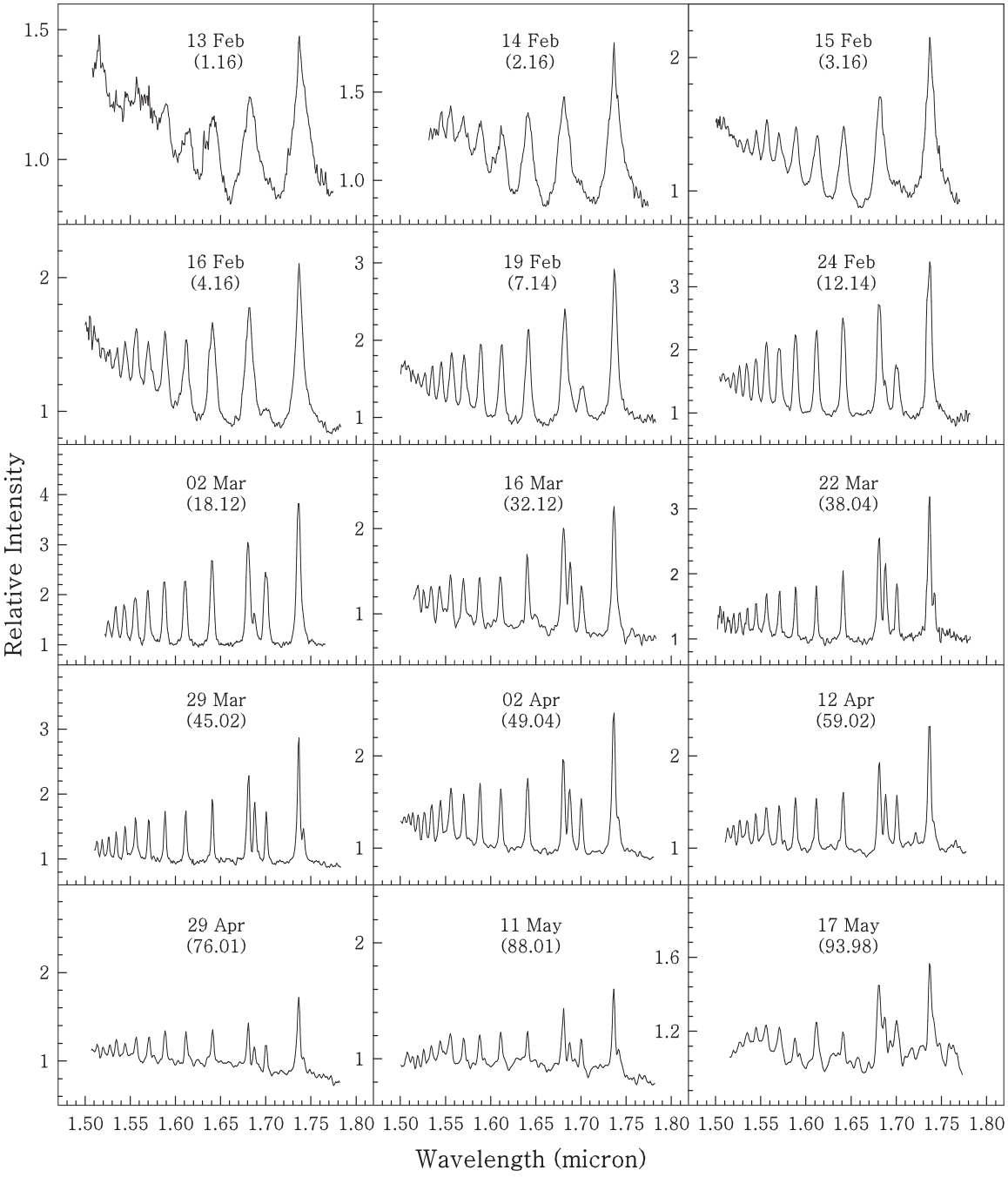

Figure 3.3: The *H* band spectra of RS Ophiuchi on different days with the flux normalized to unity at 1.65 μm. The number inside the brackets represents the days elapsed since outburst.

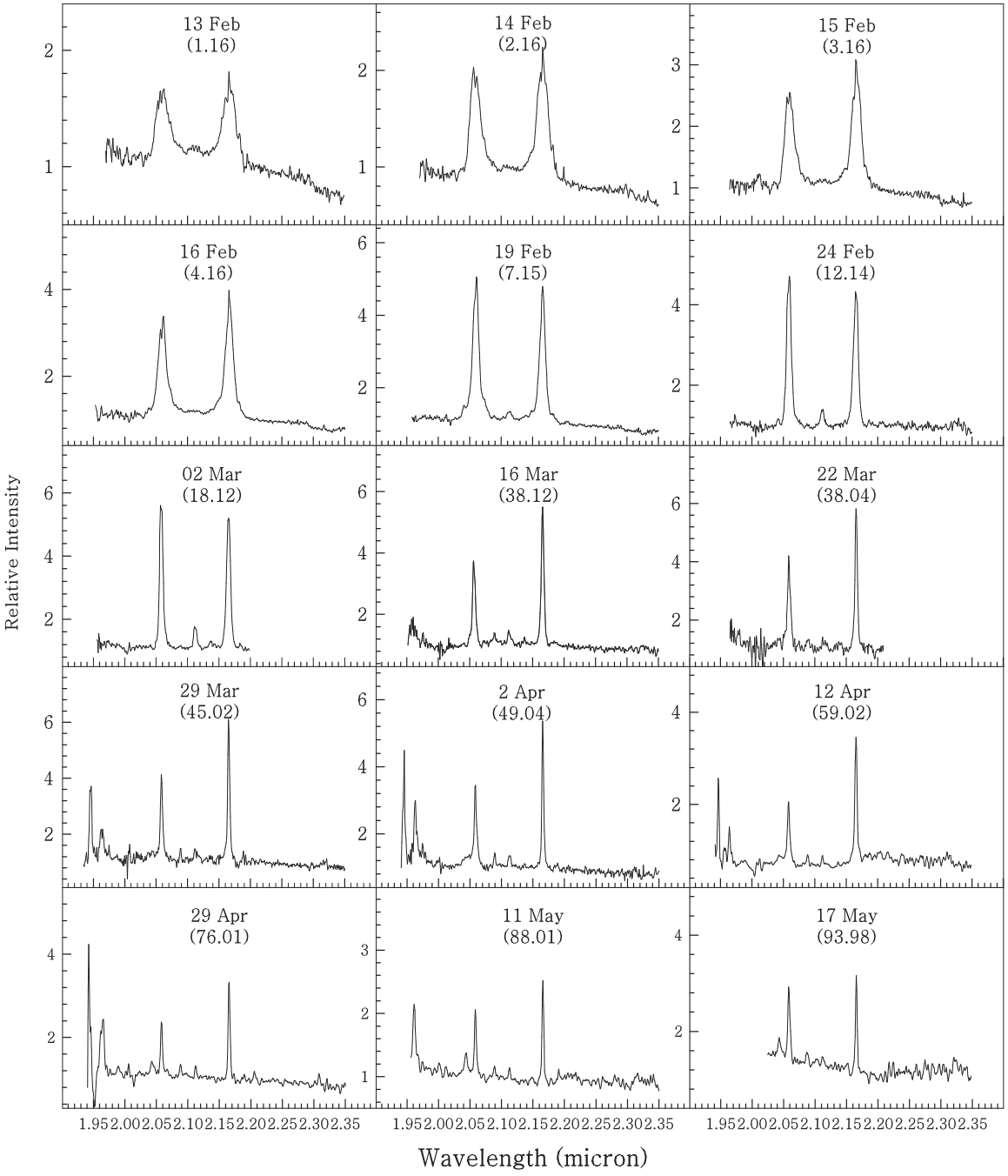

Figure 3.4: The *K* band spectra of RS Oph on different days with the flux normalized to unity at 2.2 μm. The presence of noise and weak features at $\sim$ 2.0 μm in some of the spectra are residuals from incomplete telluric subtraction as discussed in section 3.2. The number inside the brackets represents the days elapsed since outburst.

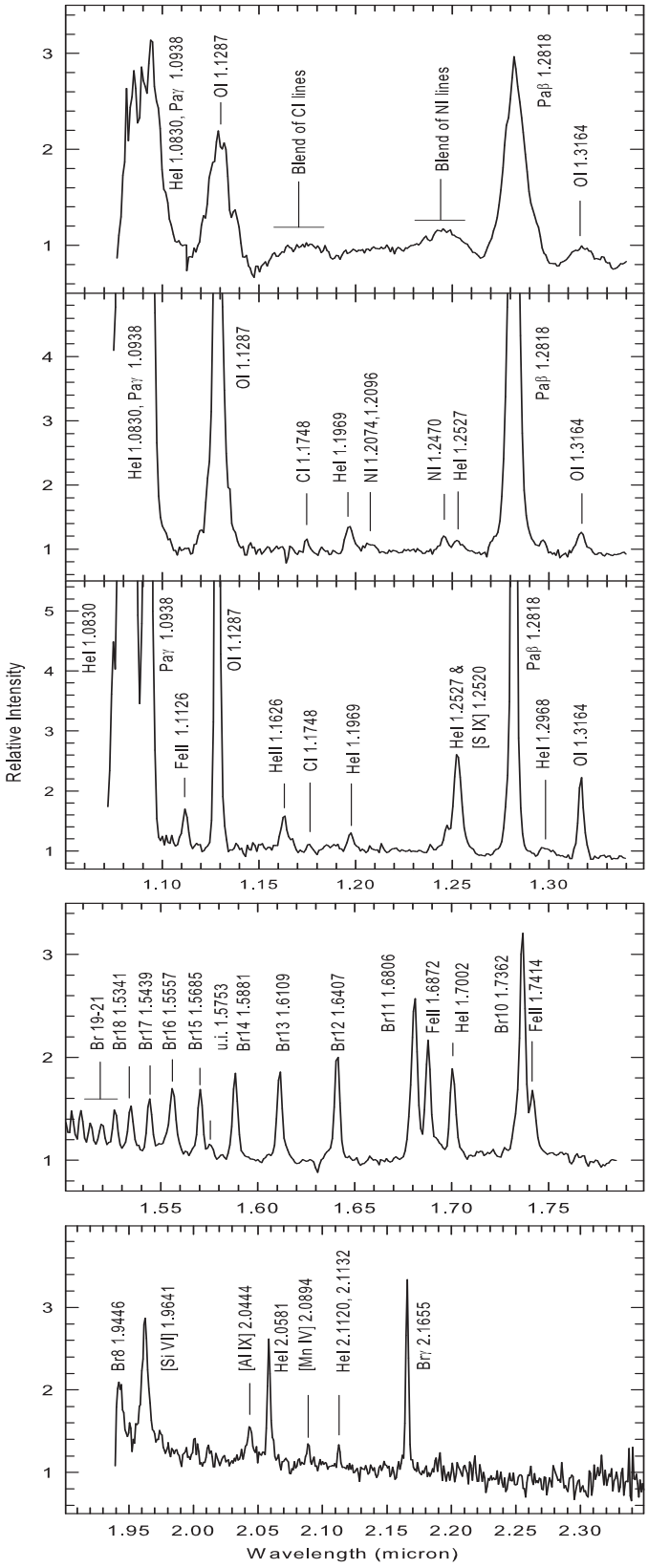

Figure 3.5: Identification of the observed lines in the *J, H* & *K* bands. The top three panels show *J* band spectra for 14 February, 24 February and 29 March 2006 respectively. The bottom two panels show the *H* and *K* band spectra of 29 March and 11 May 2006 respectively (the *K* band spectra is at bottom). Further details are provided in subsection 3.3.2 and Table 3.3.

- In Phase 1 - or the ejecta dominated stage - the ejecta expands freely into the red giant wind and produces a shock at constant velocity.
- In Phase 2, the shock wave is driven into the wind and the shocked material is so hot that there is negligible cooling by radiation losses - hence called the adiabatic phase. During this phase a deceleration is seen in the shock whose velocity v_s versus time t is expected to behave as $v_s \; \alpha \; t^{-1/3}$ assuming a r^{-2} dependence for the decrease in density of the wind.
- In Phase 3, the shocked material has cooled by radiation and here the expected dependence of the shock velocity is $v_s \; \alpha \; t^{-1/2}$.

To confirm whether these dependencies are indeed observed, we select the Paβ 1.2818μm and the OI 1.1287μm lines for detailed analysis. These lines are strong yet unblended by other lines (unlike the HeI 1.0833μm and Paγ 1.0938μm lines) ensuring a reliable estimate of their widths. We interpret the observed line widths to be due to kinematic broadening i.e. caused by the dispersion of the line-of-sight velocity component from matter at different parts of an expanding shell (which we assume to be spherical). In this case, the FWHM and FWZI (full width at half maximum and zero intensity respectively) are good indicators of the expansion velocity (i.e. the shock velocity). In particular, half the FWZI should be a reasonably good measure of the expansion velocity since the largest blue-shifted and red-shifted velocities seen in the FWZI come from those parts of the shell that are directly approaching or receding from the observer. We present the observed line widths in Table 3.4. Since the observed FWHM of the lines at later stages (beyond March 20) is comparable to the FWHM of the instrument profile (which is well approximated by a Gaussian with FWHM = 450 km/s; FWZI = 1350 km/s) we have deconvolved for the instrument broadening. For this, we have used the simple, but sufficiently adequate, approximation that the square of the observed FWHM equals the sum of the squares of the instrument and true FWHM's (and similarly so for the FWZI). This assumes a gaussian nature for the observed profiles which we find to be reasonably valid. The effect of the deconvolution is found to be rather small for the observations prior to 20 March which compose the bulk of the data. Optical depth effects could affect the lines but such effects are expected to influence the intensity and not the width of the lines. We show the temporal variation of the deconvolved widths of the selected lines with time in Figure 3.6.

Figure 3.6 first establishes that there is indeed a stage of free expansion - lasting approximately 4 days - during which the shock velocity remains approximately

constant. This behavior is more evident in the OI data vis-a-vis the Paβ data which suggests there may be a mild deceleration during this phase. Following Phase 1, a deceleration is seen and since this slowing down occurs only after the ejecta has swept up mass from the red giant wind comparable to the ejecta mass. We find that the decelerative phase, for both the OI and Paβ lines is reasonably well reproduced by power law fits of the form $t^{-\alpha}$ with α varying between 0.45 to 0.79. Using a nonlinear regression technique, the best fits were determined by maximizing the correlation coefficient R with a value of $R = 1$ describing a perfect fit. The plots in Figure 3.6 have R values of 0.977, 0.988, 0.976 and 0.975 for the FWZI and FWZM of the Paβ and OI lines respectively. A mean value of $\alpha = 0.64$ (with a standard deviation of 0.14) can be said to characterize the data which is consistent with the Swift results (Bode et al. 2006) wherein a value of $\alpha = 0.6$ is obtained. We do note that the results in Figure 3.6 do suggest the need of using more than one power law for different segments. However, our present aim is to obtain a simple yet reasonable assessment of the overall behavior of the line-widths and therefore we elect to use a single power law. We note that there seems to be a lack - or a very short-lived duration of Phase II (the Sedov-Taylor phase) in our data. While the reason for this is not clear, it is possible that the cooling of the ejecta begins very quickly. We find that the mean value of $\alpha = 0.64$ compares better to the expected value of 0.5 for Phase III rather than 0.33 expected in Phase II (Bode & Kahn 1985). Thus there are deviations in the observed data from expected model predictions. It is possible that a part of such variations arise from the assumption of spherical symmetry that is being invoked. But as the HST images (Bode et al. 2007, Harman et al. 2008), radio imaging (O'Brien et al. 2006) and interferometric results (Monnier et al. 2006) show, the ejecta remnant has deviations from spherical symmetry and also jet-like structures. Such variations in geometry are expected to affect the observed line profiles. A treatment of these effects is expected to be involved and beyond the scope of the present work. However, we find that on the whole, our results are broadly consistent with the shock model wherein a free expansion stage is expected to be seen followed by a decelerative stage characterized by a power law decay in the shock velocity. We thus believe that the observations clearly support the presence of an infrared shock wave in the recent outburst of RS Oph.

While the near-IR line emission, as seen from the Paβ and OI line behavior, is associated with a moving shock, the site of its emission within the shock structure needs to be examined. The structure of the shock is understood to consist of a cool contact surface (i.e. the region of discontinuity) positioned between the hot

compressed region consisting of the ejecta material and the hot swept-up red giant wind (e.g. Lamers & Cassinelli 1999 for a general treatment, Vaytet et al. 2007 for RS Oph specifically). The last two regions are the sites where the shocked gas is heated to the extremely high temperature of 10^8K (as determined for RS Oph; Sokoloski et al. 2006; Bode at al. 2006) and which is the source of the observed X-ray emission. Clearly the IR line emission cannot emanate from these zones because the presence of neutral OI atoms in such a hot region is not possible. Thus we think that the near-IR emission originates from the contact surface, which is considerably cooler and denser, but which still propagates with a similar velocity as the shock front thereby leading to similar kinematic behavior for the shock velocity as predicted for the X-rays (Bode & Kahn 1985).

Monnier et al. (2006) measured the near-infrared (*H* and *K* band) size of RS Oph during the recent outburst using interferometry to show that the object displays a near-constant size of ~ 3 milliarcseconds (mas) over the first 60 days of the outburst. At a distance of 1.6 kpc to RS Oph, the near-IR emission is expected to expand at the rate of 1 mas per day if associated with an expanding shock. Since this is not seen, these authors are led to the interesting conclusion that the IR continuum does not arise from an expanding fireball - a scenario favored to explain novae outbursts. In context of this, we note that the net IR emission consists of two parts - the continuum and the line emission. Regarding the line emission, the present results clearly show that it originates from an expanding shock. This does not resolve the extent and site of origin of the near-IR continuum i.e. what part could arise from the expanding shock wave vis-a-vis the fraction that arises from other sites/mechanisms (e.g. the alternative theory of Hachisu & Kato 2001). But an aspect of the Monnier et al. (2006) data, which maybe worthwhile to reexamine, is whether they do detect a faint signature associated with the expanding shock front. The reason to expect such a detection is that our *H* band spectra (also see the Evans et al. 2006 spectra), taken contemporaneously with Monnier et al. (2006), are replete with strong Brackett series lines. The combined flux contribution from these lines is estimated to be ~ 15-20 percent relative to the continuum. It would therefore appear likely that some signature of this line emission, though weaker than the continuum, should be detected and show up in expansion in the interferometric data.

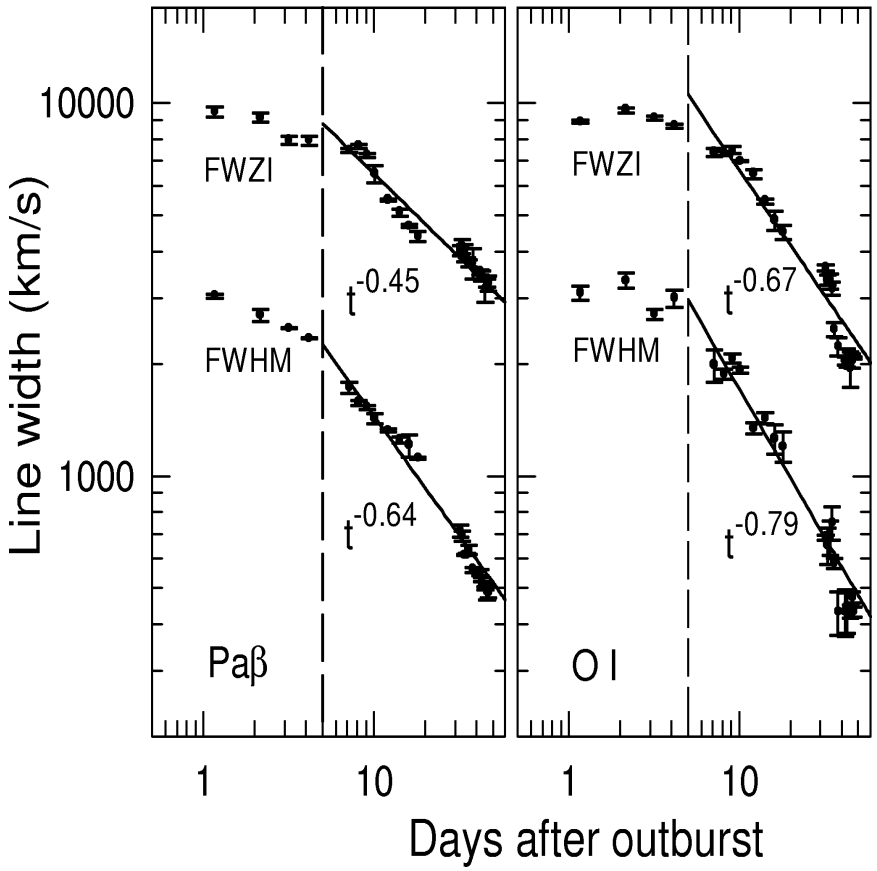

Figure 3.6: The behavior of the deconvolved line widths for the Paβ 1.2818μm and the OI 1.1287μm lines is shown. The line widths imply a free expansion phase for the infrared shock front for the first four days - the region to the left of the dashed drop lines. This phase is followed by a decelerative phase which is best described by a power law decline in the shock velocity with time. The different power laws used for fitting are marked in the figure; data points are shown with 1σ error bars. Further details can be found in the text in subsection 3.3.3.

Table 3.4: Observed widths of the Paβ and OI lines.

Days after outburst	Paβ fwhm km/s	Paβ fwzi km/s	OI fwhm km/s	OI fwzi km/s	Days after outburst	Paβ fwhm km/s	Paβ fwzi km/s	OI fwhm km/s	OI fwzi km/s
1.16	3066	9561	3136	9009	32.12	839	4236	850	3853
2.16	2738	9228	3375	9647	33.06	822	4330	824	3614
3.16	2532	8051	2764	9221	34.11	758	4189	850	3588
4.16	2381	8063	3029	8770	35.05	759	4026	904	3455
7.15	1782	7595	2046	7494	36.04	775	3955	771	2817
8.14	1632	7759	1940	7441	38.04	715	3961	664	2604
9.12	1587	7361	2126	7600	42.05	708	3768	664	2445
10.12	1489	6595	1993	7122	43.03	690	3698	664	2471
12.14	1398	5648	1435	6590	45.02	669	3452	664	2365
14.16	1326	5266	1515	5607	46.03	660	3557	691	2445
16.12	1287	4868	1355	5023	47.04	659	3557	664	2471
18.12	1203	4587	1302	4704					

3.3.4 Mass of the white dwarf

The onset of deceleration can be used to estimate the mass of the ejected shell. Following Sokoloski et al. (2006), we assume the density in the binary to be 10^9 cm^{-3} from constraints on the mass-loss rate of the red giant (Dobrzycka & Kenyon 1994) and adopt a mean initial expansion velocity in the range 3500-4000 km/s based on our results and optical reports (Buil 2006; Fujii 2006). Thus by day 4, the swept up mass (or equivalently the ejected shell mass) is estimated to have a mean value of $\sim 3\text{x}10^{-6} M_{\odot}$. This value reasonably matches with the Hachisu & Kato (2001) model for RS Oph which estimates that an ejecta mass of $\sim 2\text{x}10^{-6} M_{\odot}$ needs a mass of $1.35 M_{\odot}$ for the white dwarf. We therefore independently infer that RS Oph certainly contains a massive white dwarf with a mass close to $1.35 M_{\odot}$ - a similar conclusion is reached from alternative methods viz. from a lightcurve analysis (Hachisu & Kato 2001) and from X-ray observations (Solokoski et al. 2006).

3.3.5 Evidence for a bipolar flow

A significant finding that has emerged from studies of the present outburst of RS Oph is the presence of extended structure in the ejected material. Images from the Hubble Space Telescope, taken 155 and 449 days after outburst in the [OIII]

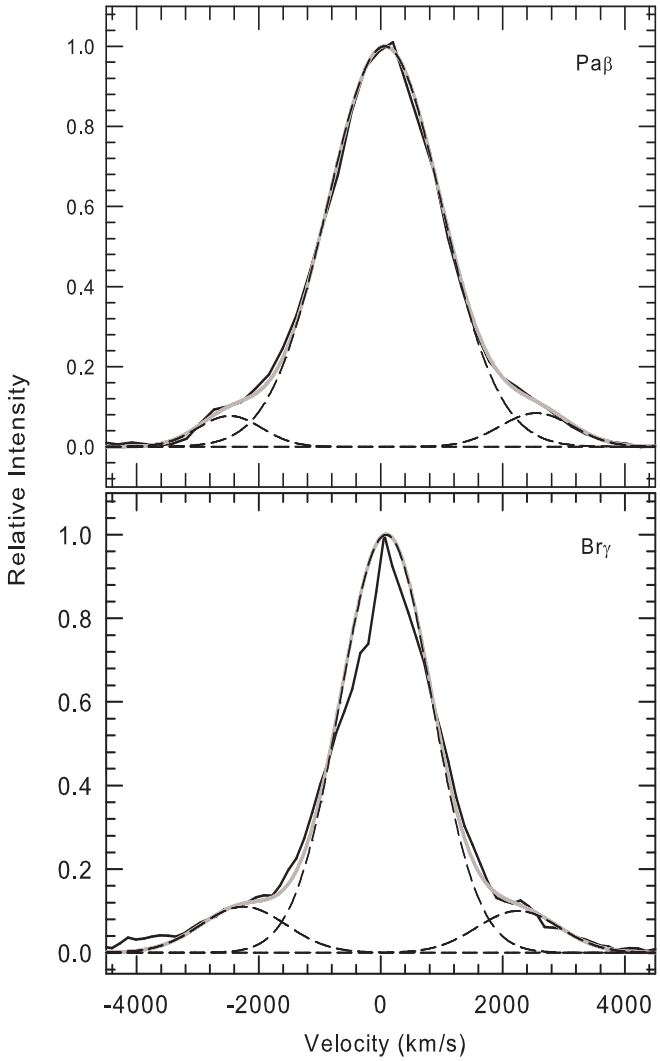

Figure 3.7: Line profiles of the Pa β and Br γ lines on Feb 16.987 showing broad wings indicative of a bipolar flow. A multigaussian fit of the profiles is shown - a gaussian for the central component and two gaussians for the satellite components in the wings. The gaussians are shown by dashed lines, their co-added sum by the gray line and the observed data by the continuous black line. Further details are provided in subsection 3.3.5.

5007Å and [NeV] 3426Å lines, clearly show an expanding hourglass shaped nebula around RS Oph (Bode et al. 2007, Harman et al. 2008). Such bipolar structure is commonly encountered in planetary nebulae and explained on the basis of the ejecta interacting with a non-uniform circumstellar environment. Alternatively, the ejection of the material could be intrinsically anisotropic but this scenario does not appear to be favored here (Harman et al. 2008). In the first scenario, if the pre-existing circumstellar material has a density enhancement in the equatorial plane then the outflowing ejecta is impeded from expanding in the equatorial region while expanding relatively more freely in the polar direction. This leads to a constriction of the nebula in the equatorial region thereby giving rise to an hourglass shape. Kinematically, this would imply that the matter in the poles would flow out with a high velocity relative to the matter in the waist of the hourglass. Evidence corroborating such a bipolar velocity flow was reported in interferometric studies by Chesneau et al. (2007) and from Hα line profile analysis by Skopal et al. (2008). By modeling the K band visibilities obtained 5.5 days after outburst, Chesneau et al. (2007) find evidence for two radial velocity fields - a slow expanding ring like structure (likely the waist of the nebula) with a velocity $\leq$ 1800 km/s and a faster structure (possibly originating from the polar regions) with a velocity of $\sim$ 2500-3000km/s. Skopal et al. (2008) obtain a similar result from their Hα profiles, taken early after the outburst, which shows a main emission component flanked by two weaker high velocity components in the wings (Figure 2 of Skopal et al. 2008).

Similar evidence for a bipolar flow is also seen from our near-IR data. To illustrate this, we present in Figure 3.7, representative profiles of the Pa β and Br γ lines on Feb 16.987. As can be seen, the profiles have a strong central component flanked by two weaker components. In both panels of Figure 3.7, we have fitted the profile with three gaussians - a central gaussian for the core emission component and two gaussians for the satellite components in the wings (the gaussians are shown by dotted lines, their sum by the gray line and the observed data by the continuous black line). It is seen that a three component gaussian fits the data reasonably well. The fits indicate the presence of two high-velocity components at radial velocities of -2540 and +2485 km/s for Pa β and at -2340 and 2160 km/s for the Br γ lines respectively (these high velocity components appear to be associated with the faster structure reported by Chesneau et al. 2007). The central components have FWHM's of $\sim$ 2200 and 1770 km/s for the Pa β and Br γ lines respectively. We can interpret the results of Figure 3.7 as follows viz. the core emission can be associated with the slower expanding material from the waist of the bipolar ejecta while the

higher velocity satellite components are associated with the flow from the polar regions. It may be mentioned that Skopal et al. (2008) draw a similar interpretation from their Hα profiles.

3.3.6 The Fe II lines at 1.6872 and 1.7414 μm

One of the more uncommon spectral features that are seen in our *H* band spectra are prominent lines of Fe II at 1.6872 and 1.7414 μm. In addition, also present in our *J* band spectrum of RS Oph is the 1.1126 μm Fe II line. This line constitutes one of the so-called "one micron Fe II lines" that are detected at 0.9997, 1.0171, 1.0490, 1.0501, 1.0863, and 1.1126 μm in novae (Rudy et al. 1991, 2000). The 1 micron lines, termed so by Rudy et al. (1991) because of their wavelength location, were first identified by Johansson (1977) in the spectrum of η Carinae and later seen in a variety of emission-line stars (Johansson & Jordan 1984; Hamann & Persson 1989; Rudy et al. 1991; Hamann et al. 1994) and in AGNs (Rudy et al. 2000, 2001; Rodriguez-Ardila et al. 2002). In comparison, the *H* band Fe II lines are rather uncommon, at least in novae spectra. In the case of novae, two of the earlier recorded instances of these lines are in the slow nova V2540 Ophiuchi (Rudy et al 2002) and possibly also in the recurrent nova CI Aquila (Lynch et al. 2004). One of the main processes for the excitation of the Fe II lines is considered to be Lyman α (Ly α) fluorescence. Additional excitation mechanisms are Ly continuum fluorescence and collisional excitation. Collisional excitation, which can play a significant role in enhancing the strength of the FeII lines (Bautista et al 2004), is discussed in greater details in subsection 3.3.6. We first consider the Ly alpha fluorescence process for the 1 micron lines. These lines specifically come from a three step process viz. the line proper comes from the decay of the $3d^5 4s^2 b^4G$ term at $\sim$ 6.72 eV above the ground state; this term being fed as a second step from decay of a $^4G^o$ term at $\sim$ 13.5eV which is originally pumped in the first step by Ly α fluorescence (Johansson & Jordan 1984).

In this context, we examine the viability of a similar Ly α excitation mechanism for the 1.6872 and 1.7414 μm lines (it appears that the excitation mechanism for these lines has been studied relatively less compared to the 1 micron lines). Using the atomic line database of Kurucz [1] we identify, at the relevant wavelengths, two Fe II lines at 1.6872 and 1.7414 μm which can undergo a similar three step Ly α excitation process. The 1.7414 μm line results from the decay of the $3d^6(^3_2F)4s\ c^4F$ term at $\sim$ 6.222

[1] http://cfa-www.harvard.edu/amp/ampdata/kurucz23/sekur.html

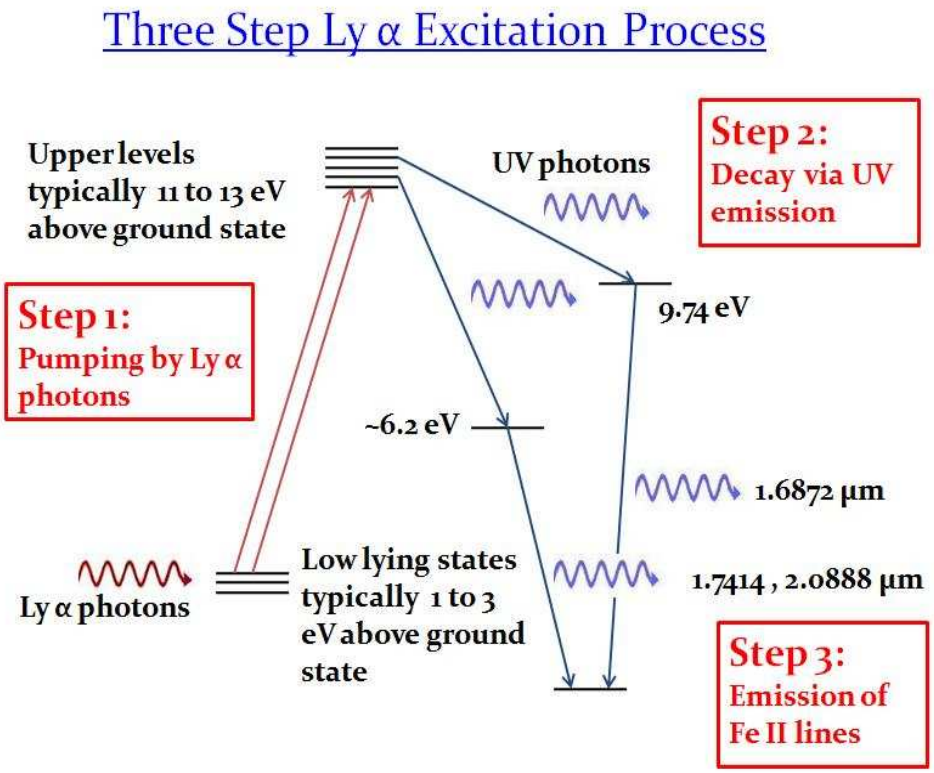

Figure 3.8: Schematic diagram explaining the three step Lyα excitation process. The FeII line at 2.0888 μm has been discussed in subsection 5.3.3.

ev above the ground state; the 1.6872 μm line from the $d^5 4s^2\ ^2G$ term at 9.743 eV. It so happens that both these upper levels of the 1.6872 and 1.7414 μm lines can be fed by not just one, but in fact by several high lying levels - each of these high lying levels capable of being pumped by Ly α photons (Figure 3.8 shows this process schematically). As examples for the 1.6872 μm line we note that photons at 1215.691 and 1215.707Å, which are closely coincident with the Ly α line center at 1215.671Å, can excite transitions from low lying levels in Fe II (at around 3.2 to 3.4 eV above ground state) to the higher excited levels (at around 13.4 to 13.6 eV). These higher levels can then decay via ultraviolet photons (at 1722.607 and 1683.961 Å respectively) to the upper level of the 1.6872 μm transition (viz. the $d^5 4s^2\ ^2G$ term) . Similarly for the 1.7414 μ line, photons at 1215.691 Å and 1215.873 Å can Ly α fluoresce from low lying levels in Fe II to the higher excited levels. These higher levels can then decay via UV photons (at 3370.341 and 3435.801 Å respectively) to the upper level of the 1.7414 μm transition (viz. the $3d^6(^3_2F)4s\ c^4F$ term). Since HI lines in novae (Ly α included) are routinely broad with widths extending upto a few thousands of km/s, additional Fe II transitions at wavelengths away from the Ly α line center could also contribute to the Ly α fluorescence process. It is noted from the Kurucz data, that there are indeed quite a few such lines - within a few Angstroms of the Ly α line center (1 Å corresponds to about 250 km/s at the Ly α wavelength) - that could also contribute to the Ly α fluorescence process. It thus appears that Ly α fluorescence is a viable mechanism for the excitation of the 1.6872 and 1.7414 μm lines.

In addition, it also needs to be examined whether Lyman continuum (Lyc) photons can also play a role in exciting these lines. If the nova ejecta is optically thick in Ly α, as is expected, then it should be optically thick in Lyc photons too - hence Lyc fluorescence could also take place. We find that this is indeed viable since several transitions of Fe II can be identified which are excited by Lyc photons to high-lying energy levels and subsequently followed by decay, via emission of an UV photon, to the upper levels of the 1.6872 and 1.7414 μm lines (one of several examples is the Fe II transition at 914.846Å between lower and upper states at 0.083 eV and 13.636 eV respectively which can be the subsequent decay of the higher excited state via a 1672.578Å line populates the upper level of the 1.7414 μm line).

Rudy et al. (2002) assigned the observed *H* band lines with FeII lines at 1.6873 and 1.7414 μm. We would agree with the identification of the 1.7414 μm line since a mechanism exists to account for its presence viz. Ly α and Lyc fluorescence as has been discussed. However, there is a possibility of an error in the identification of

the 1.6873 μm line. It is seen that actually there are two closeby lines of Fe II in this region viz at 1.68732 and 1.68719 μm respectively (air wavelengths). Identification of the observed feature with the 1.68719 μm (we refer to this as the 1.6872 μm line throughout the text) appears correct since this line, as demonstrated, can be excited by Ly α fluorescence. On the other hand the 1.6873 μm line, proposed by Rudy et al. (2002) arises in emission as a transition between the (^3F) 4s c^4F and (^5D) 4p z^4F states at $\sim$ 6.219 and 5.484 eV respectively. We are unable to identify any transition, arising from Ly α fluorescence, that can feed the upper level of this line directly or in a secondary step (as in the case of the other observed Fe II lines discussed so far). It therefore appears that the correct identification of the observed feature should be with the 1.68719 μm line.

3.3.7 Site of the near-IR line emission and studying the possibility of shock breakout

We study whether it is possible to identify the region in the ejecta from where the Fe II and the other near-IR emission lines arise. The excitation mechanism of the Fe II lines could offer a clue in this matter. While Ly α fluorescence could be a vital or possibly even the central process in exciting the Fe II lines, it may not be the sole mechanism and collisional excitation also plays a significant role. Such an inference is suggested from observations which show the absence, or greatly reduced strength from expected values, of the cascade lines that feed the upper levels of the 1 micron lines (Bautista et al. 2004 for a detailed discussion of the observational evidence). Bautista et al. (2004) show that Fe II has several high-energy pseudometastable levels and that collisional coupling between such metastable levels and radiative-emitting levels is considerable. They show that electron-impact-induced transitions from metastable levels strengthens lines throughout the emission spectrum and in particular strengthens the lines that result from secondary decay after Ly α pumping like the 1 μm lines. Model calculations of the emissivities (Bautista et al. 2004; Figure 1 therein) show that the peak emissivities of lines can be enhanced by a factor of ten or more when collisional transitions are taken into account vis-a-vis when these transitions are neglected in the calculations. The emissivities of the lines are found to be dependent strongly on the electron density and peak emissivities are seen to occur at high densities in the range 10^{10} to 10^{12} electrons/cm^3. The need for high particle densities to make these lines prominent is not surprising - it is under such conditions that the number of collisional excitations from the metastable levels can be expected to be enhanced.

In essence, the model calculations suggest that if the 1.6872, 1.7414 μm lines or the 1 μm lines are strong, then high density conditions are likely to be prevalent in the ejecta. This in turn, could offer an insight into the site of the Fe II emission. From an inspection of Figures 3.3 and 3.4 it is seen that the 1.6872 and 1.7414 μm lines remain prominent throughout the entire span of the observations. Since both lines flank the redward wings of Br 11 and Br 10 lines respectively, they are difficult to resolve as separate lines - even if they are present - during the early phases of the expansion when all the emission lines are broad. However, in spite of this, the presence of the 1.6872 μm line can be seen as a discernible inflection on the red wing of Br 11 in the 19 February spectrum. We interpret this to mean that high density conditions prevail from almost the beginning to the end of the observations in mid-May 2006 inspite of the considerable reduction in density that should be expected as the ejecta expands (in case of a geometric dilution with time i.e. n_e proportional r^{-2}, the electron density is expected to drop by a factor of around 250 to 1000 between Feb 15-19 to our last observation on 17 May).

A possible site, where such high density conditions can be generated and sustained as long as the shock lasts, is the region of discontinuity that is formed in a shock when a fast wind flows into a slow wind. Recent one dimensional hydrodynamical models have been developed by Vaytet et al. (2007) to study the structure and evolution of such a shock in the RS Oph system. Their models aim to revise and improve earlier studies (O'Brien, Bode and Kahn, 1992) by taking into account the ejection of material in the outburst as well as allowing the duration of the fast wind phase to be varied, as opposed to the instantaneous release of pure energy employed in their previous Primakoff-type models. In addition, Vaytet et al (2007) also include the effects of radiative cooling from the shocked gas which can significantly affect the dynamics of the system. Their model calculations show a complex structure for the shock front revealed through the presence of both forward and reverse shocks, with a separating contact discontinuity. In both their updated models viz. the adiabatic wind model and the radiatively cooled model, the contact discontinuity is found to be the site of high density and low temperature conditions (relative to the material in the forward and reverse shocked regions). These effects (enhancement of density and lowering of temperature) are more pronounced in the radiatively cooled model.

In view of the above, we thus propose that the Fe II emission, which is apparently favored by high-density conditions, originates from a region associated with the

contact discontinuity. In addition, Fe II is an ion of low ionization stage implying that it should originate in a zone of low kinetic temperature (a similar reasoning applies for the presence of neutral OI lines and suggests it coexists with Fe II). If our premise of associating the Fe II emission with the dense matter at the contact discontinuity is correct, then the fact that prominent Fe II emission is seen even upto $\sim$ 90 days after outburst would imply that the shockfront had not broken out even at that stage. When is breakout expected? The answer to this is complicated because of the bipolar velocity flow in the nebula. Since the polar flow is much faster than the equatorial flow (Figure 3.7, subsection 3.3.5), it should breakout much earlier. On the other hand, again from Figure 3.7, there appears to be lesser contribution to the line luminosity from the high-speed bipolar jets vis-a-vis that from the equatorial flow. Thus even if a breakout takes place in the polar direction and contribution to Fe II emission from this region ceases, the bulk of the Fe II emission will still be expected from the shockfront in the equatorial plane that has still to break out. In general, breakout will occur when the shockfront traverses a distance equal to the finite extent of the redgiant wind - this equals the product of the velocity of the red giant wind and the time elapsed since the 1985 outburst (i.e. 21 years). The velocity of the red giant wind has been estimated to be in the range 10-20 km/s (Gorbatski 1972). For this velocity range and adopting a mean value of 1000 km/s for the shockfront velocity in the equatorial plane (from the FWHM values reported here or in Das et al. 2006), breakout in the equatorial direction could be expected between 75-150 days. This timescale is consistent with our conclusion that breakout may not have occurred till even $\sim$ 90 days after outburst. The break-out time estimates are susceptible to errors because of uncertainties in the parameters involved (viz. the velocities of the red giant wind and the shockfront). However, recombination analysis of the HI lines in the following section, are reasonably in line with the conclusions drawn here.

3.3.8 Recombination analysis of the HI lines

We present in Figure 3.9 the recombination Case B analysis for the HI lines on six reasonably equispaced epochs that sample the evolution upto 94 days after the outburst. The observed spectra were flux calibrated using the *JHK* magnitudes of Table 3.2 after correcting for reddening using $E(B-V) = 0.73$ (or $A_v = 2.26$; Snijders 1987). The observed line luminosities were then compared with the Case B emissivities of Storey & Hummer (1995). Three points may be made regarding Figure 3.9. Since Case B calculations are only mildly sensitive to changes in the

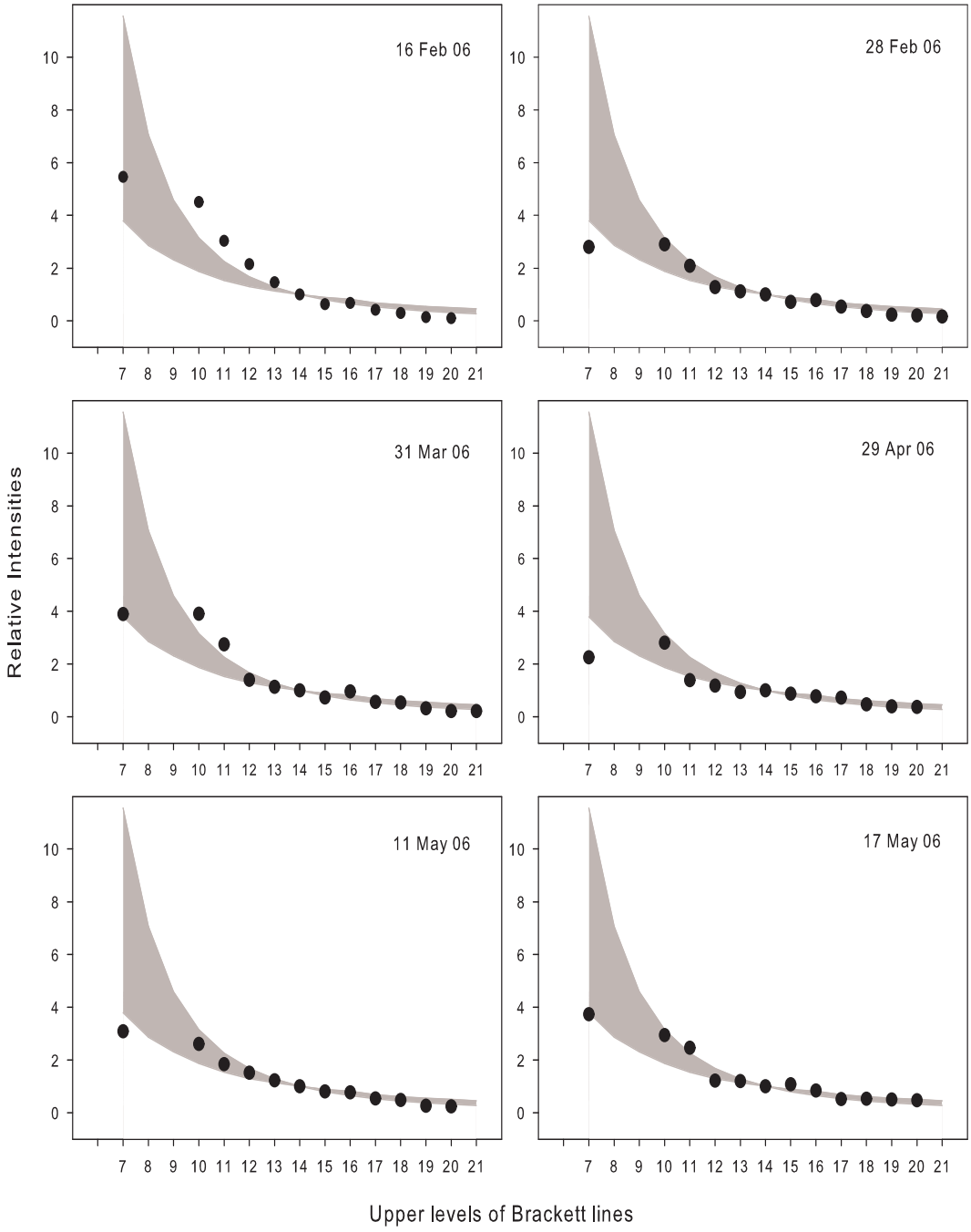

Figure 3.9: A comparison of the observed Brackett line intensities on different days with Case B predictions. The shaded area in each panel indicates the range over which the Case B model values are spread for the electron density n_e varying between 10^5 to 10^{12}cm^{-3} and temperature T between 5000K to 20000K. The Br lines have been normalized to unity at Br 14, for both Case B values and also for the observed data. The error in the strengths of the Br 10 and 11 lines is $\sim$ 30 percent and in the range of 10 to 15 percent for the other lines. Further details are given in subsection 3.3.8

electron density n_e and temperature T, we have shown by the gray shaded area, the case B predictions (normalized to unity at Br 14) for the parameter space of n_e varying between 10^5 to 10^{12} cm^{-3} and T varying between 5000 to 20000K. By showing an extended range in the parameter space, it becomes easier to establish when observed data clearly falls outside the range of plausible model values. The second point concerns the errors involved in comparing the luminosities of lines situated in different bands (Pa β in J band, Br 10-21 in H band and Br γ in K band). The robustness of the estimated line luminosities depends on how reliably the flux in the continuum has been calibrated in each of these bands which in turn depends on how reliable is the estimate of the reddening in the band concerned (the amount of extinction in each of the J,H and K bands is different). Thus as a cross-check for the extinction of A_v = 2.26 obtained by Snijders (1987), we note that modeling of the galactic interstellar extinction by Marshall et al. (2006) indicates a extinction in the direction of RS Oph of A_k = 0.21 to 0.25 (or A_v = 2.1 to 2.5 for $A_v = 10A_k$) for an adopted distance of 1.6 kpc (Snijders 1987) to the source. Thus there is a consistency in the A_v values estimated by different authors and it is unlikely that major errors are being introduced in the analysis by an incorrect estimate of A_v. The third point concerns the difficulty in estimating the equivalent widths (and hence line luminosities) of the Br 10 and 11 lines because they are so strongly blended with the Fe II lines. We have measured the equivalent widths of these lines after trying to deblend the features using gaussian fits but the exercise is not entirely satisfactory. Thus, while we do show the Br 10 and 11 lines in Figure 3.9, their strengths are subject to considerable uncertainty (of about 30 percent) and they should be accepted with caution; the formal error in the strength of the other lines is in the range of 10 to 15 percent.

Examination of the spread in the Case B values in Figure 3.9 (the gray shaded area) indicates that the higher Br lines (Br15 to 20) are really not sensitive enough to discriminate whether there are deviations between the observed data and Case B model values. The lines that are sensitive are Br γ and Pa β. In RS Oph, except for the 16 Feb 2006 data, it is seen that Br γ is consistently weaker than expected and that the Br γ/Br14 ratio is generally in the range of 2 - 4 against an expected median value of $\sim$ 6. There is also a suggestion that Br 10 and Br 11 are stronger than expected and Br 10 nearly equal to or stronger than Br γ on all days except 16 Feb. Departures in the ratio of Pa β/Br γ from Case B are also seen - this ratio is expected to be around 6 whereas we obtain values of around 6.5, 9.5, 11.5,15,11 and 6 for the six days shown in Figure 3.9. Thus the Pa β/Br γ ratio diverges

considerably from Case B on most days except Feb 16 and May 17. However, on May 17, the Br lines do not conform to Case B behavior - the Br γ/Br14 ratio is low. The general conclusion that is therefore suggested, after taking into account the behaviour of all the HI lines, is that the Feb 16 data conforms to a reasonable extent with Case B conditions; on other days there are marked deviations from it. On these days, the observed behaviour of the Br lines i.e the presence of a Br γ line that is weaker than expected when compared to the higher Br lines accompanied by the additional observation that the Br line strengths are possibly peaking around Br 10 to 11 (instead of at Br γ), suggests that the Br lines are optically thick. Such behaviour of the Br lines has been observed in other novae like Nova Ophiuchi 1998 (Lynch et al. 2000) and V4643 Sgr (Ashok et al. 2006) and also in Be stars (Banerjee et al. 2001). Such effects have been shown by Lynch et al. (2000) to arise from optical depth effects in an environment with high particle densities (n_e = 10^{10} to 10^{12}cm^{-3}) which tends to thermalize the level populations through collisions. It would thus appear that invoking high density conditions could explain the observed deviations from Case B. It is also noted that such high density conditions prevailed throughout our observations except in the very beginning at around 16 Feb 2006. At this stage, just four days after the outburst, the ejecta has been clearly shown to be in a free expansion stage. That is, it had not yet swept up enough of the red giant wind for the deceleration to begin and possibly for the dense contact surface of the shockfront to fully develop. Hence, the high density conditions, that can create a departure from Case B, were likely to be absent at this time. The Fe II line analysis of the previous subsection, which also suggested the need for high density conditions, is consistent with the line of argument suggested here.

3.3.9 Evolution of the coronal lines

We consider the temporal evolution of the [Si VI] 1.9641 μm and the [Mn XIV] 2.0894 μm coronal lines here. The uncertainty in the assignment of the latter line to [Mn XIV] has already been discussed earlier; we proceed by assuming that this assignment is correct. The observed strength of these lines on different days is presented in Table 3.5 and their temporal evolution is shown in Figure 3.10. The [Si VI] line is first detected clearly on around Mar. 26.88 ($\sim$ 42 days after outburst). It then increases in strength, peaking at around March 30.86 ($\sim$ 46 days after outburst) and subsequently declines in intensity. The [Mn XIV] line appears on Mar. 2.95 ($\sim$ 18 days after outburst), earlier than the [Si VI] line, but shows a similar evolution in the sense that it increases in strength with time and subsequently declines.

Unfortunately, no spectra were recorded between 3 to 16 March 2006 (i.e. 18 to 32 days after outburst) to monitor the evolution of the [Mn XIV] line during this period. The observed temporal behaviour of the coronal lines can be interpreted in a simple manner. The coronal lines are expected to arise from the hot, shocked gas in the shockfront. This gas, whose temperature in the very early stages was determined to be as high as $\sim 10^8$ K (Sokoloski et al. 2006), gradually cools with time. The fractional abundance of an ion (e.g. N(Si VI)/N(Si)) in a collisionally ionized, low density plasma is known to be temperature dependent. Model calculations show that the fractional abundance of Si VI peaks at a temperature of 4×10^5 K (Jordan 1969; Shull and van Steenberg, 1982) while the Mn XIV ion peaks at 1.6×10^6 K respectively (Landini and Monsignori Fossi, 1972). Since the strength of a line associated with an ion is proportional to the abundance of the ion, it is expected that the strength of the line will change as the temperature of the plasma changes (thereby changing the abundance of the ion). It would appear that this phenomenon is being manifested here. As the shocked gas in the RS Oph system cools, a temperature will be reached that is conducive for the formation of a particular ion to begin. Subsequent lowering of the temperature should see the fractional abundance of the ion reach its peak value at the optimum temperature for its production and the fractional abundance should subsequently decline as the temperature continues to decrease.

The temporal evolution of the [Si VI] and [Mn XIV] lines, as shown in Figure 3.10, is consistent with such a scenario (there is, however, a possible complication which is discussed shortly) . Further, since the 2.0894 μm line is detected earlier than the [Si VI] line (therefore at a phase when the shocked gas is relatively hotter), the analysis suggests that it is likely that the 2.0894 μm line originates from an ion with higher ionization potential than Si VI. In this sense it is consistent to identify this line with [Mn XIV] since it has a higher ionization potential of 344 eV compared to 166.8 eV for [Si VI]. Since the [Mn XIV] and [Si VI] line emission peaks on March 16.95 and March 30.86 respectively, the temperatures on these days are indicated to be 1.6×10^6 K and 4×10^5 K respectively based on the ionization balance models discussed earlier (Jordan 1969; Shull and van Steenberg, 1982; Landini and Monsignori Fossi, 1972). These temperatures may be compared with those derived from X-ray observations on nearby dates. Nelson et al. (2008) obtain a value of 6.3×10^6 K on 11-12 March 2006 (day 27.7 after outburst; Table 4 of Nelson et al. 2008). This is reasonably in agreement with the temperature of 1.6×10^6 K that we obtain on March 16.95. Ness et al. (2007) determine a temperature range of (6.3 - 8.3)$\times10^5$

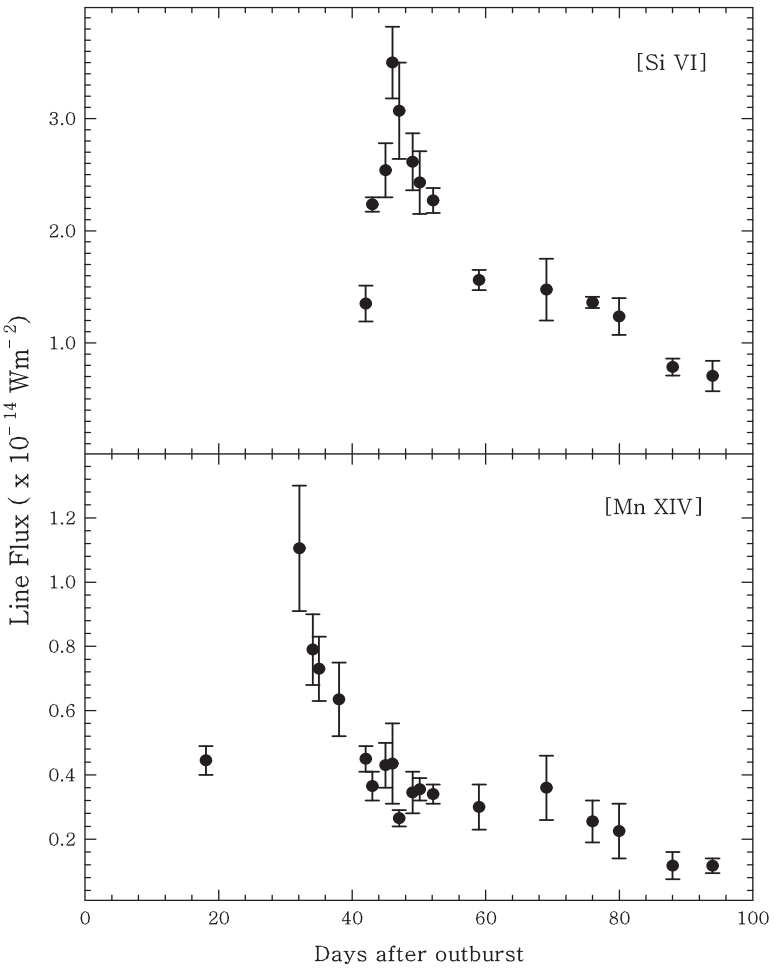

Figure 3.10: Temporal evolution of the de-reddened line strengths of the [Si VI] 1.9641 μm and [Mn XIV] 2.0894 μm lines. Further details are given in subsection 3.3.9.

K on day 39.7 after outburst (24 March 2006) while we get a value of 4×10^5 K on March 30.86. Here too, the temperature estimates are in reasonable agreement with each other.

In the case of RS Oph, a complication that arises in applying models for the fractional ion abundance, based on purely collisional effects, is that the effect of any radiation field is assumed to be negligible. X-ray spectra in the initial stages after outburst clearly indicate that the plasma in RS Oph is collisionally dominated (Nelson et al. 2008). However, these authors observe a super soft x-ray phase in RS Oph during weeks 6-10 arising from the hot central white dwarf (white dwarf) whose temperature was estimated to be 800,000K. The radiation field from the central white dwarf could thus be expected to affect the ionization balance in

Table 3.5: Evolution of the coronal lines.

Date of Observation	Days after outburst	Line flux (x 10^{-14} W m^{-2}) [Si VI]	[Mn XIV]
Mar. 2.9465	18.1165	-	0.445 ± 0.045
Mar. 16.9465	32.1165	-	1.105 ± 0.195
Mar. 18.9372	34.1072	-	0.790 ± 0.110
Mar. 19.8833	35.0533	-	0.730 ± 0.100
Mar. 22.8682	38.0382	-	0.635 ± 0.115
Mar. 26.8778	42.0478	1.350 ± 0.160	0.450 ± 0.040
Mar. 27.8644	43.0344	2.235 ± 0.065	0.365 ± 0.045
Mar. 29.8462	45.0162	2.540 ± 0.240	0.430 ± 0.070
Mar. 30.8629	46.0329	3.500 ± 0.320	0.435 ± 0.125
Mar. 31.8701	47.0401	3.070 ± 0.430	0.265 ± 0.025
Apr. 2.8736	49.0436	2.615 ± 0.255	0.345 ± 0.065
Apr. 3.9691	50.1391	2.430 ± 0.280	0.355 ± 0.035
Apr. 5.9607	52.1307	2.270 ± 0.110	0.340 ± 0.030
Apr. 12.8454	59.0154	1.560 ± 0.090	0.300 ± 0.070
Apr. 22.9392	69.1092	1.475 ± 0.275	0.360 ± 0.100
Apr. 29.8355	76.0055	1.360 ± 0.050	0.255 ± 0.065
May 3.8100	79.9800	1.235 ± 0.165	0.225 ± 0.085
May 11.8353	88.0053	0.785 ± 0.075	0.118 ± 0.043
May 17.8103	93.9803	0.705 ± 0.135	0.117 ± 0.023

the ejecta. We consider it a difficult problem, beyond the scope of this work, to assess the extent to which the white dwarf radiation field - in conjunction with collisional ionization - affects the ionization balance. We, however, note that our analysis/discussion on the [Mn XIV] line is unlikely to be affected by the super soft x-ray phase since this phase began towards the end of March (Nelson et al. 2008) after the [Mn XIV] line had peaked in intensity. However, the [Si VI] line emission, could be affected to some extent by the super-soft X-ray phase.

3.4 Summary of the work

In this chapter, we have presented near-infrared photo-spectroscopy in the *J*, *H* and *K* bands of the 2006 outburst of the recurrent nova RS Ophiuchi (RS Oph). The observations cover the period between 1 to 94 days after the eruption. The near infrared light curve is presented. An extensive set of spectra are presented, lines

identified and the general characteristics of the spectra discussed. The key result concerns the rare detection of an infrared shock wave as the nova ejecta plows into the pre-existing wind of the secondary in the RS Oph system consisting of a white dwarf primary and a red giant secondary. The evolution of the shock is traced through a free expansion stage to a decelerative phase. The behavior of the shock velocity with time is found to be broadly consistent with current shock models. The present observations also imply that the white dwarf in the RS Oph system has a high mass indicating that it could be a potential SN Ia candidate. Analysis of the HI line profiles show the presence of broad wings on both flanks of a strong central component indicating the presence of a bipolar velocity flow in the ejecta. Such a flow is kinematically consistent with the bipolar structure that the object displays in high-resolution spatial images. We discuss the behaviour and origin of the Fe II lines at 1.6872 and 1.7414 μm that are prominently seen throughout the span of the observations. It is examined and shown that Lyman α and Lyman continuum fluorescence are viable mechanisms to excite these lines. We draw upon the result, that collisional excitation can also contribute in exciting and significantly enhancing the strength of these Fe II lines, to propose that these lines originate from a site of high particle density. Such a likely site could be the high-density, low temperature contact surface that should exist in the shockfront in between the shocked ejecta and red giant wind. Recombination analysis of the HI lines indicate deviations from Case B conditions during most of the span of our observations indicating optical depth effects. It appears likely that the breakout of the shockfront had not yet occurred till the end of our observations. An analysis is made of the temporal evolution of the [Si VI] 1.9641 μm coronal line and another coronal line at 2.0894 μm which is attributed to [Mn XIV]. Assuming collisional effects to dominate in the hot coronal gas, estimates are made of the ion temperature in the gas.

CHAPTER 4

Study of the Dust Forming Nova V1280 Scorpii

4.1 Introduction

Nova V1280 Scorpii (V1280 Sco) was discovered on 2007 February 4.8 independently by Sakurai and Nakamura (2007), within a short time of each other, with a reported visual magnitude in the range 9.4 - 9.9. The nova brightened quickly to its maximum in visual light on Feb. 16.19 (m_{vmax}= 3.79, Munari et al. 2007a) to become one of the brightest novae in recent times (Schmeer 2007); V1500 Cyg in 1975 had a m_{vmax}=2.0 and nova V382 Vel 1999 had m_{vmax} =2.5. V1280 Sco has been observed in different wavelength regimes since its discovery. Early stage pre-maxima spectra was described by Munari et al. (2007a, 2007c) and Naito & Narusawa (2007a) in the visible region and by Rudy et al. (2007a, 2007b) in the infrared. The early spectrum was dominated by absorption lines of hydrogen, neutral nitrogen and carbon, and displayed deep P-Cygni profiles. After passing the maxima the spectrum turned to that typically shown by a classical nova; the lines started appearing in emission which included strong emission lines of Ca II H and K, the hydrogen Balmer series, the Na I D doublet, and Fe II 42, 49 and 74 in visible region (Buil 2007; Munari et al., 2007c). Early near-IR spectra by Das et al. (2007a) reported the presence of HI Brackett and Paschen lines and several strong C I lines. No X-ray detection was reported from the source from RXTE and SWIFT observations respectively (Swank et al. 2007; Osborne et al. 2007).

The nova has an interesting lightcurve with the possibility of more than one outburst. After passing the maxima, a smooth and slow decline followed. This was interrupted, about 24 days after discovery, by the formation of dust which was

evidenced from the sharp decline in visible light curve and a rise in the infrared continuum (Das et al. 2007b). The dust shell has been directly detected by interferometric techniques and its subsequent spatial expansion has also been tracked (Chesneau et al. 2008). Apart from providing the first direct detection of a dust shell around a classical nova, the Chesneau et al. (2008) study emphasises the important, emerging role of interferometry in the study of dust formation and dust properties in novae. We present here spectroscopic and photometric results based on observations between 14 and 125 days after the discovery. A large number of spectra were recorded, sampling the nova's evolution at regular intervals, thereby leading to one of the most comprehensive studies of a classical nova in the near-infrared.

4.2 Observations

Observations of V1280 Sco in Near-IR *JHK* were obtained at the Mt. Abu 1.2m telescope. Near-IR *JHK* spectra presented here were obtained at similar dispersions of $\sim$ 9.75 Å/pixel in each of the J, H, K bands using the Near Infrared Imager/Spectrometer with a 256×256 HgCdTe NICMOS3 array. Following the standard procedure, outlined in chapter 2, the nova spectra were ratioed with the spectra of a comparison star (SAO 184301; spectral type A0V). The lack of a suitably bright standard star close to the nova, thereby leading to our choice SAO 184301, led to some difference in airmass between the nova and standard star observations. Thus, the ratioing process, while removing telluric features sufficiently well, does leave some residuals. This applies to regions where telluric absorption is strong (specifically the 1.12 μm region in the J band and the 2 to 2.05 μm region in the K band affected by atmospheric oxygen and carbon-dioxide respectively; we have thus excluded the latter K band region from our spectra).

Photometry in the *JHK* bands was done in photometric sky conditions using the imaging mode of the NICMOS3 array. Several frames of the nova and a standard star (SAO159963 (V=4.29, J=2.89, H=2.47, K=2.33) or 2MASS J16232693 -2425291 (J=7.340,H=6.027,K=5.464)) were observed at five dithered positions. The observed data were analyzed using IRAF tasks as described in chapter 2. The log of the photometric observations and the derived *JHK* magnitudes, with typical errors in the range 0.01 to 0.03 magnitudes, are given in Table 4.1.

Table 4.1: A log of the photometric observations of V1280 Sco. The date of outburst is taken to be 2007 Feb 4.854 UT.

Date 2007 (UT)	Days since Outburst	Magnitudes		
		J	*H*	*K*
Feb. 19.972	15.118	3.33	3.05	2.78
Feb. 25.962	21.108	3.58	3.09	2.77
Feb. 27.991	23.137	4.00	3.63	3.79
Mar. 01.992	25.138	4.71	4.27	4.21
Mar. 03.996	27.142	5.42	4.43	3.55
Mar. 05.991	29.137	6.23	4.88	3.62
Mar. 07.995	31.141	6.68	5.09	3.78
Mar. 10.986	34.132	6.82	5.15	3.93
Mar. 13.979	37.125	7.21	5.45	4.03
Mar. 27.950	51.096	7.62	5.51	3.88
Mar. 28.971	52.117	7.72	5.61	3.83
Mar. 31.981	55.128	8.25	5.98	4.13
Apr. 01.972	56.118	8.29	6.04	4.19
Apr. 02.981	57.127	8.25	5.97	4.01
Apr. 03.988	58.134	8.32	6.04	3.90
Apr. 05.975	60.121	8.27	6.08	4.20
Apr. 08.982	63.128	8.27	6.05	4.05
Apr. 15.963	70.109	8.10	5.90	3.91
Apr. 18.953	73.099	7.89	5.78	3.93
Apr. 26.871	81.017	8.84	6.58	4.52
Apr. 30.890	85.04	8.85	6.70	4.62
May 02.920	87.066	8.69	6.38	4.36
May 03.922	88.068	9.10	6.71	4.49
May 04.899	89.045	9.33	6.95	4.81
May 05.920	90.066	9.06	6.79	4.63
May 06.898	91.044	8.64	6.38	4.26
May 08.910	93.056	9.13	6.77	4.62
May 15.798	99.944	8.81	6.41	4.11
May 22.800	106.946	7.26	4.94	3.06
May 30.811	114.957	7.36	5.16	3.25
Jun. 02.809	117.955	7.73	5.47	3.23
Jun. 05.791	120.937	8.08	5.73	3.67
Jun. 07.772	122.918	8.23	5.78	3.58
Jun. 10.773	125.919	8.15	5.77	3.81

4.3 Results

4.3.1 Optical lightcurve

Before presenting the results proper, we estimate some of the useful parameters for V1280 Sco. The optical lightcurve is presented in Figure 4.1. As seen, V1280 Sco is one of those few novae in which the light-curve data in the pre-maximum stage is well documented - two other novae, which come readily to mind, in which the pre-maximum ascent is similarly well studied and used to determine the onset of eruption are V1500 Cyg and PW Vul (Gehrz 1988 and references therein). After the maximum, the light curve declined steadily but was interrupted by dust formation around 24 days after discovery. We discuss in detail subsequently the dust formation phase and other specific phases in the light-curve evolution. For the present we wish to determine t_2, the time for a decline of two magnitudes in the visual band, and note that the light curve indicates that dust formation had begun even before t_2 was reached. Hence to estimate t_2, we have extrapolated the light-curve linearly in the post-maximum decline stage, as would have been the case had dust not formed at all, and thereby estimate t_2 to be approximately 21 days though slightly smaller values may also be supported. Using the MMRD relation of Della Valle and Livio (1995) we determine the absolute magnitude of the nova to be M_v = 7.88 and obtain a distance estimate to the object d = 1.25 kpc for an assumed value of A_v = 1.2 as inferred from the extinction in the direction of V1280 Sco from the work of Marshall et al. (2006). It should be noted that the estimated value of d could be subject to significant uncertainty. This arises from errors in estimating t_2, A_v and also from the intrinsic errors associated with the MMRD relations.

Henden & Munari (2007) have made post-outburst astrometric and photometric measurements of the stars in the field around V1280 Sco and generated a photometric sequence to calibrate archival plates. Using SuperCosmos plates, a comparison was made between the magnitudes of stars therein with those of Henden & Munari (2007). A good consistency is found which allows us to conclude from the SuperCosmos data that no star is seen at the nova's position down to B and R magnitudes of 20.3 and 19.3 respectively. A lower limit on the outburst amplitude A of the nova in the visual region can therefore be estimated to be in the range of $\sim$ 15.5 to 16 magnitudes. Apart from the amplitude of the outburst being rather large, the compiled data of A versus t_2 for different novae (Warner 2008) show that V1280 Sco is very much an outlier. This, together with its long rise to maximum, early dust formation and the the presence of a late-time, secondary outburst makes

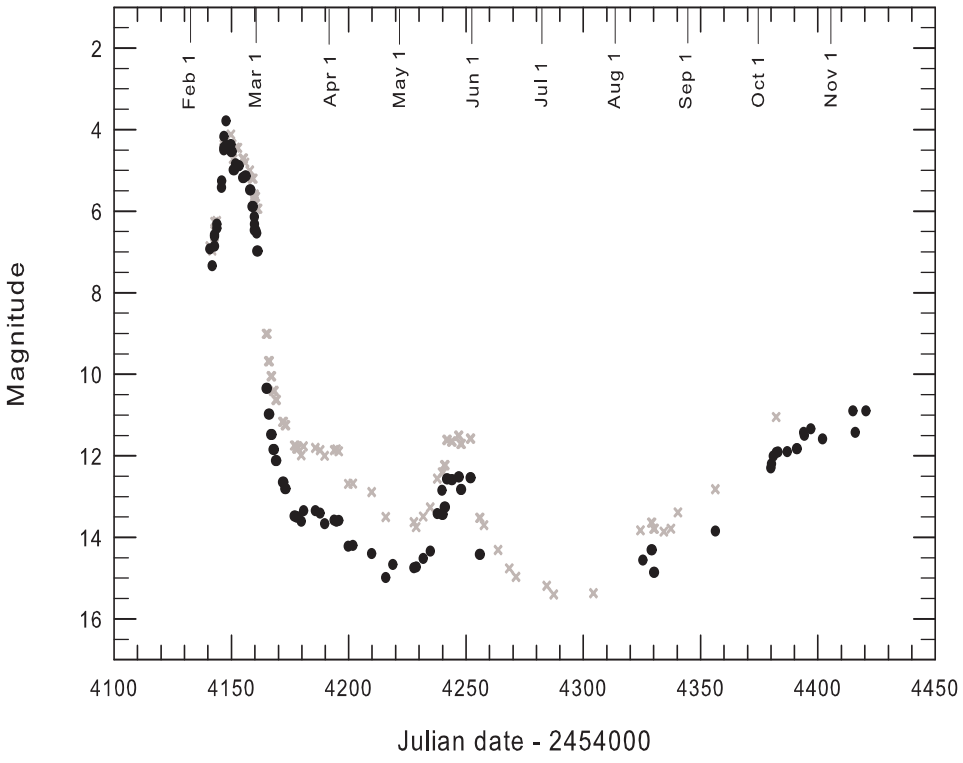

Figure 4.1: The V and R_c light curves (black circles and gray crosses respectively) of V1280 Sco from data obtained from IAU circulars, VSNET alerts, VSOLJ and AFOEV databases ((Variable Stars Network, Japan; Variable Star Observers League in Japan; Association Francaise des Observateurs d'Etoiles Variables, France).

the object somewhat unusual.

4.3.2 General characteristics of the *JHK* spectra

The log of observations for the spectroscopy is presented in Table 4.2. Instead of presenting all the spectra, we have rather chosen representative spectra sampling the observations at regular intervals which effectively convey the trend/behavior of the spectral evolution. These *JHK* spectra are presented in Figures 4.2, 4.3, and 4.4 respectively. The earliest spectra of 18 Feb show the lines to display P-Cygni structures with the absorption components considerably stronger than the emission components which are just beginning to appear. This is consistent with the near-IR spectroscopy of Rudy et al. (2007b) between 14 and 16 Feb. wherein they report that the lines of hydrogen were in absorption; emission lines almost entirely absent and Pa β and Br α were just beginning to exhibit hints of emission and P-Cygni behavior. By 19 Feb, the emission components of the P-Cygni profiles become stronger than the absorption components and by 24 February the spectra become of pure emission type typical of a classical nova soon after maximum light. The emission lines remain at significant strength thereafter till the first week of March after which they lose contrast against the rising continuum from dust emission. The formation of dust in the ejecta at around the beginning of 2007 March can also be inferred - apart from it being seen as a drop in the visible light curve - from the change seen in the slope of the near-IR continuum. In each of the *JHK* bands a rise in the continuum towards longer wavelengths is clearly seen. The development of this infrared excess, attributable to dust, is seen till the end of our observations indicating that the freshly-formed dust persists till then or is augmented by further episodes of dust formation. A detailed investigation of these aspects and analysis of the dust shell properties and kinematics is given in Chesneau et al. (2008).

4.3.3 Line identification and detailed study of spectral features

To facilitate a better understanding of the lines that contribute to a nova's spectrum, a model is developed based on local thermal equilibrium (LTE) considerations. It is likely that the model has limitations, based as it is on LTE assumptions which may not strictly prevail in an nova environment. Yet, we show that the model-generated spectra, greatly aids in a secure identification of the lines observed and also gives additional valuable insights. The synthetic spectrum is computed along similar lines as for nova V445 Pup in Ashok & Banerjee (2003) but is extended further here. The model spectra are generated by considering only those elements whose

Table 4.2: A log of the spectroscopic observations of V1280 Sco. The date of outburst is taken to be 2007 Feb 4.854 UT.

Date 2007 (UT)	Days since Outburst	Integration time (sec) J	H	K
Feb. 18.981	14.127	10	10	10
Feb. 20.006	15.152	10	10	10
Feb. 24.990	20.136	10	10	10
Feb. 25.997	21.143	10	10	10
Feb. 26.968	22.114	10	8	10
Feb. 27.972	23.118	10	8	10
Mar. 01.964	25.110	10	15	15
Mar. 03.961	27.107	20	15	20
Mar. 04.961	28.107	20	20	20
Mar. 05.965	29.111	45	20	20
Mar. 06.965	30.111	40	30	30
Mar. 07.951	31.097	60	20	20
Mar. 10.963	34.109	90	45	30
Mar. 13.950	37.096	100	40	30
Mar. 28.928	52.074	150	60	30
Mar. 31.920	55.066	300	45	30
Apr. 02.902	57.048	300	40	30
Apr. 05.905	60.051	350	60	40
Apr. 18.891	73.037	500	60	30
Apr. 27.870	82.016	500	60	45
May. 04.954	89.100	450	60	45
May. 06.833	90.979	500	45	30
May. 22.865	107.011	300	40	20
May. 30.854	114.999	350	40	30
Jun. 05.758	120.904	400	90	30
Jun. 08.836	123.982	350	60	40

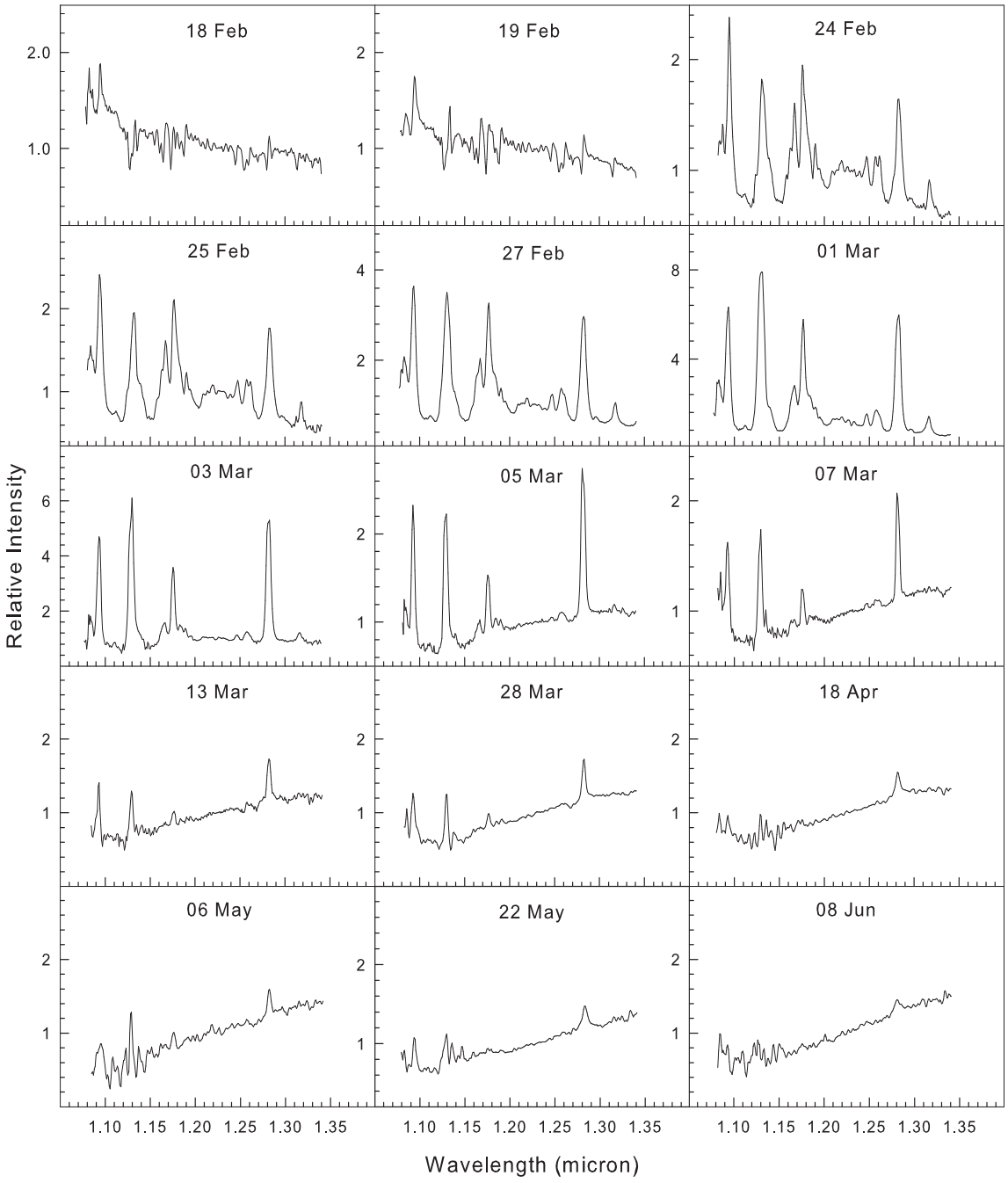

Figure 4.2: The *J* band spectra of V1280 Sco on different days with the flux normalized to unity at 1.25 μm.

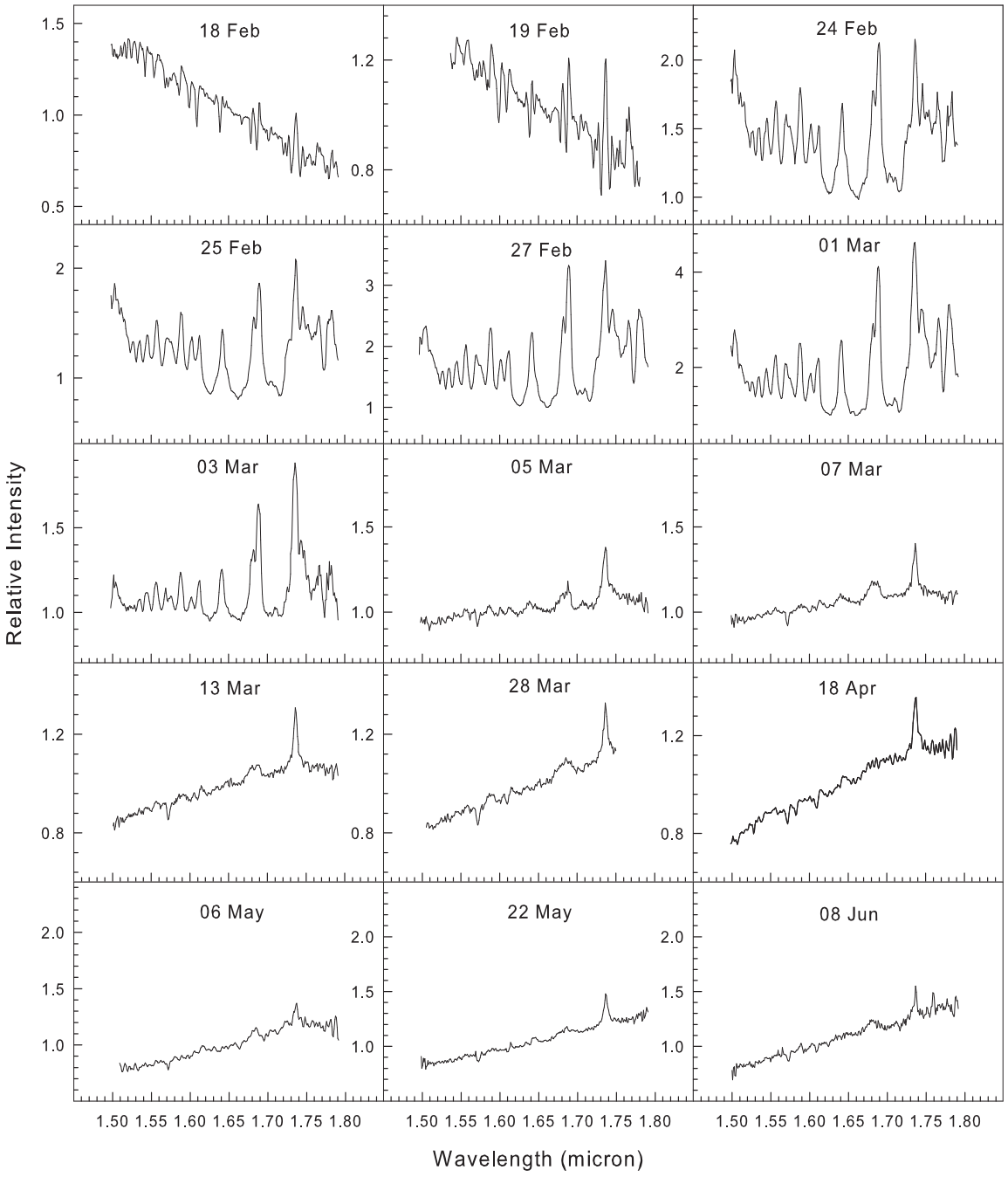

Figure 4.3: The *H* band spectra of V1280 Sco on different days with the flux normalized to unity at 1.65 μm.

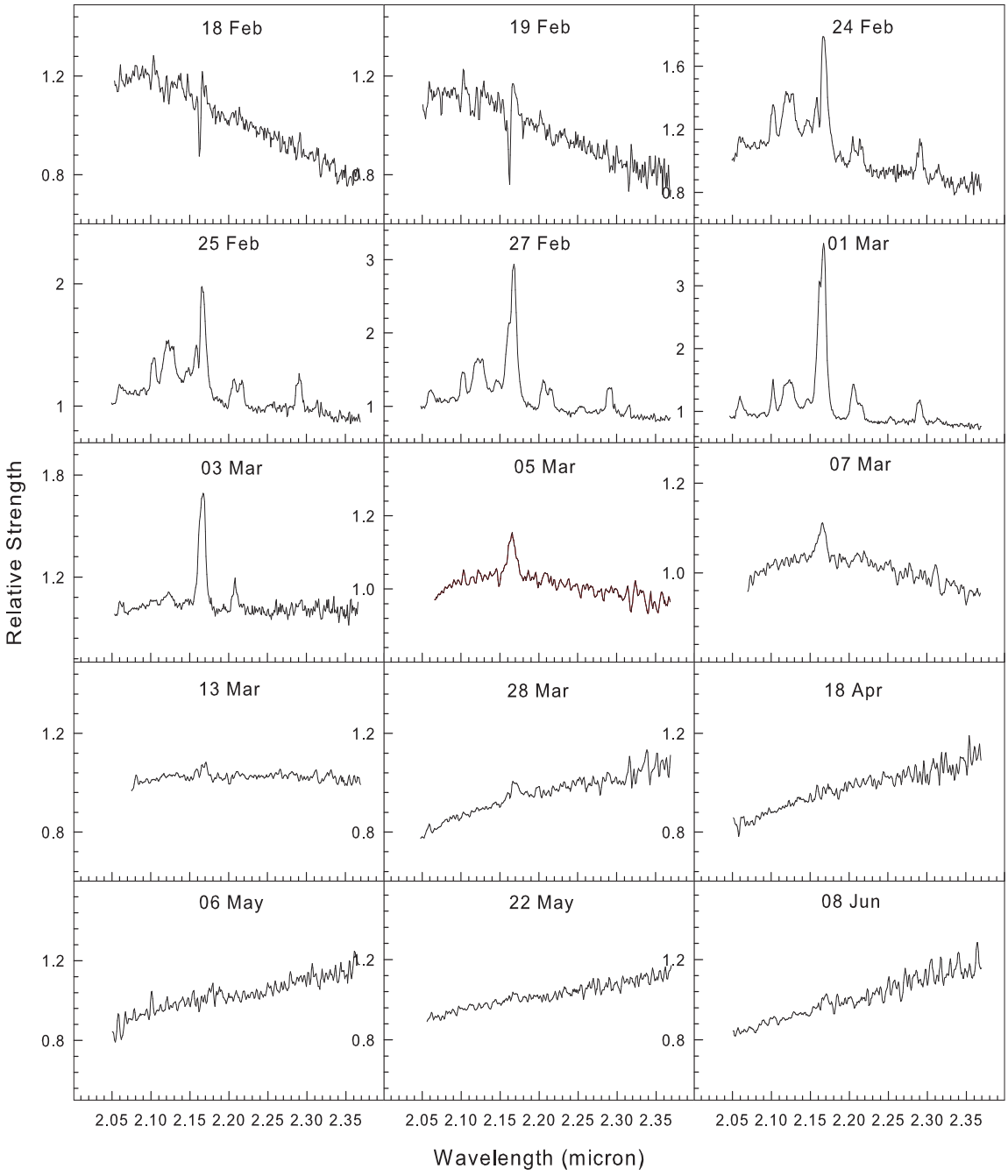

Figure 4.4: The *K* band spectra of V1280 Sco on different days with the flux normalized to unity at 2.2 μm.

lines can be expected at discernible strength. Since nucleosynthesis calculations of elemental abundances in novae (Starrfield et al. 1997; Jose & Hernanz 1998) show that H, He, C, O, N, Ne, Mg, Na, Al, Si, P, S are the elements with significant yields in novae ejecta, only these elements have been considered. For a particular element, we have first used the Saha ionization equation to calculate the fractional percentage of the species in different ionization stages (neutral plus higher ionized states). Subsequently the Boltzman equation is applied to calculate the population of the upper level from which a transition of interest arises. The transitions of interest are essentially all the stronger lines of the above elements in the region of interest (1-2.5 μm) region which was compiled from the Kurucz atomic line list[1] and National Institute of Standards and Technology (NIST)[2] line list database. From the database, for each line the statistical weight of the upper level of the transition, the energy difference between the upper energy level and the ground state; and the transition probability is also noted. Given these parameters, and the partition functions (adopted from Allen 1976; Aller 1963), the population of the upper level for a particular transition - under LTE conditions - can then be derived from the Boltzman equation and the line strength can subsequently be calculated knowing the transition probability. For simplicity we assume that the shape of each line can be reasonably represented by a Gaussian whose strength is known from the computed line strength and whose width can be adjusted to match that of the observed profiles. The co-addition of all such Gaussians - corresponding to all the lines - yields a model spectrum. In computing a model spectrum, values of certain parameters need to be assumed viz. the electron density N_e (needed in the ionization equation); the gas temperature T (needed in both the Saha and Boltzmann equations) and the assumed abundances of the elements. We have considered typical values found in nova ejecta in the early stages viz. N_e in the range 10^9 to 10^{11} cm^{-3}, $T \sim$ 4000 - 10000K and abundances in line with those of CO novae given in Starrfield et al. (1997) and Jose & Hernanz (1998).

The computed spectrum is presented, overlaid with a representative observed spectrum for comparison, in Figure 4.5 with the lines identified. The list of identified lines is given in Table 4.3. While most of the lines observed are known and identified from previous studies, there are a few subtle aspects influencing specific lines which are likely to have gone unnoticed or whose significance could be under emphasized. A better understanding of these nuances emerge from our analysis.

[1]http://cfa-www.harvard.edu/amp/ampdata/
[2]http://physics.nist.gov/PhysRefData/ASD

One such aspect is determining the relative contribution of different species to a particular spectral feature/line. Since in our model, trial spectra can be computed for one element at a time, the position and strength of all the lines of this element can be determined. Thus it becomes clear to assess whether a particular line, at a particular wavelength, has one or more species is contributing to it. On the basis of such an analysis we arrive at the following conclusions:

1. In the *J* band there is a Mg I line at 1.1828 μm in the wing of the strong Carbon lines at $\sim$ 1.1750 μm. This Mg I line, in case the nova emission lines are broad in general, may blend with the C I feature at 1.1750 μm giving the latter a broad redward wing. Alternatively it may be seen as a distinct spectral feature as seen in V1419 Aql (Lynch et al. 1995) or in our observations on later days (e.g. the spectra of 3 and 5 March). Establishing the identity of Mg lines unambiguously, and also that of Na lines, is important because we show subsequently that they are potential predictors of dust formation.

2. The region between 1.2 to 1.275 μm is a complex blend of a very large number of lines - principally those of NI and C I. This complex is routinely seen - always at low strength - in the early spectra of several nova including V2274 Cyg and V1419 Aql. Since our resolution in this region is higher than that of the V2274 Cyg and V1419 Aql spectra, we have tried to identify individual lines in the complex. Since most of the individual spectral features in this region are weak it is necessary to ensure their reliability. Thus, the data of 5 Feb was examined - since four, high S/N spectra are available for this date - and it was ensured that individual features repeat in all the four spectra. Subsequent line identification that followed, by comparing with the synthetic spectrum, is largely satisfactory but not completely so. The majority of the observed features are reproduced at the correct wavelengths in the synthetic spectrum except for the observed 1.2074, 1.2095 μm C I blend and the unidentified line at 1.2140 μm which are not. The NI 1.2461, 1.2469 μm feature is one of the stronger features in the complex and while it has been attributed solely to NI by Rudy et al. (2003), it is likely that there is some contamination of this line with O I 1.2464 μm. In fact, the excess strength shown by this line in the synthetic spectrum is due to the contribution of the O I line in addition to the NI line. The contribution of O I however has made the line look too strong.

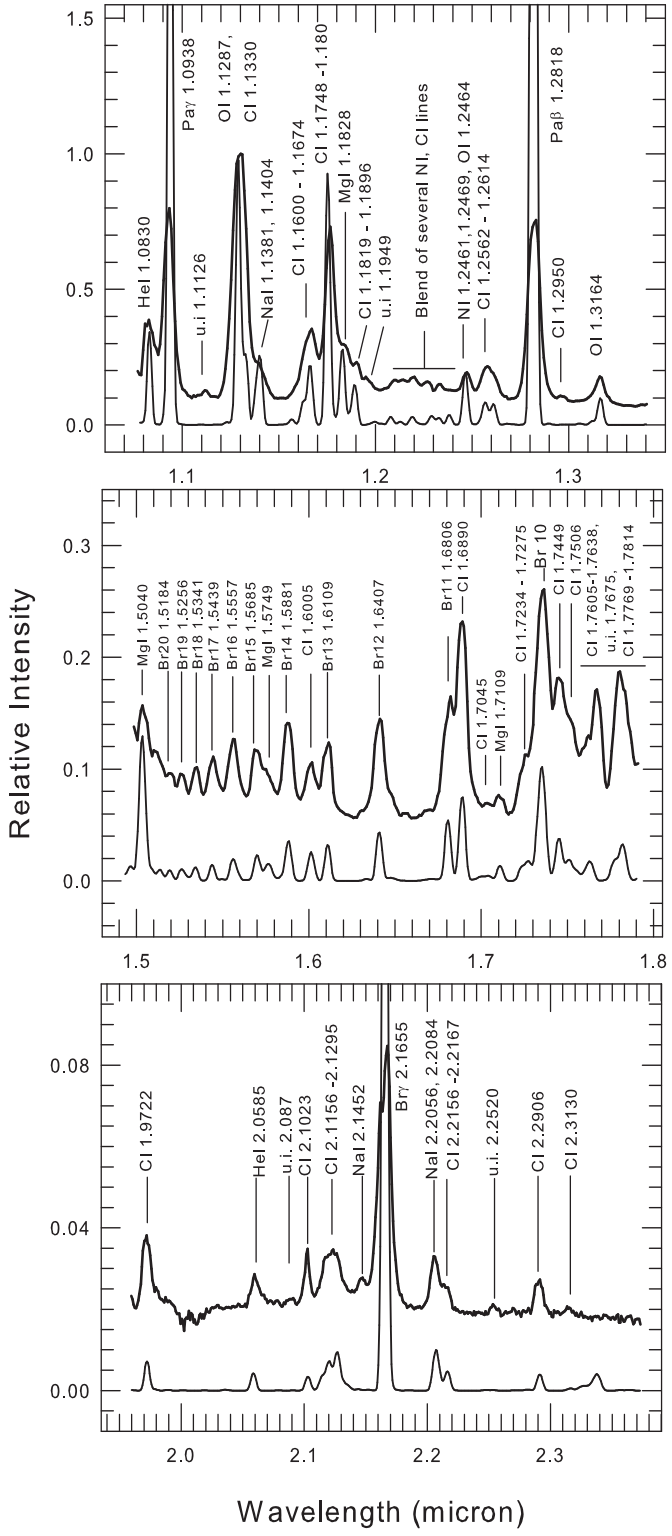

Figure 4.5: Line identification in the *J*,*H* & *K* bands shown from top to bottom respectively. In each panel, the upper plot (darker shade) is the observed data of 1 March; the lower curve (lighter shade) is the synthetic spectrum (details in subsection 4.3.3). More details on the lines are given in Tables 4.3. The observed spectrum was calibrated with the observed *JHK* magnitudes and normalized to unity w.r.to the 1.1287 μm O I line whose peak strength is 5.6×10^{-15} W/cm^2/μm. The absorption features at $\sim$ 2.0 μm are residuals from improper telluric subtraction (discussed in section 4.2).

3. The blended feature comprising of the O I 1.1287 μm and C I 1.1330 μm lines shows considerable evolution with time. In the initial phase, for spectra between 24 Feb and ~ 5-7 March, the O I and C I lines contribute to the blend in comparable amounts. But with time the O I line begins to dominate possibly due to a increase of the Ly β flux with time as the central remnant becomes hotter. That Ly β fluorescence is certainly influencing the 1.1287 μm line can be inferred from its large relative strength compared to the continuum excited 1.3164 O I line. The 1.1287 μm O I - C I 1.1330 μm blended feature shows a broad red wing at 1.14 μm. There appears to be strong case to believe, from the results of our synthetic spectrum, that Na I lines at 1.1381 and 1.1404 μm are responsible for this red wing. There are two Carbon lines in this region which could contaminate the Na I lines but the effect of these C I lines is found to be very marginal from our model spectrum. It is also noted that the same Na I features are seen in the spectrum of V2274 Cen and identified by Rudy et al. (2003) as potentially arising from Na I.

4. In the *H* band, the recombination lines of the Brackett series are most prominent and readily identifiable. But the presence of a C I line at 1.6 μm, which could be mistaken as just another member of the Brackett series, should not be missed. If a recombination analysis of the Hydrogen lines is to be done, caution is needed in estimating line strengths of Br 11 which can be severely blended with the strong C I feature at 1.6890 μm and Br10 at 1.7362 μm which is again blended with C I lines. Other Br lines, whose strengths are affected but to much lesser extent, are Br14 at 1.5881 μm (blended with C I 1.5853 μm and O I 1.5888 μm) thereby making it appear artificially stronger than Br12 contrary to what is expected in a Case B scenario; Br12 at 1.6407 μm is contaminated with several weak C I lines between 1.6335 μm and 1.6505 μm thereby giving Br12 a broad appearance on both wings. A specifically interesting feature at 1.579 μm on the redward flank of Br15 (1.5701 μm is due to Mg I; magnesium and sodium lines are discussed subsequently.

Before proceeding with other conclusions regarding line identification, it is relevant to point out at this stage that the early spectrum of V1280 Sco is very similar to that of the dust forming novae V2274 Cyg and V1419 Aql (Rudy et al. 2003, Lynch et al. 1995). A comparison of the 0.75-1.35 μm early spectra of these last two novae is given in Figure 8 of Rudy et al. (2003) to show the striking similarity in spectral

features between them and examination of the *J* band spectra shows that there is a one-to-one replication of spectral features in the case of V1280 Sco also. All three novae show a spectrum rich in H,C, O and N. Rudy et al. (2003) discuss in detail why it is not always easy to distinguish between CO and ONeMg novae based on near-infrared spectroscopy alone. But they show that by considering several observational features together viz. the rate of decline, the expansion velocity, the formation of dust and the presence of C I lines that V2274 Cyg is strongly indicated to have a CO white dwarf (WD). By virtue of the same arguments, it would appear that V1280 Sco is also a CO nova. This is further supported by the classification of V1280 Sco as a FeII nova based on its early optical spectrum (Munari et al. 2007) - Fe II novae are associated with explosions on CO white dwarfs (Williams 1992). It is intended to present results on three other novae which we have studied recently viz. V476 Scuti, V2615 Oph (Das et al. 2009; also see chapter 5 in this thesis) and V2575 Oph. All three show rather similar spectra as V1280 Sco with prominent carbon lines and furthermore they all went on to form dust - a propensity shown preferentially by CO novae (Starrfield et al. 1997; Gehrz 1988). It is therefore tempting to think that a tentative hypothesis is emerging, subject to proper validation, that the characteristic near-IR spectrum shown by these nova is a hallmark of the CO class of novae. On a more definitive note, we hope to convincingly show that there are certain features in the spectrum of V1280 Sco that appear to be reliable, generic predictors whether dust will form in novae ejecta or not. A return is now made to a few other traits in the spectrum in Figure 4.5 that deserve elaboration.

5. Apart from the 1.1828 μm line, the other Mg I lines that we detect are those at 1.5040, 1.5749 and 1.7109 μm . The 1.5040 μm and 1.7109 μm are also suggested by Rudy et al (2003) to be due to Mg I - we are convinced that this association is correct even if the 1.5040 μm line is at the edge of our observed spectral window. The feature at 1.5749 μm, blending with the wings of Br 15 is certainly Mg I and may escape detection at lower resolutions where it could blend with lines of the Brackett series. The 1.5749 μm line can become quite strong, stronger than the adjacent Br lines as in the case of V2615 Oph and a correlated increase in the strength between this line and other Mg I lines is also clearly seen in V2615 Oph. The identification of the Mg I lines is therefore felt to be secure. Regarding lines arising from Na, apart from those at $\sim$ 1.4 μm , the other lines that are definitively identified are those at 2.2056 and 2.2084 μm. These lines are known to occur in novae e.g in V705 Cas (Evans et al. 1996). However, in the synthetic spectrum, we have trouble

reproducing the 2.1045 μm feature - again associated with Na I (e.g. Evans et al. 1996) - at its observable strength. The identification is therefore uncertain.

6. The C I feature at ~ 2.12 μm is actually a blend of several C I lines; the principal ones being at 2.1156, 2.1191, 2.1211, 2.1260 and 2.1295 μm.The superposition of these closely spaced lines gives the overall feature its unusually broad appearance.

7. There are a few weak lines which remain unidentified. One of these is the 1.1126 μm line which appears consistently in our spectra and which is often seen in the spectra of novae; Rudy et al. (2003) suggest its association with Fe II. However,our model shows that if this line is due to Fe II then several other lines of Fe II should also be seen - in the *H* band especially. Hence we are doubtful about its origin. Similarly, a weak line is consistently seen at 2.2520 μm, prominently present too in the spectrum of V705 Cas (Evans et al. 1996), which eludes identification but which may be due to CO^+ (Dalgarno et al. 1997).

It may be noted that the Hydrogen line strengths are considerably overestimated in our model, particularly the stronger lines viz. Pa β and Br γ. One possibility, that could cause such behavior, is that the assumption that LTE conditions prevail is a simplification. But this could be resolved if optical depth effects are considered. To illustrate this, we note that even if a non-LTE situation is considered, as in Case B computations, then some difficulty may still persist in explaining the observed relative strengths of the H lines. For e.g., Pa β at 1.2818 μm is seen to be weaker than Pa γ at 1.0938 although Case B predicts the other way around (typically Paβ/Paγ = 1.6 is expected). As we understand it, the optical depth in a line is proportional to the column density and the oscillator strength of the line. While the column density for all H lines will be the same, the oscillator strength decreases considerably for the weaker lines in a series (i.e. it is lower for Pa γ as compared to Pa β). This effectively causes the strength of Pa β to be reduced much more than for Pa γ. Rigorous modeling demonstrating this effect is given in Lynch et al. (2000) and an observed example is seen in nova N Sgr 2001 (Ashok et al. 2006) where Br γ is seen to be much weaker than later Br series lines like Br 10, 11 etc. In the present case optical depth effects seem to be present, which if taken into account, is quite likely to reduce the strength of the stronger H lines and bring them in better

agreement with the observed spectrum. In comparison to H, the optical depth in the lines of the other elements is expected to be significantly less - and hence their strengths remain unaffected - because of their considerably lower column densities (as a consequence of their lower abundances).

It was also found that use of a single temperature for the emitting gas fails to simultaneously reproduce the observed strengths of lines from all the elements. Though a complex interplay between the Saha and Boltzmann equations is involved, one of the principal reasons for this failure we believe, can be traced to the considerable diversity in ionization potentials (I.P) of the elements contributing to the spectrum. The observed lines in the spectrum are from neutral species. If a higher temperature is considered (~ 10,000K), then the ionization equation indicates that elements like Na and Mg with low I.Ps of 5.139 and 7.646 eV respectively have a larger fraction of their atoms in higher stages of ionization and very few in the neutral state. Therefore the lines from the neutral species of these elements are found to be extremely weak - the reduction in strength is compounded by the additional fact that they have low abundances. In comparison to Na and Mg, higher temperatures favor a relatively larger fraction of neutral species for H, C, N and O because of their significantly higher I.Ps (13.6, 11.26, 14.53 and 13.62 eV respectively). On the other hand, instead of a high temperature, the use of only a single lower temperature (~ 3500-4500K) enhances the strength of Na and Mg lines to an unacceptable extent - they become too strong vis-a-vis lines of other elements.

It therefore becomes necessary to consider the possibility of temperature variation in the ejecta. We have adopted the simplest scenario viz. there exists a hot zone in the ejecta outside which lies a relatively cooler region. This involves invoking the least number of free parameters i.e. two temperature values for the hot and cool zone. Physically, the assumption of temperature variation in the nova shell does not appear unduly unreasonable - the formation of dust in V1280 Sco does indicate that there must a cool region in the ejecta - though the temperature stratification is expected to be more complex than being characterized by just two temperature values. But our aim, as mentioned earlier, is to get a better qualitative idea of the characteristics of the emission lines seen. The model computation in Figure 4.5 is therefore made on this basis using temperatures of 8300 and 3800K for the hot and cool zones with their respective emitting volumes being in the ratio of ~ 3:1. All other parameters are assumed to be the same in both zone viz. abundances, electron density etc. In this manner we are able to reproduce reasonable agreement

between observed and computed lines strengths of all elements except Hydrogen (which as explained earlier could be significantly affected by optical depth effects). The abundances that we used in Figure 4.5, in terms of mass fractions, are 0.41, 0.21, 0.147, 0.096, 0.13, 0.0051 and 0.0010 for H, He, C, N, O, Ne and Na-Fe respectively. which are reasonably consistent with that expected in CO novae (e.g. model CO4 of Jose & Hernanz, 1998). However, we do not intend to stress that our model calculations determines elemental abundances in V1280 Sco or validates the assumption of LTE prevailing. But it appears that departure from LTE conditions may not be too severe in the early stages when the density in the ejecta is high.

A conclusion that emerges from the analysis, and of which we feel fairly convinced, is the following. The presence of lines of particularly Na and also Mg, associated as they are with low excitation and ionization conditions, necessarily implies the existence of a cool zone. Such a zone is conducive for dust formation. In the coming subsection, using observational evidence for corroboration, we validate the claim that whenever these lines are seen it is also likely to be accompanied by dust formation in the nova.

Table 4.3: List of observed lines in the *JHK* spectra of V1280 Sco

λ (μm)	Species	Other contributing lines & remarks
1.0830	He I	
1.0938	Pa γ	
1.1126	u.i	Fe II?
1.1287	O I	
1.1330	C I	
1.1381	Na I	C I 1.1373
1.1404	Na I	C I 1.1415
1.1600-1.1674	C I	strongest lines at 1.1653, 1.1659,1.16696
1.1748-1.1800	C I	strongest lines at 1.1748, 1.1753, 1.1755
1.1828	Mg I	
1.1819-1.1896	C I	strongest lines at 1.1880, 1.1896
1.1949	u.i	
1.2074,1.2095	N I	blended with C I 1.2088
1.2140	u.i	
1.2187,1.2204	N I	

Continued on next page

Table 4.3 – continued from previous page

λ (μm)	Species	Other contributing lines & remarks
1.2249,1.2264	C I	
1.2329	N I	
1.2382	N I	
1.2461,1.2469	N I	blended with O I 1.2464
1.2562,1.2569	C I	blended with O I 1.2570
1.2601,1.2614	C I	
1.2659	u.i	
1.2818	Pa β	
1.2950	C I	
1.3164	O I	
1.5040	Mg I	blended with Mg I lines at 1.5025,1.5048
1.5184	Br 20	
1.5256	Br 19	
1.5341	Br 18	
1.5439	Br 17	
1.5557	Br 16	
1.5685	Br 15	
1.5749	Mg I	blended with Mg I lines at 1.5741,1.5766 & C I lines at 1.5784
1.5881	Br 14	blended with C I line at 1.5853
1.6005	C I	
1.6109	Br 13	
1.6335	C I	
1.6419	C I	
1.6407	Br 12	blended with C I lines between 1.6335-1.6505
1.6806	Br 11	
1.6890	C I	
1.7045	C I	
1.7109	Mg I	
1.7200-1.7900	C I	Several C I lines in this region (see Figure 4.5)
1.7362	Br 10	Affected by C I 1.7339 line

Continued on next page

Table 4.3 – continued from previous page

λ (μm)	Species	Other contributing lines & remarks
1.9722	C I	
2.0585	He I	
2.0870	u.i	
2.1023	C I	
2.1138	O I	This line may be present
2.1156-2.1295	C I	blend of several C I lines strongest being 2.1156,2.1191,2.1211, 2.1260,2.1295
2.1452	Na I?	
2.1655	Br γ	
2.2056	Na I	
2.2084	Na I	
2.2156-2.2167		blend of C I lines at 2.2156,2.2160,2.2167
2.2520	u.i	
2.2906	C I	
2.3130	C I	

4.3.4 Can we predict which novae will form Dust from early infrared spectra?

Considerable attention has been paid to understanding the dust formation process in novae and the fundamental physical conditions necessary for dust grain formation (Gehrz 1988, Evans 2001). It would appear that several parameters are involved in determining whether a nova has the ability to produce dust. Correlations between dust formation and parameters like ejection velocity and speed class have been examined but it is still not completely understood which novae will go on to form dust. Gehrz (1988) shows that for dust formation to take place efficiently, it is necessary that a sufficiently high particle density be available at the dust condensation point - the high density being necessary to enable the nucleation of grains to take place. It is also evident that low temperatures must prevail in the dust forming zone to enable dust to condense. Dust may fail to form in novae with

low metal abundances. PW Vul and HR Del are examples of dust-poor novae which probably had low CNO abundances - probably solar-like - whereas the novae that have formed thick dust shells have had an enrichment of CNO elements (Gehrz 1988 and references therein). Rudy et al. (2003) have found a significant correlation between novae in which CO (carbon monoxide) emission is seen and their dust producing capacity. They consider the known novae in which the first overtone of CO has been detected viz. V2274 Cyg, NQ Vul, V842 Cen, V705 Cas, V1419 Aql (Rudy et al. 2003, Ferland et al. 1979, Hyland & Mcgregor 1989, Wichmann et al. 1990; Evans et al. 1996; Lynch et al. 1995). All of these novae produced prolific amounts of dust. Rudy et al. (2003) comment that the association of dust with CO may not be totally unexpected, given that CO formation maybe a precursor for dust formation (Rawlings 1988; Evans 1996) since CO emission could cool the regions sufficiently that dust formation can occur. Additionally, the low-temperature,high density, metal-rich environment needed for CO production also favors the production of dust.

Among these physical parameters, the signature of a low-temperature condition can also be inferred from the presence of Na and Mg lines. We have therefore inspected the *JHK* spectra of these novae to see whether Na and Mg lines were present in their spectrum. In addition, since high densities in the ejecta seems a pre-requisite for dust formation, only the early spectra were inspected because the density is expected to be high at this stage before expansion thins it. Beginning with V2274 Cyg, this object showed lines of Na I 1.1381, 1.1404, 2.2056, 2.2084 μm and the Mg I 1.5040 and 1.7109 μm lines are also detected (Rudy et al. 2003) in spectra taken 18 days after outburst. The 1.1828 and 1.5749 μm Mg I lines are not seen but that appears to be due to inadequate resolution in distinguishing them from nearby lines with which they could be blended (see Table 4.3). In V1419 Aql, during the early stages, among the *JHK* spectra only the early *J* band spectrum is available taken 18 days after maximum light - the Mg I 1.1828 line is clearly detected in it (Lynch. et al. 1995). 1.6-2.2 μm spectra of NQ Vul were recorded by Ferland et al (1979) 19 days after the outburst. The S/N in these spectra is low but the Na I 2.2056, 2.2084 μm features are clearly discerned and listed as observed features. V705 Cas was extensively studied by Evans et al (1996) with *K* and *L* band spectra recorded at three epochs prior to strong dust formation in this nova which took place $\sim$ 62 days after outburst. V705 Cas is an archetypal example in which dust formation was accompanied by a drastic drop of $\sim$ 7 magnitudes in the visual light curve. The *K* band spectra of V705 Cas taken a day before maximum

and 26.5 days after peak light very prominently show the lines of Na I 2.2056, 2.2084 μm respectively and also the line at 2.1045 μm which is attributed to Na I (Evans et al. 1996). In the case of V842 Cen, while 1-5 μm IR spectra have certainly been recorded (Hyland & Mcgregor, 1989; Wichmann et al. 1990, 1991) we are unable to examine the *JHK* region of the spectra - to infer about the presence of specific Na I/Mg I lines - as they do not appear to be published. The published Hyland & Mcgregor (1989) spectra cover the 2.9-4.1 μm region emphasizing the PAH features detected in this while the Wichmann et al (1990) spectrum covers only the 2.27-2.43 μm region i.e. the focus is on the CO first overtone emission seen in the object. However Wichmann et al. (1991) do report that emission lines of Na I were seen, apart from other lines of H, He, C, O, N, in the 1-4 μm region. Thus all these four dust forming novae had lines of Na I and/or Mg I in their spectra.

Apart from these novae, we were unable to locate early *JHK* spectra of other novae to increase the sample size to test our hypothesis. However, we have some unpublished data on V476 Scuti and V2575 Oph. Preliminary results indicate both novae formed dust - from sharp declines seen in their light-curves accompanied by the buildup of an infrared excess. From our recent studies, we find that nova V2615 Oph (Das et al. 2009, also see chapter 5 of this thesis), in which strong first overtone CO emission was observed, formed dust also. Quite consistently, Na I and Mg I lines are seen in the spectra of these objects too. And finally, they are seen in the present case of V1280 Sco; though it must be noted that CO did not form in this nova and yet it formed dust. Thus there appears to be a extremely good one-to-one correlation between the presence of NaI/MgI lines and the dust forming potential of a nova. Their presence, in early infrared spectra, could therefore predict dust-formation. All of these novae appear to be rich in heavy elements. Abundance calculations show this for V842 Cen (Andrea et al. 1994) while for the other novae, for which abundance calculations are unavailable, a metal-rich ejecta can be inferred indirectly from the prominent/strong lines of C, N, O seen in their *JHK* spectra (especially the lines of Carbon). In essence, dust formation in novae can be expected when conditions of low temperatures and high densities are satisfied along with the possible pre-requisite of an enhancement in heavy elements.

4.3.5 Evidence for sustained mass loss

Examination of the Brγ 2.1655 μm feature in the data of 24, 25, 27 Feb and 01 March (Figure 4.6) shows that there appears to be an additional line on the blue wing of Brγ. However, we are not able to identify this feature with any known line and therefore looked for alternative reasons for its origin. As it turns out, it is caused by the continued presence of the absorption component of a P-Cygni feature that persists quite long after the outburst began - atleast till 01 March. To demonstrate this, a velocity plot of Brγ region is shown in Figure 4.6 on different days. The earliest spectra of Feb. show classic P-Cygni profiles. What may be noted however is that the position of the P-Cygni absorption component in the earliest spectra closely tracks the trough seen in the peak of the Br gamma line at later stages (Feb 24 to March 01). The trough it may be seen, by splitting the peak/profile of the Br gamma line into two components, creates the impression of an additional line being present which however is not the case. The profiles in Figure 4.6 can instead be interpreted as follows. A P-Cygni profile arises in an outward accelerating wind and is a indicator of mass loss. The initial P-Cygni structure arises from mass loss during the rise to maximum or epochs close to it. As this matter moves away from the central remnant, the line profile associated with it is expected to become purely of emission-type. However if strong mass loss continues, then superposed on this emission component will be the P-Cygni component arising from the continuing mass loss. The addition of these two components, as can be visualized, can lead to the profiles of the observed shape in Figure 4.6. In effect, Figure 4.6 indicates that observational evidence is seen that mass-loss continues from the nova up to 1-3 March 2007 i.e. it lasts for atleast 25-27 days after the outburst began. This estimate for the duration of the mass-loss ($T_{\rm ml}$) is likely to be a lower limit for the process of mass ejection could continue longer but at reduced mass-loss rates insufficient to create the necessary absorption column density to produce a discernible P-Cygni absorption component on the overall profile. Our finding gives direct observational evidence for sustained mass-loss and a constraint on its duration.

A comparison could be made between theoretical estimates of $T_{\rm ml}$ and its observed value from the grid of nova models developed by Prialnik and Kovetz (1995) and Yaron et al. (2005) providing numerical estimates for key quantities characterizing a nova outburst and properties of the ejecta. The different models are computed by varying the three basic and independent parameters that control a nova outburst viz the mass ($M_{\rm WD}$) and temperature of the white dwarf and the mass accretion rate on the white dwarf. One of the central timescale parameters that they compute is

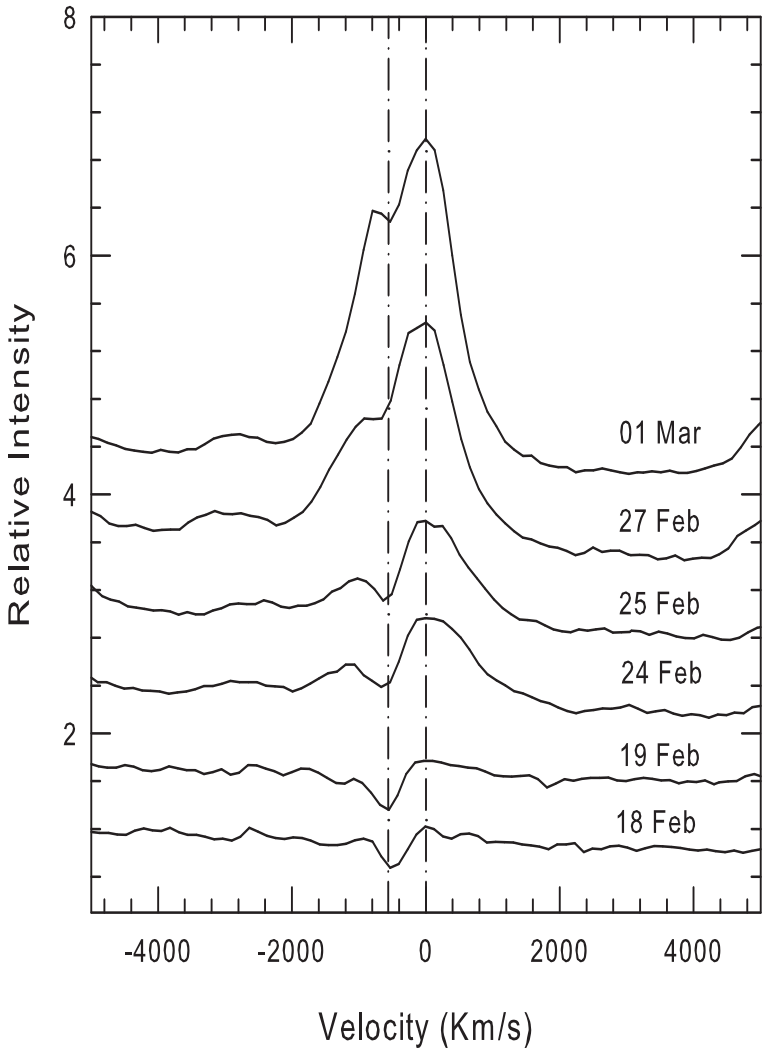

Figure 4.6: The time evolution of the Brackett γ 2.1655μm line showing the P-Cygni profile in the early stages with its absorption feature at ~ -575 km/s blueward of the emission peak. An absorption component, coincident in wavelength with the P-Cygni absorption trough position, persists near the peak of the profile for several days indicating continuing mass loss (see text of subsection 4.3.5 for details).

$T_{\rm ml}$ which is shown to be of the order of t_3 (the time for a decline of 3 magnitudes in the visual). The early formation of dust in V1280 Sco makes it difficult to estimate t_3. But if we proceed along the lines as our estimate of t_2, then t_3 should be in the range of 30-40 days. This seems to be satisfactorily consistent with the observed lower limit for the mass-loss timescale of about 25-27 days. Together with the observed estimate of $T_{\rm ml}$ if the known outburst amplitude (A) and the expansion velocity ($V_{\rm exp}$) are also considered; then the grid of models can be used to estimate $M_{\rm WD}$ since A and $V_{\rm exp}$ are two other observable parameters predicted by the computations. In this context, it appears that a value of $M_{\rm WD}$ towards the higher end (1-1.25 $M_{\odot}$) may be supported. For e.g. one of the models with $M_{\rm WD}$ = 1.25 $M_{\odot}$ predicts a maximum velocity, average velocity, outburst amplitude and $T_{\rm ml}$ with values of 1230 km/s, 678 km/s, 14.3 magnitudes and 22 days respectively. This agrees reasonably with the A and $V_{\rm exp}$ values observed in V1280 Sco. However, this estimate of $M_{\rm WD}$ has to viewed with due caution given the uncertainties in the observable quantities (we have only a lower limit on $T_{\rm ml}$ and on A) in addition to the complicated behaviour of V1280 Sco which shows evidence for a second episode of significant mass loss about $\sim$ 100 days after the first outburst (see subsection 4.3.7). It is also noted that a high white dwarf mass would imply a ONeMg rather than a CO white dwarf in this nova. But the infrared spectrum definitely supports a CO classification. Thus there could be a possible inconsistency here, which though not firmly established, could still be kept in mind.

4.3.6 The initial fireball phase of V1280 Sco

V1280 Sco was first caught brightening on Feb 4.5 (Sakurai & Nakamura 2007) when it was found to be at 9.4-9.9 magnitudes in the visible. Within the next $\sim$ 12 days it brightened by nearly 5.8 mags to reach its maximum on Feb 16.2 at V=3.79 (Munari et al. 2007). During this prolonged rise to maximum, extensive optical photometry of the object has been documented; not many novae have had been studied so well in the pre-maximum rise. Thus the available data permits a study to be made of the early fireball expansion in the nova along similar lines as in PW Vul (Gehrz et al. 1988). In Figure 4.7, using B,V,$R_{\rm c}$,$I_{\rm c}$ and JHK magnitudes, when available, reasonably good blackbody fits are obtained to the data thereby allowing a blackbody temperature $T_{\rm bb}$ to be derived. The blackbody temperatures obtained are consistent with the observation that the nova pseudosphere generally shows an A to F spectral type at outburst.The blackbody angular diameter $\theta_{\rm bb}$ in arcseconds

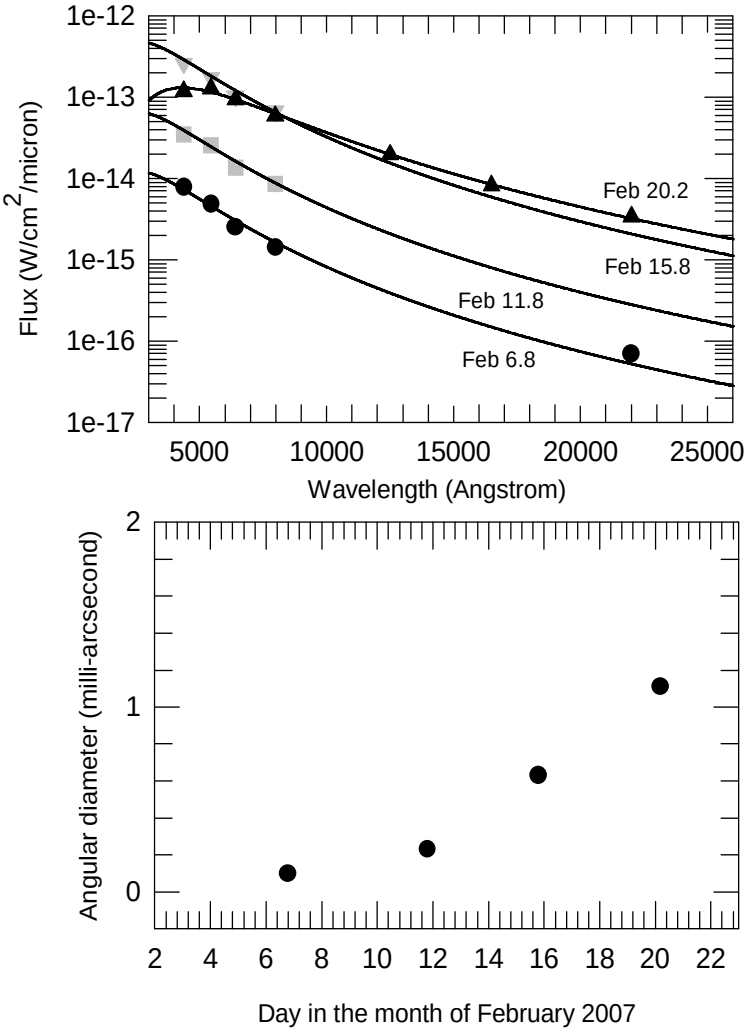

Figure 4.7: The top panel shows the observed SED's on different dates fitted by black body fits after correcting for A_v = 1.2. The same black body temperature of 11000K is found to fit the data of Feb 5.8, 11.8 and 15.8 while for Feb. 20.2 a temperature of 6750K is used. The bottom panel shows the fireball expansion in V1280 Sco during pre-maximum and peak phase.

is then obtained from (e.g. Ney & Hatfield 1978)

$$\theta_{\rm bb} = 2.0 \times 10^{11} (\lambda F_\lambda)_{\rm max}{}^{1/2} T_{\rm bb}{}^{-2} \quad (4.1)$$

where $(\lambda F_\lambda)_{\rm max}$ is in W/cm^2 and $T_{\rm bb}$ in Kelvin. The estimate of $\theta_{\rm bb}$ will always be a lower limit since it is applicable for a black body (Ney & Hatfield 1978; Gehrz et al. 1980). For a gray body, the actual angular size can be larger, since the right hand side of equation 4.1 should then be divided by $\epsilon^{1/2}$, where ϵ the emissivity has a value less than unity for a gray body.

The angular diameter values are plotted in the lower panel of Figure 4.7 and clearly show the expansion of the fireball. Though subject to some uncertainty, it would appear the expansion rate was marginally slower between 6 to 12 Feb. but subsequently increased thereafter to $\sim$ 0.105 mas/day. This angular expansion rate is approximately a factor of three smaller than the mean rate of 0.35 mas/day determined from the interferometric data. As a consequence of this, values of parameters such as the angular size and the distance to the nova, when derived from the interferometric and fireball approach will not match. For example, the March 23 interferometric data for which the shell size was well constrained, estimates its diameter to be 12-13 mas in comparison to $\sim$ 4.1 mas obtained by extrapolating the data in Figure 4.7. We show in Figure 4.8 and 4.9 the results from Chesneau et al. (2008) demonstrating the expansion of the nova shell. The Chesneau et al. (2008) results estimate a mean distance of 1.6 kpc for an adopted expansion velocity for the ejecta of 500km/s ; a similar choice of the expansion velocity will yield a distance three times larger using the fireball approach (since the distance is inversely proportional to the angular expansion rate). It is thus necessary to understand why this inconsistency arises between the two methods. The most likely source for this disagreement is that diameters derived from equation 4.1 are lower limits being applicable to a true blackbody which may not be the case here. The physical reasons which cause a departure in the nature of the emission from black to gray - as seems to be applicable here - are not entirely clear to us. Is it associated with clumpiness in the matter or the matter becoming optically thin? The fireball expansion data, extrapolated back to zero angular size, shows that the onset of the eruption began around 2.5 Feb, almost 2.35 days before the day of discovery and nearly 13.7 days before maximum light. A comparison could be made with V1500 Cyg and PW Vul, two other rare instances where the early fireball expansion was documented sufficiently well to enable estimating the onset of ejection. In both these novae, ejection began well before maximum light viz.

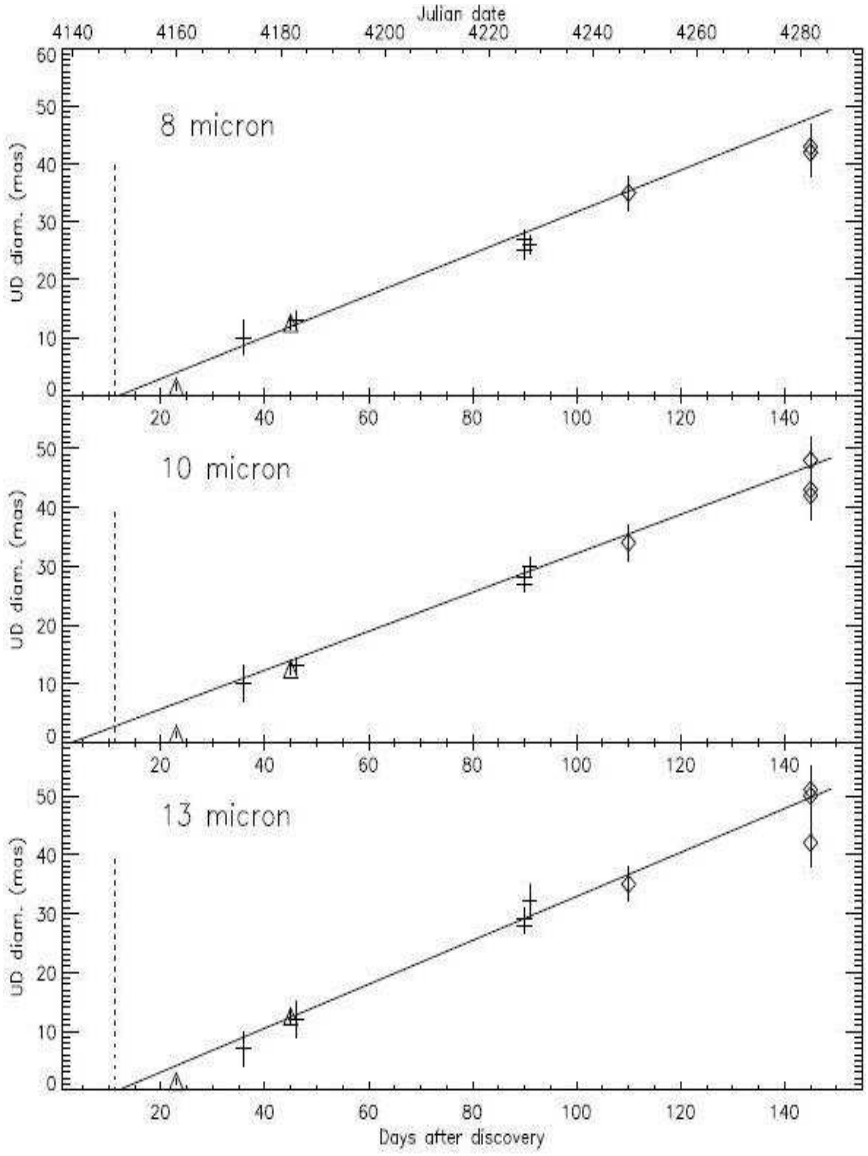

Figure 4.8: Temporal evolution of the dust shell in V1280 Sco at 8 μm (top), 10 μm (middle) and 13 μm (bottom) together with the best polynomial fits of a linear expansion model, obtained from interferometric observations from VLTI. The figure has been adapted from Chesneau et al. 2008. The dotted vertical line represents the time of maximum light (t = 11 d). The crosses stand for the points, directly inferred from the visibilities; the squares represent the diameters measured after t = 110 d; and the triangles represent the The AMBER measurements at t = 23 d and t = 45 d. From the plot it is found that the first dust shell originates from material launched a few days before the maximum light. For more details see Chesneau et al. 2008.

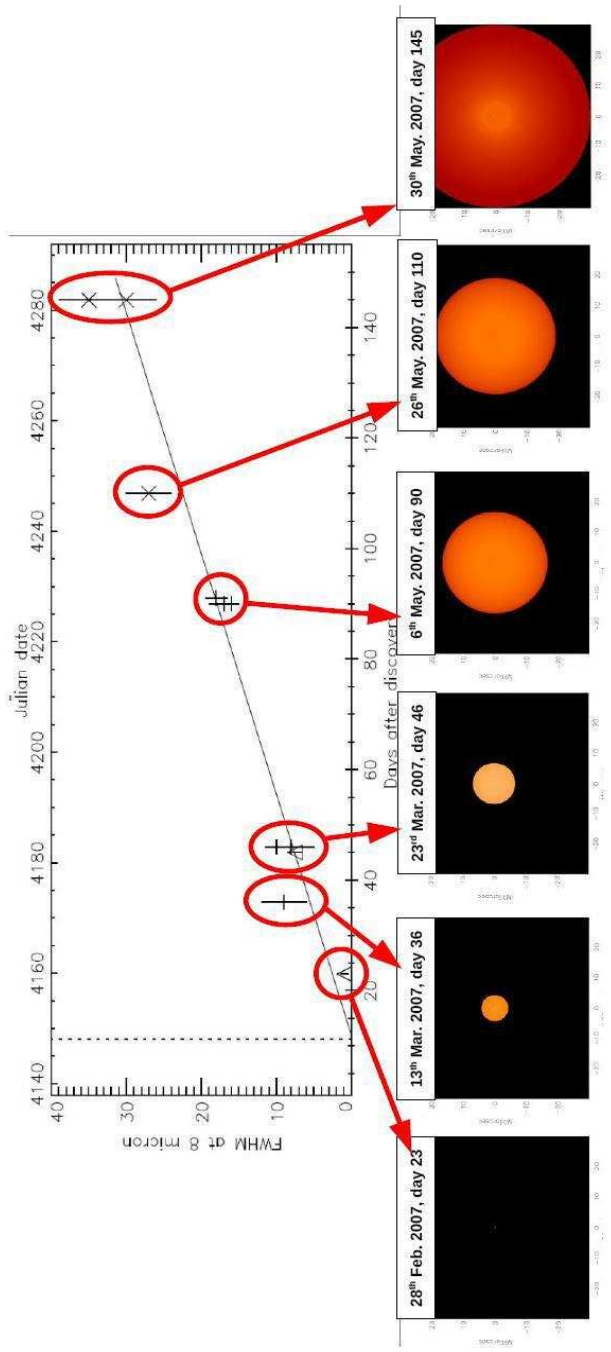

Figure 4.9: This figure shows, schematically, how the angular size of the dust shell around V1280 Sco increased with time. The sizes have been estimated from the observed data at 8 μm in infrared (Chesneau et al. 2008).

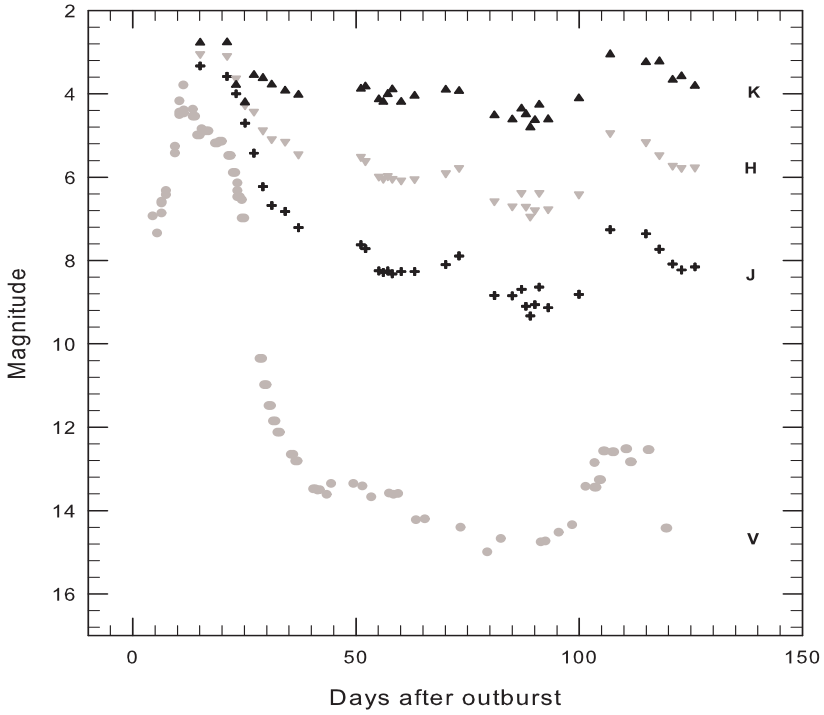

Figure 4.10: The *JHK* lightcurve of V1280 Sco from Mt. Abu observations overlaid on the *V* band lightcurve for comparison (*V* band - grey circles; *J* band - black plus signs; *H* band - grey downward triangles; *K* band - black upward triangles).

1.8 and 9 days for V1500 Cyg and PW Vul respectively (Gehrz 1988 and references therein).

4.3.7 The *JHK* light curve of V1280 Sco

The *JHK* light curve is presented in Figure 4.10 along with the visible light curve to enable a comparison. The first onset of dust around 12 days after maximum shows a sudden drop in the *V* magnitude. The contribution from the dust to the infrared affects the near-IR bands whose magnitudes do not drop so sharply. The contribution to the *K* band is the greatest indicating the dust emission peaks at even longer wavelengths. That this is indeed so can be seen from the 0.5 - 13 μm SED plots of the object by Chesneau et al. (2008). These plots, though obtained at different epochs, show the SED to generally peak at 3 μm or slightly beyond indicating a blackbody temperature for the dust of $\sim$ 1000K. Such peak temperatures for the dust are typically found in novae (Gehrz et al. 1988). Figure 4.10 shows that on the whole, the *K* band brightness remains quite high throughout our observations indicating the constant presence of dust during this time. The dust shell formed in V1280 Sco is not as optically thick as in novae like Nova Serpentis

1978 (Gehrz et al. 1980) or NQ Vul (Ney & Hatfield 1978) where the bulk of the entire emission at shorter wavelengths is absorbed and re-radiated by the dust into the IR. By fitting blackbody curves to our *JHK* magnitudes and the *N* band fluxes of Chesneau et al. (2008), we estimate for V1280 Sco, that the ratio of the maximum infrared luminosity to the outburst luminosity (from data in Figure 4.7) is ~ 0.06. This ratio is found to be close to unity for optically thick novae like Nq Vul, LW Ser etc. The fact that the IR luminosity is much less than the outburst luminosity, but that the dust is thought to cause the decline in the visual band, is suggestive of a clumpy shell. The clumps are individually optically thick, but do not cover the whole of the sky as seen from the nova. The decline in the *V* band could then occur when an optically thick clump of dust forms along the line of sight.

A notable feature of the light-curve behaviour is the strong brightening seen at $\sim$ 110 days after outburst. This is seen in the *V* band and also *JHK* bands. If the *V* band brightening was to arise because of destruction of the dust shell, then an increase in the IR fluxes would not be expected. Since this is not the case, the observed behavior possibly indicates that a second outburst or significant episode of mass loss has taken place at this stage. Such rebrightenings, at late stages, are occasionally known to occur in novae (e.g. V1493 Aql; Venturini et al. 2004) but the cause for it is open to interpretation. The interferometric results (Chesneau et al. 2008) indicate the possibility of a second dust shell forming from the matter ejected in this rebrightening. Though our IR observations could not be continued beyond 126 days after the outburst, the *V* band photometry shows that V1280 Sco had another phase of rebrightening in October-November 2007 (Munari & Siviero, 2007) which lasted for several days. On the whole the object has exhibited a complex light curve.

4.4 Summary of this chapter

In this chapter, we have presented spectroscopic and photometric results of Nova V1280 Sco which was discovered in outburst in early 2007 February. The large number of spectra obtained of the object leads to one of the most extensive, near-infrared spectral studies of a classical nova. The spectra evolve from a P-Cygni phase to an emission-line phase and at a later stage is dominated by emission from the dust that formed in this nova. A detailed model is computed to identify and study characteristics of the spectral lines. Inferences from the model address the vexing question of which novae have the ability to form dust. It is demonstrated,

and strikingly corroborated with observations, that the presence of lines in the early spectra of low-ionization species like Na and Mg - indicative of low temperature conditions - appear to be reliable indicators that dust will form in the ejecta. It is theoretically expected that mass loss during a nova outburst is a sustained process. Spectroscopic evidence for such a sustained mass loss, obtained by tracing the evolution of a P-Cygni feature in the Brackett γ line, is presented here allowing a lower limit of 25-27 days to be set for the mass-loss duration. Photometric data recording the novas extended 12 day climb to peak brightness after discovery is used to establish an early fireball expansion and also show that the ejection began well before maximum brightness. The *JHK* light curves indicate the nova had a fairly strong second outburst $\sim$ 100 days after the first.

CHAPTER 5

Study of V2615 Ophiuchi - A Nova with Prominent CO Emission

5.1 Introduction

V2615 Ophiuchi (V2615 Oph) was discovered by Nishimura (2007) at a visual magnitude of 10.2 on 2007 March 19.812 UT. No star was visible at the position of the nova on a film taken by Nishimura on 2007 March 17.82 UT and earlier survey films since 2005 (limiting mag 11.5-12). The discovery report was supplemented by several other observers from observations obtained close to and around the time of discovery. These reports, in conjunction with the lack of a detection of the nova in images taken just a few days prior to discovery, imply that the nova was discovered a few days before maximum light which was reached on 28 March.

The early low-resolution optical spectra (410-670 nm, resolution 1500) of V2615 Oph by Naito and Narusawa (2007b) on March 20.84 UT showed Balmer-lines having P-Cyg features and Fe II lines (multiplets 42, 49, 74), suggesting that the nova is a "Fe II"- type nova. The FWHMs of the Hα, Hβ, and Hγ emissions were 920, 810, and 790 km/s, and the displacement of the P-Cyg absorptions from the Balmer emission peaks were 940, 820, and 830 km/s, respectively. Early optical spectra were also obtained by Munari et al. (2007b, 2008) on Mar. 22.17 and 24.18 UT. On March 22.17 UT, the spectrum was characterized by weak emission lines with P-Cygni profiles. The strongest emission lines were due to Fe II multiplets 27, 28, 37, 38, 42, 48, 49, 55, and 74; Si II multiplets 2, 3, 4 and 5; N I multiplet 3; Ca II H and K; Na I D1 and D2; and O I 777.2-nm (the O I line showed the sec-

ond strongest emission component after Hα). With respect to the peak of the Hα emission, the absorption terminal velocity was -1415 km/s, and the mean velocity -910km/s. In comparison to the March 22.17 UT spectrum, the Mar. 24.18 UT spectra show large changes: mainly a marked reduction in equivalent width of emission lines and reduction in outflow velocity of absorption components of P-Cyg profiles.

Infrared observations of V2615 Oph have been made by Das et al. (2007) and Rudy et al.(2007) - some of the findings in Rudy et al. (2007) are discussed in details subsequently. The highlight of the Das et al. (2007c) report was the detection of first-overtone CO emission in the nova - similar emission has been recorded previously in only a few novae. In this chapter, we present *JHK* spectrophotometry of V2615 Oph between March 28 and June 9. The spectroscopic results are fairly extensive as spectra have been obtained on 15 occasions during this period.

5.2 Observations

The Near-Infrared *JHK* spectrophotometric data of V2615 Oph presented here were acquired at the Mount Abu 1.2m telescope. The first observation was recorded on the night of 2007 March 28 while the nova was close to the optical maximum. The nova was then observed regularly until the arrival of the monsoon, when inclement weather brought our monitoring to an end. The instrument used was the Near Infrared Imager/Spectrometer with a 256×256 HgCdTe NICMOS3 array. The observation logs for spectroscopy and photometry are presented in Tables 5.1 and 5.2 respectively. Near-IR *JHK* spectra were obtained at similar dispersions of ~ 9.75 Å/pixel in each of the J, H, K bands. General procedures for acquiring data have been described in chapter 2. In each band, spectra were recorded at different positions along the slit (slit width ~1 arcsec) to provide for the background subtraction. To remove telluric features in the spectra of V2615 Oph, we obtained spectra of a nearby standard star (SAO 184301; spectral type A0V) at a similar airmass as the target.

V2615 Oph was monitored photometrically in the JHK bands for 85 days after discovery. Photometric observations were performed under photometric sky conditions using the imaging mode of the NICMOS3 array. In each of the J, H, K filters, several frames at 5 dithered positions offset typically by 20 arcsec, were obtained of both the nova and a selected standard star (2MASS J16232693 -2425291; J=7.340,H=6.027,K=5.464). Near-IR *JHK* magnitudes were then derived using the

Table 5.1: A log of the spectroscopic observations of V2615 Oph. The date of outburst is taken to be 2007 March 19.812 UT.

Date 2007 (UT)	Days since Outburst	Integration time (sec) J	H	K
Mar. 28.928	09.116	60	45	45
Mar. 31.917	12.105	60	60	60
Apr. 02.901	14.089	45	40	60
Apr. 03.893	15.082	60	40	45
Apr. 05.904	17.092	60	45	60
Apr. 06.890	18.078	60	60	60
Apr. 07.915	19.103	75	75	75
Apr. 16.942	28.130	90	90	90
Apr. 18.888	30.076	90	75	90
Apr. 27.869	39.057	90	60	90
Apr. 30.830	42.018	90	90	90
May. 02.835	44.023	90	90	90
May. 06.832	48.020	90	60	60
May. 08.840	50.028	90	90	90
Jun. 09.846	82.034	500	120	90

IRAF aperture photometry task APPHOT. The derived *JHK* magnitudes are given in Table 5.2, the typical errors associated with them lie in the range of 0.02 to 0.04 magnitudes.

5.3 Results

5.3.1 Optical and near-infrared lightcurve

The optical lightcurve of V2615 Oph is presented in Figure 5.1. The object was discovered about 9 days before its maximum which was reached on 2007 March 28 at V = 8.52. On the whole, the object shows a steady post-maximum decline in brightness of 0.05 mag/day for the first $\sim$ 80 days after maximum. Subsequently there is a steep decline in the lightcurve due to dust formation - this aspect is addressed shortly while discussing the near-IR light curve. From the lightcurve we estimate t_2 and t_3 - the time for a drop of 2 and 3 magnitudes respectively in the visual brightness - to be 33 and 58 days respectively. The use of these values of t_2 and t_3 in various MMRD relationships (della Valle et al. 1995, Capaccioli et al. 1989, Cohen 1988 for t_2; Schmidt 1957 for t_3) leads to closely similar values for the absolute visual

Table 5.2: A log of the photometric observations of V2615 Oph. The date of outburst is taken to be 2007 March 19.812 UT.

Date 2007 (UT)	Days since Outburst	Magnitudes J	H	K
Mar. 28.993	09.181	6.26	5.83	5.39
Mar. 31.961	12.149	6.94	6.51	5.90
Apr. 02.970	14.158	6.49	6.07	5.54
Apr. 05.993	17.181	6.54	6.14	5.64
Apr. 07.956	19.144	6.93	6.57	6.18
Apr. 15.979	27.167	7.36	7.07	6.53
Apr. 16.981	28.169	7.22	6.97	6.46
Apr. 18.940	30.128	7.30	6.96	6.62
Apr. 26.885	38.073	7.76	7.53	7.09
Apr. 30.906	42.094	7.98	7.68	7.18
May. 02.932	44.120	8.14	7.84	7.07
May. 06.934	48.122	8.13	7.72	6.79
May. 08.882	50.070	7.94	7.32	6.26
Jun. 09.887	82.075	9.31	7.62	5.34

magnitude - a mean value of M_v = 7.16 ± 0.12 is obtained. The extinction toward the object can be estimated in two ways. Rudy et al. (2007c), using the strength of the OI lines, have determined the reddening prior to dust formation to be E(B-V) = 1.0 (or A_v = 3.1 magnitudes). This leads to a distance estimate of D = 3.25 kpc to the object. To show that this value of A_v is reasonable, we use the extinction data of Marshall et al. (2006) which shows that A_{Ks} is constant at = 0.34-0.36 beyond 3 and upto 12 kpc in the direction of V2615 Oph. Thus, assuming $A_v/A_{Ks} \sim 11$ (Koornneef 1983), a maximum value of A_v = 3.85 is suggested toward V2615 Oph thereby leading to a lower limit on the distance of D = 2.3 kpc. For the present study we adopt the distance estimate from the Rudy et al (2007) findings viz. D = 3.25 kpc.

Our IR observations, begun close to optical maximum, show a steady decline for the first 42 days. After this each of the J,H,K magnitudes show an increasing trend possibly indicating the onset of dust formation. However, no corresponding sharp decline in the optical light curve is seen at this stage implying that any dust, that may have formed, is likely to be optically thin. Rudy et al. (2007c) have reported 0.4 to 2.5 μm spectroscopy of V2615 Oph on May 7 2007 and 0.8 to 5.5 μm spectroscopy on 2007 May 31. They find that the nova evolved dramatically between the two observations (i.e between May 7 and May 31) due to the formation of dust. The

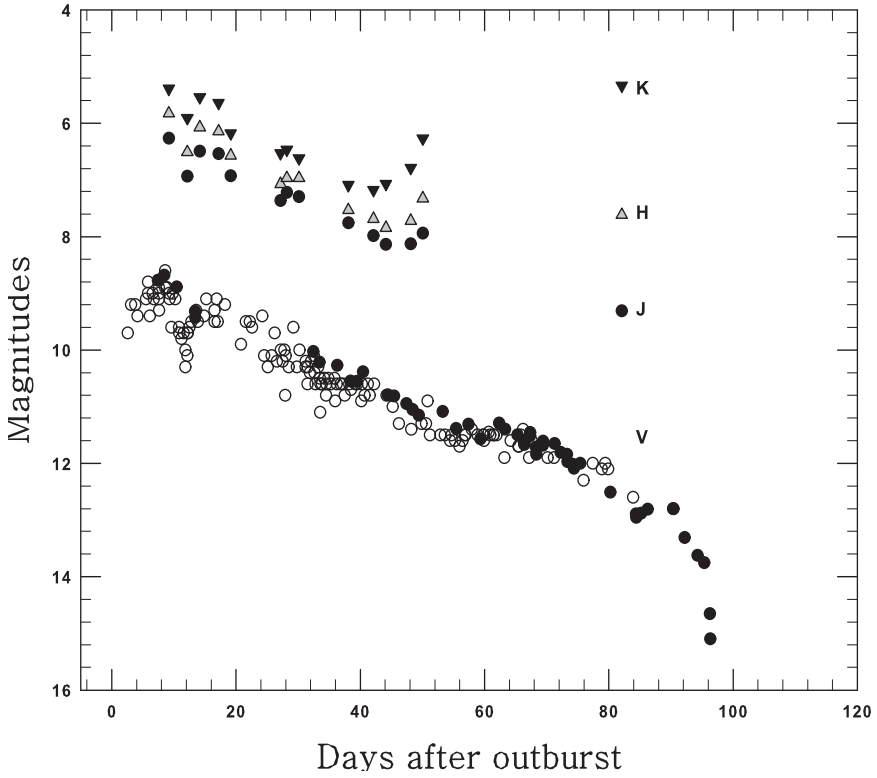

Figure 5.1: The V band lightcurve is shown at the bottom (photoelectric/CCD measurements shown by filled circles ; visual estimates by open circles) based on data from IAU circulars, AAVSO (American Association of Variable Star Observers) and AFOEV databases (Association Francaise des Observateurs d'Etoiles Variables, France). At the top are shown the near-IR J, H and K band light curves based on the present observations (J : filled circles, H : gray triangles - up; K : black triangles - down.)

reddening derived from the OI lines increased from E(B-V)=1.0 to 1.3 in their data. Our last observations on 9 June 2007 show a significant infrared excess due to emission by the newly formed dust.

5.3.2 General characteristics of the JHK spectra

The lines in the earliest spectrum of 28 March, when the nova was at maximum light, show P-Cygni structure with a prominent absorption component. By following the Pa β line for example, it is seen that the P-Cygni absorption component persists for at least 10 days (upto 7 April) indicating that mass loss extends over a prolonged period. The minimum of the absorption component is found to be displaced from the emission peak by $\sim$ 950 km/s on 28 March but this value changes closer to $\sim$ 1400-1500 km/s for 31 March and other subsequent dates upto 7 April.

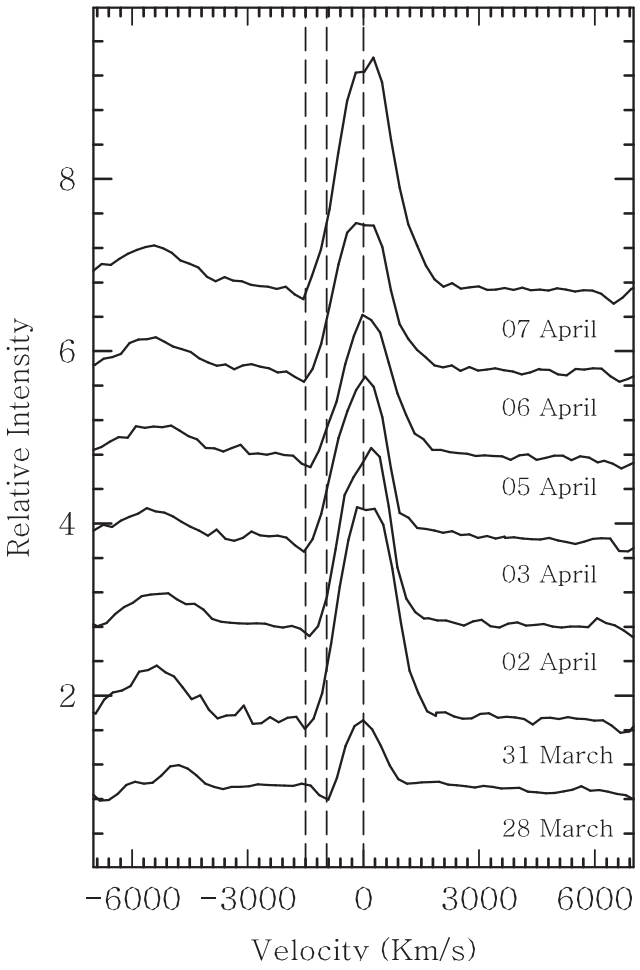

Figure 5.2: The Paschen β 1.2818 μm line is presented on different days to show the evolution of the profile. The two dotted lines, at left of the line center, are positioned at -950 and -1500 km/s respectively to indicate the change in position of the P-Cygni absorption minimum with respect to the emission peak (further details are in the text of subsection 5.3.2)

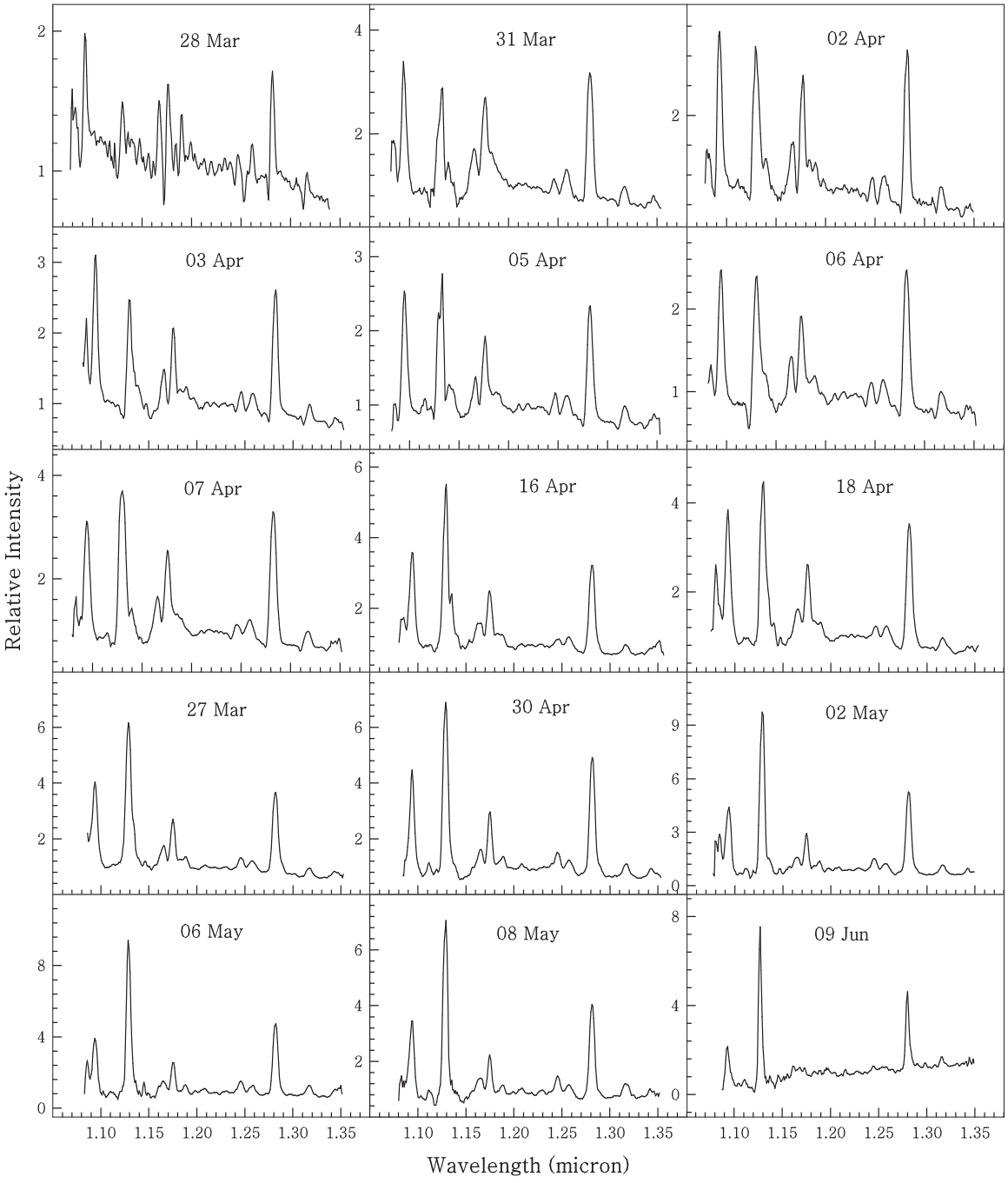

Figure 5.3: The J band spectra of V2615 Oph on different days with the flux normalized to unity at 1.25 μm.

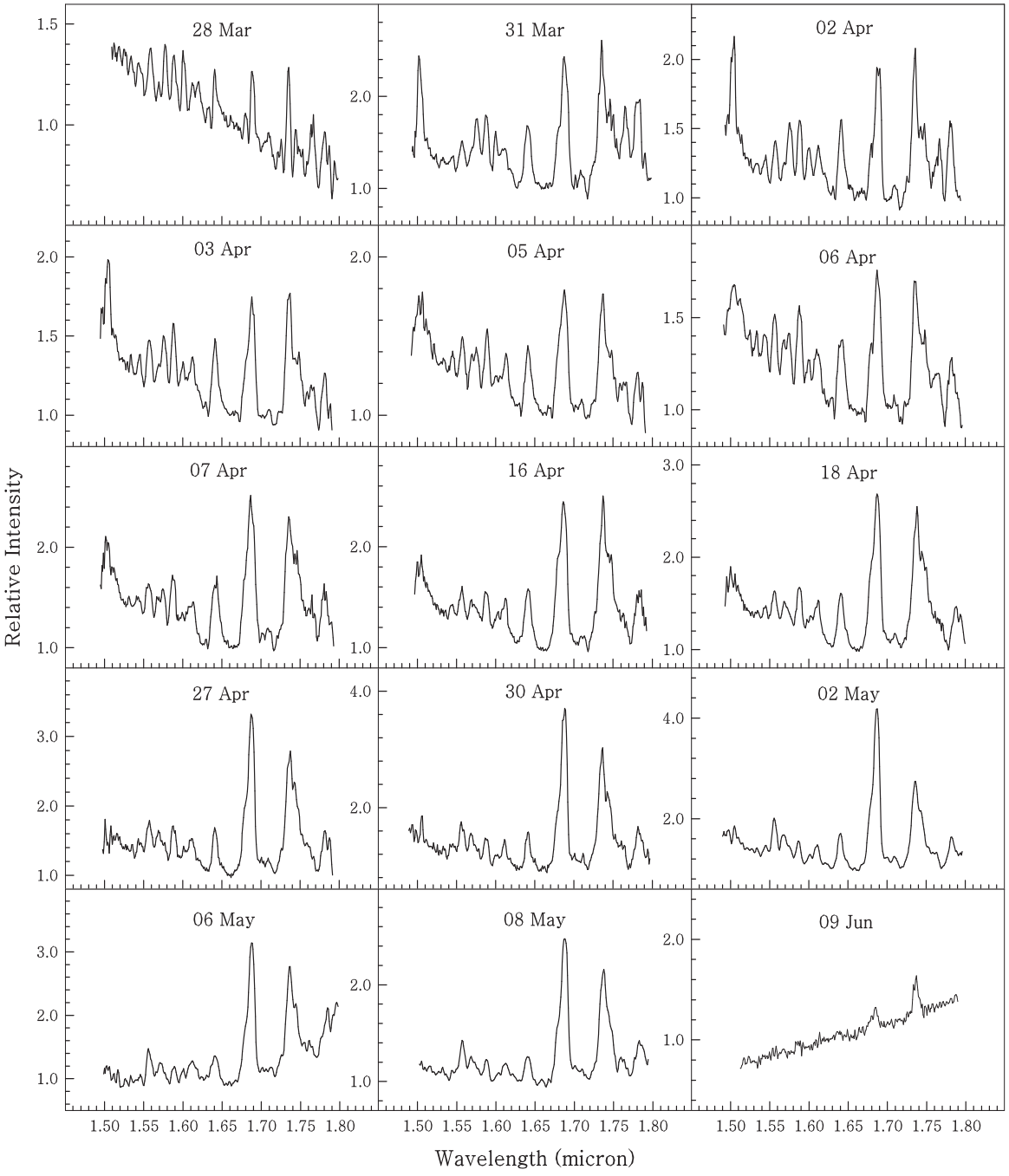

Figure 5.4: The *H* band spectra of V2615 Oph on different days with the flux normalized to unity at 1.65 μm.

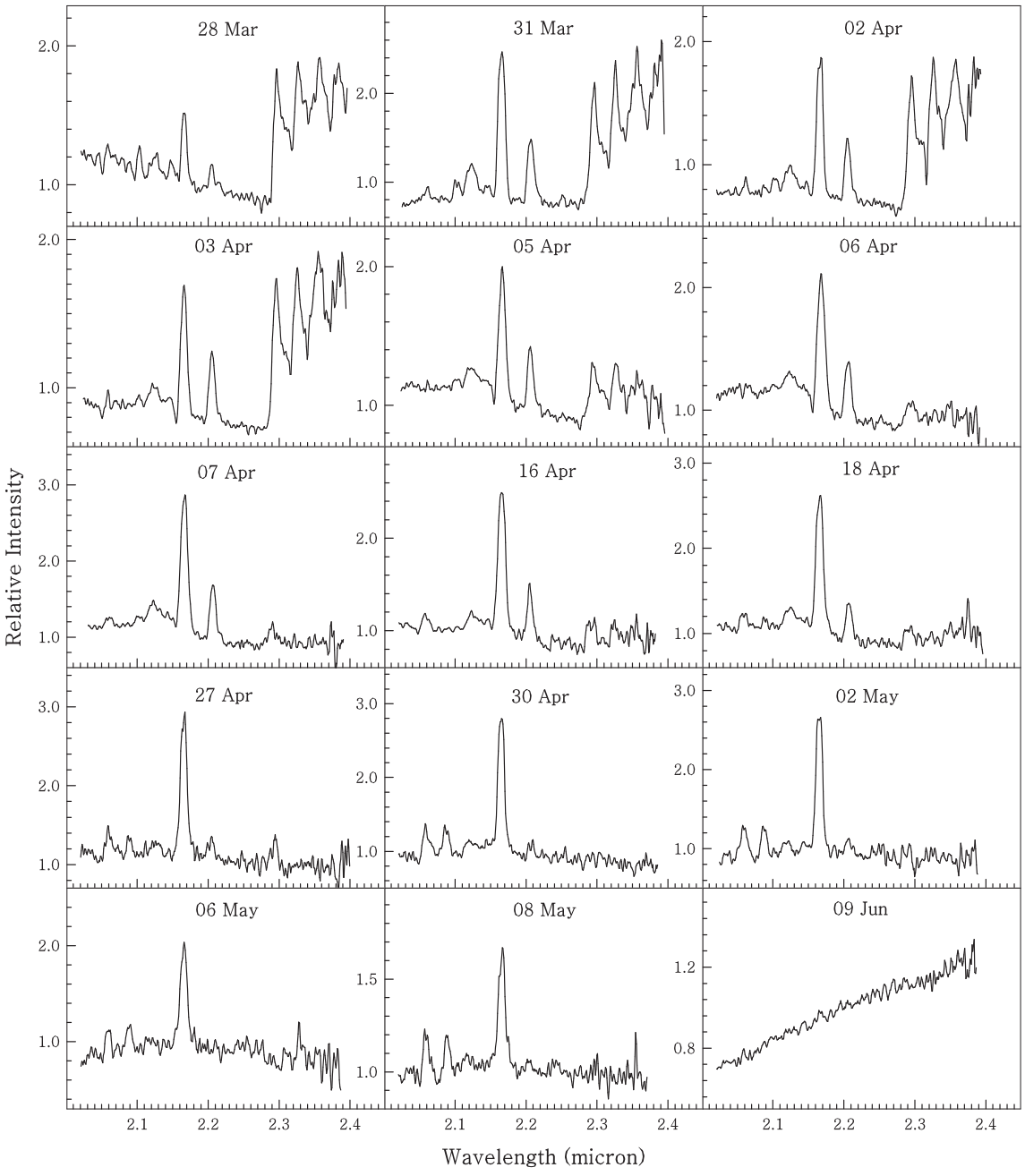

Figure 5.5: The K band spectra of V2615 Oph on different days with the flux normalized to unity at 2.2 μm.

Variations, of a similar nature, in the outflow velocities were also noted by Munari et al (2007b) on 22 and 24 March - when the nova was on its rise to maximum light. Clearly, the mass loss process and its kinematics during the early stages is not uniform.

Mosaics of the the *J*, *H* and *K* band spectra are presented in Figures 5.2, 5.3, and 5.4 respectively. The early spectrum of V2615 Oph is typical of a carbon-oxygen nova (CO nova) - examples of which are V2274 Cyg (Rudy et al. 2003), V1419 Aql (Lynch et al. 1995) and V1280 Sco (Das et al. 2008). In addition to lines of H, He, N and O, these novae show strong lines of carbon e.g in the *J* band in the 1.16 to 1.18 μm wavelength region. In contrast, such carbon lines are weak in the spectra of ONeMg novae e.g. in the novae V597 Pup and V2491 Cyg (Naik et al. 2009). The IR-based classification of V2615 Oph is consistent with its optical classification as a FeII type nova (Naito & Narusawa 2007b). Fe II novae are believed to be associated with explosions on CO white dwarfs (Williams 1992). We have presented the line identification in Table 5.3 but do not show them marked on the spectra as a separate figure. However, since the lines are very similar to those seen in V1280 Sco, the line-identification figure for V1280 Sco could be referred to which contains greater details (Das et al. 2008 or chapter 4 of this thesis). The most prominent lines in the *JHK* spectra of V2615 Oph are the Paschen and Brackett hydrogen recombination lines; the Lyman β and continuum fluoresced OI lines at 1.1287 and 1.3164 μm; the HeI lines at 1.0830 μm and 2.0585. Strong carbon lines are seen in the *J* band and also in the *H* band redwards of Br 11. Among subtle features, the presence of a C I line at 1.6 μm, which could be mistaken as just another member of the *H* band Brackett series lines, should not be missed. The region between 1.2 to 1.275 μm contains the complex blend of a large number of NI and C I lines that are often seen in the early spectra of CO novae. The presence of several lines of NaI and MgI (the prominent ones being at 1.1404, 1.5040, 1.5749, 2.2056 and 2.2084 μm) are worth noting as it may be inferred, from their presence, that dust will form in a nova. During the analysis of V1280 Sco, one of the conclusions that emerged, was that the lines of NaI particularly, and also of MgI, are associated with low excitation and ionization conditions (Das et al. 2008). Such conditions necessarily imply the existence of a cool zone which is conducive for dust formation. This was observationally corroborated in the case of several novae, in which these lines were detected, and which proceeded to form dust (e.g. V2274 Cyg (Rudy et al. 2003), V1419 Aql (Lynch. et al. 1995), NQ Vul (Ferland et al. 1979), V705 Cas (Evans et al. 1996), V842 Cen (Wichmann et al. 1991), V1280 Sco (Das et al. 2008); for a more

detailed discussion see Das et al. 2008 or chapter 4 of this thesis). The presence of these lines in V2615 Oph, and the dust formation witnessed subsequently, is consistent with this scenario. The formation of dust is clearly reflected in the last spectrum of 9 June. Each of the spectra in the individual *J*, *H* and *K* bands show the continuum level increasing to longer wavelengths showing the development of an infrared excess associated with dust.

Table 5.3: List of observed lines in the *JHK* spectra of V2615 Oph.

λ (μm)	**Species**	**Other contributing lines & remarks**
1.0830	He I	
1.0938	Pa γ	
1.1116	u.i.	
1.1126	Fe II	
1.1287	O I	
1.1330	C I	
1.1381,1.1404	Na I	
1.1600-1.1674	C I	strongest lines at 1.1653, 1.1659,1.16696
1.1748-1.1800	C I	strongest lines at 1.1748, 1.1753, 1.1755
1.1828	Mg I	
1.1880	C I	blended with C I at 1.1896
1.2074,1.2095	N I	blended with C I at 1.2088
1.2187,1.2204	N I	
1.2249,1.2264	C I	
1.2329	N I	
1.2382	N I	
1.2461,1.2469	N I	
1.2562,1.2569	C I	
1.2818	Pa β	
1.3164	O I	
1.3465	N I	
1.5040	Mg I	
1.5184	Br 20	

Continued on next page

Table 5.3 – continued from previous page

λ (μm)	Species	Other contributing lines & remarks
1.5256	Br 19	
1.5341	Br 18	
1.5439	Br 17	
1.5557	Br 16	
1.5685	Br 15	
1.5749	Mg I	
1.5881	Br 14	
1.6005	C I	
1.6109	Br 13	
1.6407	Br 12	
1.6806	Br 11	
1.6890	C I	
1.7109	Mg I	
1.7200-1.7900	C I	Several C I lines
1.7362	Br 10	
2.0585	He I	blended with u.i. 2.0620
2.0888	u.i.	Fe II ? (see subsection 5.3.3)
2.1023	C I	
2.1156-2.1295	C I	blend of several C I lines
2.1452	Na I	
2.1655	Br γ	
2.2056,2.2084	Na I	
2.2156-2.2167	C I	
2.29-2.40	CO	Δv=2 bands
2.2906	C I	
2.3130	C I	
2.3348,2.3379	Na I	

The most interesting spectral features in V2615 Oph are the first overtone CO bands in the *K* band which is discussed in coming sections. The other atomic lines in V2615 Oph are similar to those seen in carbon-oxygen novae and which were discussed in our earlier work on V1280 Sco - hence they are not discussed further here. There is, however, an unidentified line at 2.088 μm which is discussed below.

5.3.3 An unidentified line at 2.0888 μm: possibly a FeII line excited by Lyman α fluorescence?

We note the presence of an emission line at $\sim$ 2.0890 μm in the K band that is seen fairly prominently in the spectra from 27 April onwards. We propose that this is a FeII line and additionally investigate whether this line could be excited by Lyman α (Lyα) fluorescence. In the near-infrared, there are a few FeII lines seen in the spectra of novae, which are believed to be primarily excited by Lyman α and Lyman continuum fluorescence. Among these are the so-called "one micron Fe II lines" at 0.9997, 1.0171, 1.0490, 1.0501, 1.0863, and 1.1126 μm seen in several novae (Rudy et al. 1991, 2000). In addition, two other Fe II lines at 1.6872 and 1.7414 μm in the H band, are also proposed to be pumped by the same mechanism (Banerjee et al. 2009). The H band lines are prominently detected in the 2006 outburst of recurrent nova RS Oph (Banerjee et al. 2009 or chapter 3 of this thesis), in the slow nova V2540 Ophiuchi (Rudy et al 2002) and possibly also in the recurrent nova CI Aquila (Lynch et al. 2004). These H band lines could be present in the spectra of other novae too, but have evaded detection because of blending with the Br 11 (1.6806 μm) and CI lines at 1.6890 and 1.7449 μm which lie close by. However these lines are well resolved in RS Ophiuchi (Banerjee et al. 2009), especially during the later stages of its outburst when all line widths in RS Oph become small - due to deceleration of the shocked, emitting gas - and blending effects are thereby minimal.

The excitation mechanism of the Fe II lines appears to be a three step process (Johansson & Jordan 1984; Bautista et al. 2004 and references therein, Banerjee et al. 2009). FeII is first excited from low-lying levels by Lyα or Lyc to a high energy level (typically 11 to 13 eV above ground state) which decays, in the second step, to feed the upper level associated with the observed FeII line (the decay of this upper level, in the third step, leads to the line proper). The 2.0888 μm line results from the decay of the $3d^6(^3_2F)4s\ c^4F$ term at $\sim$ 6.209 eV above the ground state. It so happens that this term can be fed by not just one, but in fact by several high lying levels - each of these high lying levels capable of being pumped by Ly α photons. As illustrative examples, it is noted that photons at 1213.738, 1214.067, 1216.239, 1216.272 and 1217.152 Å, which are reasonably coincident with the Ly α line center at 1215.671Å, can excite transitions from the low lying (5D) 4s a^4D term in Fe II (at 1.076 eV above ground state) to the higher excited levels ((5D) 4p 4F, (5D) 4p 4D and (3P) 4p 4P respectively at around 11.3 eV). Since HI lines in novae (Ly α included) are broad with widths extending upto a few thousands of km/s (1 Angstrom corre-

sponds to about 250 km/s at the Ly α wavelength), these photons could contribute to the flourescence process, even though they are not coincident with the Ly α line centre. These higher levels at 11.3 eV can then decay via ultraviolet photons to the upper level of the 2.0888 μm transition. The Kurucz atomic data [1] on which the present analysis is based, indicates there are additional Lyα fluorescing candidate lines (apart from the five discussed here), all within a few Angstroms of the Ly α line center - that could also contribute to the Ly α fluorescence process. Therefore, the 2.0888 μm line could be excited by Ly alpha flourescence, if its identification with Fe II is correct.

A few cautionary words regarding the identification of the 2.0888 μm with FeII may be in order. In case the Fe II identification is correct, then a few other Fe II lines - as mentioned earlier - could also be expected viz. lines at 0.9997, 1.0171, 1.0490, 1.0501, 1.0863, 1.1126, 1.6872 and 1.7414 μm. Unfortunately the first four of these lines are not covered in our spectra while it is difficult to make any definitive conclusion about the 1.0863 μm line which is in a region of low signal since it is at the edge of our spectral window. However the 1.1126 μm line is seen. It is also difficult to draw a firm conclusion whether the 1.6872 and 1.7414 μm lines are present. Unfortunately both these lines occur at positions close to strong CI and HI lines (Table 5.3) which could lead to line blending. In essence, further detections of the 2.0888 μm line in other novae is desirable to enable a secure identification.

5.3.4 Modeling the CO emission

The CO emission is modeled by assuming the gas to be in thermal equilibrium characterized by the same rotational and vibrational temperature. The populations of different levels can be determined from the Boltzmann distribution with the energy $\varepsilon_{J,v}$ of any individual rovibrational level, with rotational and vibrational quantum numbers (J, v), being given by

$$\begin{aligned}\varepsilon_{J,v} = BJ(J+1) - DJ^2(J+1)^2 + w_e(v+1/2) \\ -w_e x_e(v+1/2)^2 + w_e y_e(v+1/2)^2\end{aligned} \tag{5.1}$$

The first two terms in the above correspond to the rotational energy (higher order terms are neglected) and the remaining terms to the vibrational energy. The values used for the rotational constants are B = 57635.96828(12) MHz and D = 183.5058(22) KHz respectively for $^{12}C^{16}O$ and 55101.0138(23) MHz and 167.668(5)

[1] http://cfa-www.harvard.edu/amp/ampdata/kurucz23/sekur.html

KHz for $^{13}C^{16}O$ respectively. In our calculations we do not consider other isotopic species like $^{12}C^{17}O$, $^{14}C^{16}O$ etc. since they are expected to have low abundances. For the vibrational equilibrium constants the values used are w_e = 2169.75589(23) cm^{-1}, $w_e x_e$ = 13.28803(5) cm^{-1}, $w_e y_e$ = 0.0104109(43) cm^{-1} for ^{12}CO; w_e = 2141.162 cm^{-1} , $w_e x_e$ = 12.711 cm^{-1}, $w_e y_e$ = 0.0107 cm^{-1} for ^{13}CO. All the molecular constants are taken from the NIST database [2] except for the vibrational constants for ^{13}CO which are adopted from Benedict et al. (1962).

The line luminosity E of each rovibrational transition can be calculated from knowing the population of the upper level involved in the transition, the associated transition probability for the line (Goorvitch 1994) and the photon energy ($h\nu$) associated with the transition. To enable a comparison of the model value with the observed data, the line luminosity E calculated above, which is in units of ergs/sec, needs to be converted into units of the observed flux (we use units of ergs/s/cm^2/μm). This conversion is achieved by first dividing E by $4\pi D^2$ (where D is the distance to the source) and subsequently scaling E to a unit of wavelength. In implementing the last step, it is assumed that each rotational line is gaussian in shape. Then, the peak intensity of such a gaussian (plotted with its ordinate units in ergs/s/cm^2/μm; abscissa in units of μm) can be determined analytically by ensuring that the integrated area under this gaussian matches the known quantity $E/4\pi D^2$. The gaussian line profiles of all the rotational lines are thus generated and co-added together to generate the resulting envelope of the CO emission. To this envelope we add the appropriate continuum, the level of which is determined from broad band photometry of Table 5.2, to provide a model CO emission spectrum for a particular day. Such model spectra matching the observed data of 28 and 31 March; and 2 and 3 April are shown in Figure 5.5. The parameters that are fed as inputs for the modeling are the total mass of the CO gas (M_{CO}), the $^{12}C/^{13}C$ ratio (designated as α) and the gas temperature (T_{CO}). Once M_{CO} and α are chosen, the total number of ^{12}CO and ^{13}CO molecules are fixed - thus the level populations in thermal equilibrium at a temperature T_{CO} can be calculated and the emerging spectrum determined. The estimated model CO flux is therefore an absolute quantity but it could however be subject to certain errors. One of these is the value of the distance D to the source - the model CO flux scales as D^2.

Different combinations of the parameters M_{CO}, α and T_{CO} were tried to find the best fit between model spectra and the observed data. The characteristics of the

[2] http://physics.nist.gov/PhysRefData/MolSpec

CO emission remains fairly constant between 28 March and 3 April. The profiles of Figure 5.6 are reasonably well modeled with closely similar values of T_{CO} and M_{CO} in the range of 4000 - 4300K and 2.75x10^{-8} to 3.25x10^{-8} $M_{\odot}$ respectively. Some of the difficulties encountered in the modeling, and also possible sources of errors involved therein, are as follows. It is noted that changes brought about in the spectra by either changing T_{CO} or changing M_{CO} can be similar in the following respect. Increasing either of these quantities enhances the absolute level of the CO emission. However, the contributions of these two parameters can be distinguished by the fact that increasing M_{CO} just scales up the overall level of the CO emission level. On the other hand, increasing T_{CO} not only increases the CO flux but additionally changes the intensities of the different vibrational bands, relative to each other, within the first overtone. Therefore, vibrational bands from v≥5, would help the analysis, but they are located in regions of poor atmospheric transmission, beyond the spectral coverage and the v=5-3 band is barely covered.

While making the fits we note that the CO bands are likely contaminated by CI lines at 2.2906 and 2.2310 μm and from NaI lines at 2.3348 and 2.3379 μm. The position of these lines are marked in the bottom panel of Figure 5.6 and there are discernible structures at these positions, in most of the profiles, indicating these lines are present. The 2.29 μm (v = 2-0) band would appear to be affected, especially by the CI 2.2906 line which can be significant in strength in carbon-oxygen novae (Rudy et al. 2003; Das et al. 2008) and whose presence is possibly responsible for lack of agreement between model and observed data in this region. In view of the above, we have relied more on the fits to the higher bands (the v = 3-1 and 4-2 bands) while estimating the CO parameters. We have also assumed the CO emission to be optically thin. For the assumptions and constraints outlined above, the formal fits of Figure 5.6 yield estimates of T_{CO} of 4100, 4000, 4100 and 4300K (with an error of ± 400K) for 28 March, 31 March, 2 April and 3 April. We find that a constant CO mass of 3.0x10^{-8} $M_{\odot}$, or at most a marginal variation of M_{CO} between 2.75x10^{-8} to 3.25x10^{-8} $M_{\odot}$, can account for the observed profiles on the four days. The fits shown in all panels of Figure 5.6 are made for the same mass of 3.0x10^{-8} $M_{\odot}$ and the implications of a fairly constant mass is discussed shortly.

As in earlier studies on the $^{12}C/^{13}C$ ratio in a few novae, discussed in the following subsection, we are also able to place only a lower limit on this ratio viz. $^{12}C/^{13}C$ is greater than 2. If this ratio is decreased below 2, the ^{13}CO contribution becomes rather prominent i.e. the ^{13}CO bandheads begin to prominently appear in the

synthetic spectra resulting in poor model fits. The determined lower limit for the $^{12}C/^{13}C$ ratio may be compared with that expected from theoretical calculations. For carbon-oxygen novae like V2615 Oph, the expected $^{12}C/^{13}C$ ratio in the ejecta has been computed (e.g. Jose and Hernanz 1998; Starrfield et al. 1997) and shown to be dependent on the white dwarf mass among other parameters. Different models by Jose and Hernanz (1998) show that this ratio is approximately constrained between 0.3 to 0.65 for a white dwarf mass between 0.8 to 1.15 $M_{\odot}$; Starrfield et al. (1997) find the $^{12}C/^{13}C$ ratio to decrease from 2.4 to 0.84 as the white dwarf mass increases form 0.6 to 1.25 $M_{\odot}$. However, our observations and modeling seem to indicate that ^{13}C is possibly not synthesized to the high levels predicted by the theoretical models.

To calculate the CO column density, we assume that the CO is uniformly spread in a shell of thickness ΔR and volume $4\pi R^2\Delta$R. The radius R of the shell is estimated kinematically knowing the time elapsed since outburst and the velocity of the shell. A value of $\sim$ 1450 km/s is adopted for the shell velocity based on the P-Cygni terminal velocity reported by Munari et al. (2007b) and similar values of the FWHM of the near-IR lines as found in this work. The column density, which is proportional to $(M_{CO}\Delta R)/(4\pi R^2\Delta R)$, is then independent of the thickness of the shell. In this manner we determine the CO column densities to be $7.5\text{x}10^{18}$, $4.1\text{x}10^{18}$, $3.8\text{x}10^{18}$ and $2.9\text{x}10^{18}$ cm^{-2} on 28 March, 31 March, 2 April and 3 April respectively.

It maybe useful to present similar results in other known novae in which the first overtone of CO has been detected. These are V2274 Cyg (Rudy et al. 2003), NQ Vul (Ferland et al. 1979), V842 Cen (Hyland & Mcgregor 1989, Wichmann et al. 1990, 1991), V705 Cas (Evans et al. 1996) and V1419 Aql (Lynch et al. 1995). The CO mass M_{CO} was determined to be $10^{25.5\pm0.5}$ gms (i.e. $1.6\text{x}10^{-8}$ $M_{\odot}$) in NQ Vul by Ferland et al. (1979) from observations 19 days after outburst or 20 days before the large visual fading associated with dust formation. A limit of $^{12}C/^{13}C$ greater than 3.0 and a temperature T_{CO} = 3500 ± 750K were determined for the object. In V2274 Cyg, Rudy et al. (2003) from observations 17 days after discovery, determined M_{CO} = $8\text{x}10^{-9}$ $M_{\odot}$, $^{13}C/^{12}C \geq 0.83 \pm 0.3$ and T_{CO} = 2500K. In nova V705 Cas, observations by Evans et al. (1996) taken at two epochs i.e. one day before maximum light and 26.5 days after maximum light yielded estimates for M_{CO} of $(2.8 \pm 0.2)\text{x}10^{-10}$ $M_{\odot}$ and $(3.8 \pm 0.2)\text{x}10^{-10}$ $M_{\odot}$ respectively and T_{CO} equal to 4300 ± 300K & 4500 ± 300K respectively. They estimate the $^{12}C/^{13}C$ ratio to be ≥ 5 and the CO column density to be $2\text{x}10^{17}$ cm^{-2} for M_{CO} equal to $1.0\text{x}10^{-10}$ $M_{\odot}$. Apart from the above sources,

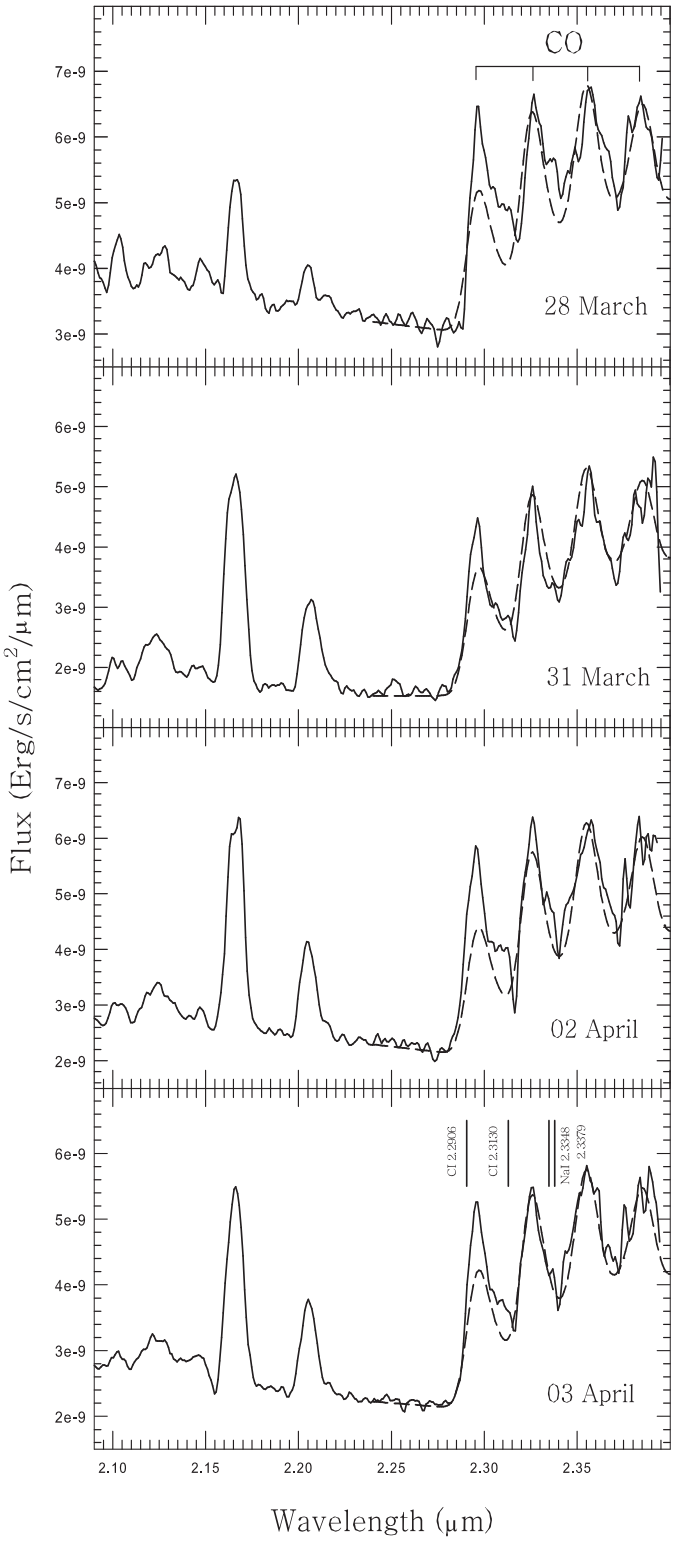

Figure 5.6: Model fits (dashed lines) to the observed first overtone CO bands in V2615 Oph. The fits are made for a constant CO mass of 3.0x10^{-8} $M_{\odot}$ on all days while the temperature of the gas T_{CO} is estimated to be 4100, 4000, 4100 and 4300K (with an error of ± 400K) for 28 & 31 March and 2 & 3 April respectively. The bottom panel shows the position of certain CI and NaI lines that complicate the modeling. The other prominent lines seen in the spectra are Br γ at 2.1655 μm; NaI 2.2056, 2.2084 μm blended with weaker emission from CI 2.2156, 2.2167 μm lines and other CI lines between 2.1 and 2.14 μm. The position of the $^{12}C^{16}O$ bandheads are shown in the top panel.

the $^{12}C/^{13}C$ ratio has also been estimated in two other novae. In DQ Her this ratio was found to be ≥ 1.5 by Sneden and Lambert (1975); in V842 Cen observations between days 29 and 45 after outburst by Wichmann et al. (1991) show the $^{12}C/^{13}C$ ratio to be 2.9 ± 0.4.

5.3.5 Evolution of the CO emission

The detection of CO over a significant duration of time in the present observations, presents an opportunity - not available before - to study the formation and destruction of CO during a nova outburst. The earliest theoretical studies of the chemistry of novae were done by Rawlings (1988) in the form of pseudo-equilibrium chemical models of the pre-dust-formation epoch. These models, which were developed with the main aim of explaining the observed presence of CO in novae, found that the outer parts of the ejecta have to be substantially more dense and less ionized than the bulk of the wind for substantial molecule formation to occur. For this to occur carbon has to be neutral. In a neutral carbon region, the carbon ionization continuum, which extends to less than 1102 Å, shields several molecular species against the dissociative UV flux from the central star. A more refined model for molecule formation in the nova outflow in the early stages is presented in Pontefract and Rawlings (2004; hereafter PR) - we try to correlate the present observational findings with the results in this work. The PR studies are a major extension of their earlier models with only one major qualitative point of departure viz. neutral-neutral reactions are now shown to be more important than photoreactions in determining the nova chemistry.

A significant result in PR is the prediction of the evolution of the fractional CO abundance with time. Two models are considered - model A considers oxygen rich ejecta and model B considers carbon rich ejecta. Figure 5.7 is reproduced here from PR which show the evolution of the fractional abundance of different molecules and radicals, including CO, with time. It is seen that in both models, the CO abundance remains constant upto about 2 weeks after outburst ($\sim$ 12 days in case A and $\sim$ 15 days in case B). This behaviour, and the length of its duration, seems to be generic to the models. During this phase the CO is saturated - that is to say, all the available oxygen or carbon, whichever has the lower abundance, is completely incorporated into forming CO. After this there is a sharp decline in the CO abundance as CO is destroyed mostly by reactions with N and N^+. During this stage, from Figure 5.7, we estimate an approximate decrease in CO by a factor of 1000 in $\sim$ 27days for model A

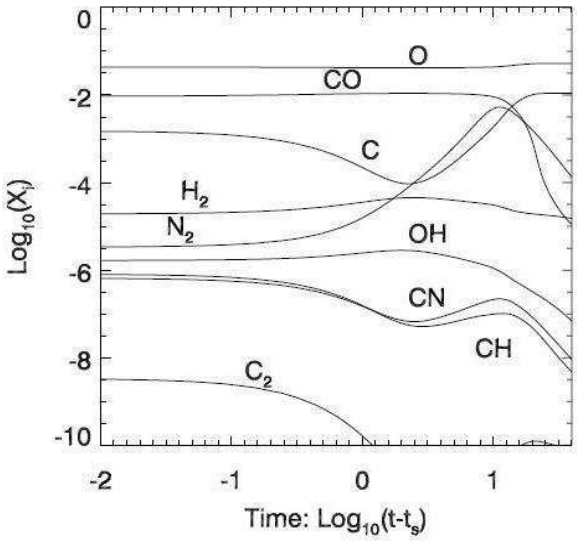

(a) Results from model A

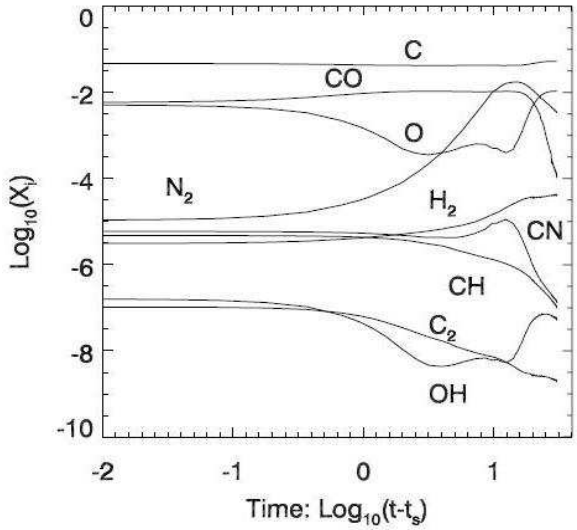

(b) Results from model B

Figure 5.7: This figure, taken from Pontefract & Rawlings (2004), shows time-dependence of the fractional abundances of selected species predicted by model calculations. Time is measured in units of days time, post visual maximum. Two models are considered - model A considers oxygen rich ejecta and model B considers carbon rich ejecta.

and a decrease by a factor of 100 in ~ 16 days for model B. The present data allows to check on these two vital aspects of the model predictions viz. the existence of a short-lived saturated phase followed by a phase involving rapid destruction of CO.

The present observations and modeling show that the CO mass was constant between 28 March and 3 April i.e. for a period of 7 days. This puts a lower limit on the duration of the saturated phase since our observations commenced on 28 March, nearly 8-9 days after the beginning of the outburst on Mar. 19.812 UT. It is possible that the CO emission was present, and at similar levels, between March 19 and March 28 also. After all, CO has been seen very early after commencement of the eruption as in the case of V705 Cas (Evans et al. 1996). If that is the case, then the upper limit on the saturated-phase timescale would be around 15 days. Thus the evidence indicates that a phase does exist when the CO mass is constant and whose duration t_s is constrained within $7 \leq t_s \leq 16$ days. This observational finding conforms well with the predicted timescales of ~ 12-15 days from the PR model calculations.

Between 3 April and 5 April there is a sudden decrease in the CO strength. It is difficult to meaningfully model the 5 April data, and hence derive the CO parameters, because the relative contribution of the CI 2.2906 μm line is considerable at this stage. Also the signal-to-noise ratio in the region around the CO emission region begins to get low now. However, if we assume that T_{CO} has not changed drastically between 3 and 5 April, then from the diminished CO flux on the latter date, we estimate that M_{CO} has decreased by a factor of 3. Beyond this date, the decrease in the CO emission continues to take place, with a possible restrengthening again on 16 April, to finally drop below measurable limits by 27-30 April. But the data beyond 5 April is of inadequate quality to make a quantitative assessment of the strength of the CO emission beyond this stage (or indeed whether CO is even present on some of the days; the presence of the CI lines complicates the assessment further). However, a quantitative assessment can certainly be made with a good degree of surety - there is a phase of rapid reduction in the CO emission after 3 April. The initial decrease is indeed rapid - the spectra over a 4 day gap, between 3 April and 7 April, have only to be compared to establish this. This quantitative behaviour i.e. the rapid destruction of CO following the saturated phase is again largely consistent with the predictions of the theoretical model by PR.

It is also possible to estimate the CO:C ratio, though with substantial uncertainties,

at different stages of the CO evolution and compare it with model predictions. We assume the entire ejecta mass to be in the range of 10^{-5} to 10^{-6} $M_{\odot}$ which is fairly representative for the mass of novae ejecta. Carbon can be assumed to comprise about 10 percent of this mass as indicated by model calculations for elemental abundances (Jose and Hernanz, 1998) in CO novae like V2615 Oph. Thus, in the initial saturated phase when M_{CO} is found to be 3x10^{-8} $M_{\odot}$, the CO:C ratio is determined to lie in the range between 10^{-1} and 10^{-2}. This would clearly rule out the PR models in which the initial abundances of carbon are less than oxygen (model A) and be consistent with model B (carbon rich) where a CO:C ratio of $\sim 10^{-1}$ is expected. At later stages, after the destruction of CO, M_{CO} is difficult to estimate precisely but it is certainly lower than one-tenth of its value during saturation. This suggests that CO:C is in the range 10^{-2} to 10^{-3} and likely to be even lower. This is again reasonably consistent with the PR results which find that in most models, regardless of whether the ejecta is O or C rich the CO:C ratio decreases with time and is less than 10^{-3} at a time greater than 50 days.

5.4 Summary of this chapter

In this chapter we have presented near-infrared (1 - 2.5 μm) spectroscopic and photometric results of Nova V2615 Ophiuchi which was discovered in outburst in 2007 March. Our observations span a period of $\sim$ 80 days starting from 2007 March 28 when the nova was at its maximum light. The evolution of the spectra are shown from the initial P-Cygni phase to an emission-line phase and finally to a dust formation stage. The characteristics of the *JHK* spectra are very similar to those observed in a nova outburst occurring on a carbon-oxygen white dwarf. We analyze an observed line at 2.088 μm and suggest it could be due to FeII excited by Lyman α fluorescence. The highlight of the observations is the detection of the first overtone bands of carbon monoxide (CO) in the 2.29 - 2.40 μm region. The CO bands are modeled to estimate the temperature and mass of the emitting CO gas and also to place limits on the ^{12}C/^{13}C ratio. The CO bands are recorded over several epochs thereby allowing a rare opportunity to study its evolution from a phase of constant strength through a stage when the CO is destroyed fairly rapidly. We compare the observed timescales involved in the evolution of the CO emission and find a good agreement with model predictions that investigate the chemistry in a nova outflow during the early stages.

CHAPTER 6

Summary and Scope For Future Work

We summarize, in this chapter, the work contained in this thesis with emphasis on the important and new results that have been obtained. The scope for future work, as an extension of and related to the current studies, is also discussed.

6.1 Summary

The thesis presents the near-Infrared (1-2.5 μm) spectroscopic and photometric studies of the following three novae:

1. RS Ophuchi (RS Oph), the well known recurrent nova. The recent outburst have been discovered on 2006 February 12.83 UT. Our observations of this nova commenced immediately after outburst and extended upto 94 days after outburst.

2. V1280 Scorpii (V1280 Sco), a classical nova. It was discovered in outburst on 2007 February 4.85 UT. This object was observed for 125 days after outburst.

3. V2615 Ophiuchi (V2615 Oph), a classical nova. This was discovered on 2007 March 19.812 UT and was followed for next 80 days.

These objects were observed extensively using the 1.2m telescope (+NICMOS) at Mount Abu Infrared Observatory, India. The important results obtained from the extensive studies of these novae are described below.

6.1.1 Results from the study of RS Oph

1. We report the rare detection of an infrared shock wave as the nova ejecta plows into the pre-existing wind of the secondary in the RS Oph system. The evolution of the shock is traced through a free expansion stage to a decelerative phase. The behavior of the shock velocity with time is found to be broadly consistent with current shock models.

2. From the present observations we estimate the white dwarf mass to be 1.35 $M_{\odot}$. This implies that the white dwarf in the RS Oph system has a high mass and it could be a potential SNIa candidate.

3. We discuss the behaviour and origin of the Fe II lines at 1.6872 and 1.7414 μm that are prominently seen throughout the span of the observations. It is examined and shown that Lyman α, Lyman continuum fluorescence and aditionally collisional excitation are viable mechanisms to excite these lines.

4. We draw upon the result, that collisional excitation can also contribute in exciting and significantly enhancing the strength of these Fe II lines, to propose that these lines as well as the near-IR emission originate from a site of high particle density. Such a likely site could be the high-density, low temperature ($\sim 10^4$ K) contact surface that should exist in the shockfront in between the shocked ejecta and red giant wind.

5. From recombination analysis of the HI lines, we notice deviations from Case B conditions during most of the span of our observations indicating optical depth effects.

6. Since the *H* band Fe II lines, which originate from the contact surface, are observed till the end of our observations, it appears likely that the breakout of the shockfront had not yet occurred till the end of our observations.

7. An analysis is made of the temporal evolution of the [Si VI] 1.9641 μm coronal line and another coronal line at 2.0894 μm which is attributed to [Mn XIV]. Assuming collisional effects to dominate in the hot coronal gas, we estimate the coronal temperature to be 1.6×10^6 K and 4×10^5 K on 2006 March 16.95 and March 30.86 respectively.

8. Analysis of the HI line profiles show the presence of broad wings on both flanks of a strong central component indicating the presence of a bipolar velocity flow (at radial velocities of -2540 and +2485 km/s for Pa β and at

-2340 and 2160 km/s for the Br γ lines respectively) in the ejecta. Such a flow is kinematically consistent with the bipolar structure that the object displays in high-resolution spatial images.

9. The photometric data shows that the behavior of the infrared lightcurve is quite similar to that of the 1985 outburst. Though it is known that the visual lightcurve behaves similarly from outburst to outburst, an equivalent comparison for the near-infrared lightcurve had not been possible earlier for lack of data.

6.1.2 Results from the study of V1280 Sco

1. The key result concerns the issue of predicting which novae will form dust. We have identified diagnostic lines which are shown to reliably aid in such a prediction. It is demonstrated, and strikingly corroborated with observations, that the presence of lines in the early spectra of low-ionization species like Na and Mg - indicative of low temperature conditions - appear to be reliable indicators that dust will form in the ejecta.

2. A synthetic LTE spectrum is generated to facilitate line identification to qualitatively study different aspects of the observed spectral features. Our model could identify a few weak but significant features those had gone unnoticed in the previous studies.

3. From the synthetic spectrum we estimate the relative abundances of different species in terms of mass fractions, are 0.41, 0.21, 0.147, 0.096, 0.13, 0.0051 and 0.0010 for H, He, C, N, O, Ne and Na-Fe respectively. This indicates that the metal abundance in the nova ejecta is very high relative to the cosmic abundance - this is expected in general for novae.

4. The presence of a persisting absorption structure in the Br γ line is interpreted as evidence for sustained mass-loss during the outburst and used to set a lower limit of 25-27 days for the mass loss duration.

5. We have made a study of the early fireball expansion in the nova. We calculate the angular diameter on different days and show how the fireball expanded. Though subject to some uncertainty, it would appear the expansion rate was marginally slower between 6 to 12 Feb. but subsequently increased therafter to $\sim$ 0.105 mas/day.

6. Consistent with the nova's prolonged climb to maximum, it is shown that the actual outburst commenced very early indeed - approximately 13.7 days before maximum light.

6.1.3 Results from the study of V2615 Oph

1. The key observational result is the detection of first overtone bands of carbon monoxide (CO) in the 2.29 - 2.40 μm region. The CO bands are recorded over several epochs thereby allowing a rare opportunity to study its evolution from a phase of constant strength through a stage when the CO is destroyed fairly rapidly.

2. The CO bands are modeled to indicate an initial phase when the CO is saturated and whose duration t_s is constrained in the range $7 \leq t_s \leq 16$ days. During this phase, the gas temperature and mass are found to be fairly constant in the range of 4000 - 4300K and 2.75×10^{-8} to 3.25×10^{-8} $M_{\odot}$ respectively.

3. From the modeling we estimate the ratio of $^{12}C/^{13}C$ to be ≥ 2. This imply that ^{13}C is possibly not synthesized to the high levels as predicted by the theoretical models.

4. We also determine the CO column densities to be 7.5×10^{18}, 4.1×10^{18}, 3.8×10^{18} and 2.9×10^{18} cm^{-2} on 28 March, 31 March, 2 April and 3 April 2007 respectively.

5. Following the saturated phase, the CO is found to be destroyed fairly fast. The observed timescales involved in the evolution of the CO emission and the estimated CO:C ratio are compared with model predictions and found to be in good agreement.

6. We analyse an observed line at 2.088 μm and suggest it could be due to FeII. It is shown that this line is likely excited by Lyman α fluorescence process.

6.2 Scope of future work

In this closing section it would be appropriate to indicate a few suggestions for future work. I plan to complete the following tasks in continuation of the present studies. First, as already mentioned a fairly large number of novae have been observed (Chapter 2) during the course of the studies presented here. Out of

these, three novae could be analyzed and studied in details. However, a significant amount of observations were obtained for a few other novae. In addition, from the preliminary analysis of the data, we find that few of these novae show rather interesting features. For example, V476 Scuti formed optically thin dust, V5558 Sgr had an unusual light curve displaying multiple outbursts accompanied by narrow spectral lines and V2575 Oph was caught in the initial stage when the spectral lines were in absorption. I will complete the analysis of the remaining data on these objects and publish the results. These results should add to further insights into the infrared development of novae as described in this dissertation.

Second, apart from the novae observed by me, systematic infrared observations of other novae have been going on for a decade or more from the Mount Abu observatory. Using the entire database of these observed novae, one of our prime aims will be to classify novae in the infrared along similar lines as that proposed by Williams (1992) based on optical spectra. Such an attempt at an infrared classification, based on the spectra, has not been made earlier. It is particularly important to make such a scheme in the near-infrared, since an infrared classification of a nova will supplement its classification and properties in the optical regime where a wealth of past measurements already exist. It is felt that such a study should add value to our understanding of the nova phenomenon. Progress in this direction has already commenced and we hope to complete the investigation in the near future.

Bibliography

Allen C.W., 1976, *Astrophysical Quantities*, Athlone Press, London and Dover.

Aller L.H., 1963, *The Atmospheres of the Sun and Stars*, Ronald Press, New York.

Andrea J., Drechsel H. & Starrfield S., 1994, *A&A*, 291, 869.

Ashok N. M. & Banerjee D. P. K., 2002, *BASI*, 30, 851.

Ashok N. M. & Banerjee D. P. K., 2003, *A&A*, 409, 1007.

Ashok N. M., Banerjee D. P. K., Varricatt W. P. & Kamath U. S., 2006, *MNRAS*, 368, 592.

Banerjee D. P. K., Bobra A. D. & Subhedar D. V., 1997, *BASI*, 25, 555.

Banerjee D. P. K., Janardhan, P. & Ashok, N. M., 2001, *A&A*, 380, L13.

Banerjee D.P.K., Das R.K. & Ashok N.M., 2009, to be published in *MNRAS*, arXiv0903.3794.

Bautista M. A., Rudy R. J. & Venturini C. C., 2004, *ApJ*, 604, L129.

Benedict W. S., Herman R., Moore G. E. & Silverman S., 1962, *ApJ*, 135, 277.

Bessel M. S., Castelli F. & Plez B., 1998, *A&A*, 333, 231 (err. 337, 321).

Bode M. F., & Kahn F., 1985, *MNRAS*, 217, 205.

Bode M. F., O'Brien T. J., Osborne J. P., Page K. L., Senziani F., Skinner G. K., Starrfield S., Ness J. -U., Drake J. J., Schwarz G., Beardmore A. P., Darnley M. J., Eyres S. P. S., Evans A., Gehrels N., Goad M. R., Jean P., Krautter J. & Novara G., 2006, *ApJ*, 652, 629.

Bode M. F., Harman D. J., O'Brien T. J., Bond H. E., Starrfield S., Darnley M. J., Evans A. & Eyres S. P. S., 2007, ApJ, 665, L63.

Bode M. F. & Evans A., eds., 2008, *Classical Novae*, Cambridge University Press.

Boyarchuk A. A. & Antipova L. I., 1990, *Lect. Notes Phys.*, 369, 97.

Brandi E., Quiroga C., Mikolajewska J., Ferrer O. E. & Garcia L. G., 2009, *A&A*, 497, 815.

Buil C. 2006, *CentralBureauElectron.Telegrams*, 403.

Buil C., 2007, *IAU Circ.*, 8812.

Capaccioli M., della Valle M., Rosino L. & D'Onofrio M., 1989, *AJ*, 97, 1622.

Casatella A. & Viotti R., eds., 1990, *Physics of Classical Novae*, Springer, Berlin.

Chesneau O., Nardetto N., Millour F., Hummel C., Domiciano de Souza A., Bonneau D., Vannier M., Rantakyrö F., Spang A., Malbet F., Mourard D., Bode M. F., O'Brien T. J., Skinner G., Petrov R. G., Stee P., Tatulli E. & Vakili F., 2007, *A&A*, 464, 119.

Chesneau O., Banerjee D. P. K., Millour F., Nardetto N., Sacuto S., Spang A., Wittkowski M., Ashok N. M., Das R. K., Hummel C., Kraus S., Lagadec E., Morel S., Petr-Gotzens M., Rantakyro F. & Schöller M., 2008, *A&A*, 487, 223.

Ciardullo R., Tamblyn P., Jacoby G. H., Ford H. C. & Williams R. E., 1990, *AJ*, 99, 1079.

Clark D. H. & Stephenson F. R., 1977, *The Historical Supernovae*, Oxford: Pergamon Press.

Cohen J. G., 1988, in *The Extragalactic Distance Scale*, ASP Conf Ser., Vol. 4, eds. van den Bergh S. & Pritchet C. J., Astron. Soc. Pac., San Francisco, p. 114.

Dalgarno A., Stancil P. C. & Lepp S., 1997, *ApSS*, 251, 375.

Darnley M. J., Bode M. F., Kerins E. J., Newsam A. M., An J., Baillon P., Belokurov V., Calchi Novati S., Carr B. J., Crézé M., Evans N. W., Giraud-Héraud Y., Gould A., Hewett P., Jetzer Ph., Kaplan J., Paulin-Henriksson S., Smartt S. J., Tsapras Y. & Weston M., 2006, *MNRAS*, 369, 257.

Das R.K., Ashok N. M., & Banerjee D. P. K., 2006, *IAU Circ.*, 8673.

Das R.K., Banerjee D.P.K. & Ashok N.M., 2006, *ApJ*, 653, L141.

Das R.K., Ashok N.M. & Banerjee D.P.K., 2007a, *Central Bureau Electron. Telegrams*, 864.

Das R.K., Ashok N.M. & Banerjee D.P.K., 2007b, *Central Bureau Electron. Telegrams*, 866.

Das R.K., Ashok N.M. & Banerjee D.P.K., 2007c, *Central Bureau Electron. Telegrams*, 925.

Das R.K., Banerjee D.P.K. & Ashok N.M. & Chesneau O., 2008, *MNRAS*, 391, 1874.

Das R.K., Banerjee D.P.K. & Ashok N.M., 2009, *MNRAS*, 398, 375.

della Valle M., 1991, *A&A*, 252, L19.

della Valle M., Bianchini A., Livio M. & Orio M., 1992, *A&A*, 266, 232.

della Valle M. & Livio M., 1995, *ApJ*, 452, 704.

Dobrzycka D. & Kenyon S.J., 1994, *AJ*, 108, 2239.

Duerbeck H. R. in *Classical Novae*, Second Edition, 2008, eds. Bode M.F & Evans A., Cambridge University Press, p. 4.

Evans A., Callus C. M., Albinson J. S., Whitelock P. A., Glass I. S., Carter B. & Roberts G., 1988, *MNRAS*, 234, 755.

Evans A., Geballe T. R., Rawlings J. M. C. & Scott A. D., 1996, *MNRAS*, 282, 1049.

Evans A., 2001, in *Dust formation in nova winds*, *ApSS*, 275, 131.

Evans A., Kerr T., Yang B., Matsuoka Y., Tsuzuki Y., Bode M. F., Eyres S. P. S., Geballe T. R., Woodward C. E., Gehrz R. D., Lynch D. K., Rudy R. J., Russell R. W., O'Brien T. J., Starrfield S. G., Davis R. J., Ness J. -U., Drake J., Osborne J. P., Page K. L., Adamson A., Schwarz G. & Krautter J., 2007a, *MNRAS*, 374, L1.

Evans A., Woodward C. E., Helton L. A., van Loon J. Th., Barry R. K., Bode M. F., Davis R. J., Drake J. J., Eyres S. P. S., Geballe T. R., Gehrz R. D., Kerr T., Krautter J., Lynch D. K., Ness J. -U., O'Brien T. J., Osborne J. P., Page K. L., Rudy R. J., Russell R. W., Schwarz G., Starrfield S. & Tyne V. H., 2007b, *ApJ*, 671, L157.

Fekel F.C., Joyce R.R., Hinkle K.H. & Skrutsie M.F., 2000, *AJ*, 119, 1375.

Ferland G. J., Lambert D. L., Netzer H., Hall D. N. B. & Ridgway S. T., 1979, *ApJ*, 227, 489.

Fujii M., 2006, *IAU Circ.*, 8869.

Gallegher J. S. & Code A. D., 1974, *ApJ*, 189, 303.

Gehrz R. D., Grasdalen G. L., Hackwell J. A. & Ney E. P., 1980, *ApJ*, 237, 855.

Gehrz R.D., 1988, ARA&A, 26, 377.

Gehrz R. D., Harrison T. E., Ney E. P., Matthews K., Neugebauer G., Elias J., Grasdalen G. L. & Hackwell J. A., 1988, *ApJ*, 329, 894.

Gehrz R. D., Truran J. W., & Williams R. E., 1993, in *Protostars and Planets III*, eds. E. H. Levy & J. I. Lunine, Tuscon: Univ. Arizona Press, p. 75.

Gehrz R.D., Truran J. W., Williams R. E. & Starrfield S., 1998, *PASP*, 110, 3.

Gehrz R. D., 2002, in *Classical Nova Explosions*, eds. Hernanz M. & José J., NewYork: American Institute of Physics, p. 198.

Gehrz R.D., 2008, in *Classical Novae*, Second Edition, eds. Bode M.F. & Evans A., Cambridge University Press, p. 175.

Gerasimovic B. P., 1936, *Pop. Astr.*, 44, 78.

Goorvitch D., 1994, *ApJS*, 95, 535.

Gorbatski V. G., 1972, *Soviet Astronomy*, 16, 32.

Hachisu I. & Kato M., 2000, ApJ, 536, L93.

Hachisu I. & Kato M., 2001, *ApJ*, 558, 323.

Hamann F. & Persson S. E., 1989, *ApJS*, 71, 931.

Hamann F., Simon M., Carr J. S. & Prato L., 1994, *ApJ*, 436, 292.

Harman D. J., Bode M. F., Darnley M. J., O'Brien T. J., Bond H. E., Starrfield S., Evans A., Eyres S. P. S., Ribeiro V. A. R. M. & Echevarria J. M., 2008, *ASPC*, 401, 246.

Henden A. & Munari U., 2007, *IBVS*, 5771.

Hirosawa K., 2006, *IAU Circ.*, 8671.

Hubble E., 1929, *ApJ*, 69, 103.

Hjellming R. M. & Wade C. M., 1970, *ApJ*, 162, L1.

Hjellming R. M., 1974, in *Galactic and Extragalactic Radio Astronomy*, eds. Vershuur G. L. & Kellermann K. I., NewYork: Springer, p. 159.

Hyland A.R. & McGregor P.J., 1989, IAU Symposium No. 135, *Interstellar Dust*, ed. L.J. Allamandola & A.G.G.M. Tielens (NASA CP-3036; Washington: NASA), 495.

Iben I. Jr. & Livio M., 1993, *PASP*, 105, 1373.

Iijima T., 2006, *IAU Circ.*, 8675

Johansson S., 1977, *MNRAS*, 178, 17.

Johansson S. & Jordan C., 1984, *MNRAS*, 210, 239.

Jordan C., 1969, *MNRAS*, 142, 501.

Jose J. & Hernanz M., 1998, ApJ, 494, 680.

Joy A. H., 1940, *PASP*, 52, 324.

Joy A. H., 1956, *ApJ*, 124, 317.

Kantharia N. G., Anupama G. C., Prabhu T. P., Ramya S., Bode M. F., Eyres S. P. S. & O'Brien T. J., 2007, *ApJ*, 667, L171.

Koornneef J., 1983, *A&A*, 128, 84.

Kraft R. P., 1962, *ApJ*, 135, 408.

Kraft R. P., 1964, *ApJ*, 139, 457.

Krautter J., Ögelman H., Starrfield S.,Wichmann R. & Pfeffermann E., 1996, *ApJ*, 456, 788.

Krautter J., 2002, in *Classical Nova Explosions*, eds. Hernanz M. & José J., NewYork: American Institute of Physics, p. 345.

Krautter J., 2008, in *Classical Novae*, Second Edition, eds. Bode, M.F. & Evans A., Cambridge University Press.

Lamers H.J.G.L.M., & Cassinelli, J.P. 1999, *Introduction to Stellar Winds*, Cambridge University Press, UK.

Landini M. & Monsignori Fossi B. C., 1972, A&AS, 7, 291.

Liller W. & Mayer B., 1987, *PASP*, 99, 606.

Livio M. & Truran J. W., 1992, *ApJ*, 389, 695.

Livio M., 2000, in *Type Ia Supernovae: Theory and Cosmology*, eds. Niemeyer J. C. & Truran J. W., Cambridge Univ. Press, Cambridge.

Lynch D.K., Rossano G.S., Rudy R.J. & Puetter R.C, 1995, *AJ*, 110, L2274.

Lynch D. K., Rudy R. J., Mazuk S. & Puetter R. C., 2000, *ApJ*, 541, 791.

Lynch D. K., Wilson J. C., Rudy R. J., Venturini C., Mazuk S., Miller N.A. & Puetter R. C., 2004, *AJ*, 127, 1089.

MacDonald J., 1984, *ApJ*, 283, 241.

Marshall D. J., Robin A. C., Reyle C., Schultheis M. & Picaud S., 2006, *A&A*, 453, 635.

McLaughlin D. B., 1939, *Pop. Astr.*, 47, 410, 481, 538.

McLaughlin D. B., 1945, *PASP*, 57, 69.

McLaughlin D. B., 1960, in *Stellar Atmospheres*, ed. Greenstein J. L., Chicago: University of Chicago Press.

Monnier J.D., Barry R. K., Traub W. A., Lane B. F., Akeson R. L., Ragland S., Schuller P. A., Le Coroller H., Berger J.-P., Millan-Gabet R., Pedretti E., Schloerb F. P., Koresko C., Carleton N. P., Lacasse M. G., Kern P., Malbet F., Perraut K., Kuchner M. J. & Muterspaugh M. W., 2006, *ApJ*, 647, L127.

Munari U., Valisa, P., Dalla Via G. & Dallaporta S., 2007a, Central Bureau Electron. Telegrams, 852.

Munari U., Siviero A., Valentini M., Ochner P. & Dallaporta S., 2007b, Central Bureau Electron. Telegrams, 906.

Munari U. & Siviero A., 2007c, Central Bureau Electron. Telegrams, 1099.

Munari U., Henden A., Valentini M., Siviero A., Dallaporta S., Ochner P. & Tomasoni S., 2008, *MNRAS*, 387, 344.

Naik S., Banerjee D. P. K. & Ashok N. M., 2009, *MNRAS*, 394, 1551.

Naito H. & Narusawa S., 2007a, *IAU Circ.*, 8803.

Naito H. & Narusawa S., 2007b, *IAU Circ.*, 8824.

Nelson T., Orio M., Cassinelli J. P., Still M., Leibowitz E. & Mucciarelli P., 2008, *ApJ*, 673, 1067.

Ness J. -U., Starrfield S., Beardmore A. P., Bode M. F., Drake J. J., Evans A., Gehrz R. D., Goad M. R., Gonzalez-Riestra R., Hauschildt P., Krautter J., O'Brien T. J., Osborne J. P., Page K. L., Sch*önrich* R. A. & Woodward C. E., 2007, *ApJ*, 665, 1334.

Ness J. -U., Drake J. J., Starrfield S., Bode M. F., O'Brien T. J., Evans A., Eyres S. P. S., Helton L. A., Osborne J. P., Page K. L., Schneider C. & Woodward C. E., 2009, *AJ*, 137, 3414.

Ness J. -U., Schwarz G. J., Retter A., Starrfield S., Schmitt J. H. M. M., Gehrels N., Burrows D. & Osborne J. P., 2007, *ApJ*, 663, 505.

Ney E. P. & Hatfield B. F., 1978, *ApJ*, 219, L111.

Nishimura H., 2007, *IAU Circ.*, 8824.

O'Brien T. J., Bode, M. F. & Kahn, F. D., 1992, *MNRAS*, 255, 683.

O'Brien T.J., Bode M. F., Porcas R. W., Muxlow T. W. B., Eyres S. P. S., Beswick R. J., Garrington S. T., Davis R. J. & Evans A., 2006, Nature, 442, 279.

*Ö*gelman H., Beuermann K., & Krautter J., 1984, *ApJ*, 287, L31.

*Ö*gelman H., 1990, in *Physics of Classical Novae*, eds. Cassatella A. & Viotti R., Berlin: Springer, p. 148.

*Ö*gelman H., & Orio M., 1995, in *Cataclysmic Variables*, eds. Bianchini A., della Valle M. & Orio M., Astrophys. Space Sci. Lib., 205, p. 11.

Orio M., 1999, *Phys. Rep.*, 311, 419.

Orio M., 2004, *Rev. Mex. AA (Serie de Conferencias)*, 20, 182.

Osborne J. P., Page K., Starrfield S., Ness J. -U., Krautter J., Bode M., Orio M., Schwarz G., O'Brien T. & Belloni T., 2007, *The Astronomer's Telegram*, 1010.

Payne-Gaposchkin C., 1957, *The Galactic Novae*. Amsterdam: North-Holland.

Pontefract M. & Rawlings J. M. C., 2004, *MNRAS*, 347, 1294.

Prialnik D. & Kovetz A., 1995, *ApJ*, 445, 789.

Rawlings J. M. C., 1988, *MNRAS*, 232, 507.

Rodriguez-Ardila A., Viegas S. S., Pastoriza M. G. & Prato L., 2002, *ApJ*, 565, 140.

Rosino L.& Iijima T., 1987, in *RS Ophiuchi and the recurrent nova phenomenon*, ed. Bode M. F., VNU Science press, Utrecht, p. 27.

Rudy R. J., Rosano G.S. & Puetter R. C., 1991, *ApJ*, 383, 344.

Rudy R. J., Puetter R. C., Mazuk S. & Hamann F., 2000, *ApJ*, 539, 166.

Rudy R. J., Lynch D. K., Mazuk S., Venturini C. C. & Puetter R. C., 2001, *PASP*, 113, 916.

Rudy R. J., Lynch D. K., Mazuk S., Venturini C. C., Puetter R. C.& Perry R. B., 2002, *BAAS*, 34, 1162.

Rudy R. J., Dimpfl W. L., Lynch D. K., Mazuk S., Venturini C. C., Wilson J. C., Puetter R. C. & Perry R. B., 2003, *ApJ*, 596, 1229.

Rudy R. J., 2007a, *IAU Circ.*, 8845.

Rudy R. J., Lynch D. K. & Russell R. W., 2007b, *IAU Circ.*, 8809.

Rudy R. J., Russell W., Lynch D. K., Mazuk S., Pearson R. L., Woodward C. E., Puetter R. C. & Perry R. B., 2007c, *IAU Circ.*, 8846.

Rupen M. P., Mioduszewski A. J. & Sokoloski J. L., 2008, *ApJ*, 688, 559.

Sakurai Y. & Nakamura Y., 2007, *IAU Circ.*, 8803.

Schmeer P., 2007, *VSNET-alert* 9227.

Schmidt Th., 1957, *Zeitschrift für Astrophysik*, 41, 182.

Seaquist E. R. & Bode M. F., 2008, in *Classical Novae*, Second Edition, eds. Bode, M.F. & Evans A., Cambridge University Press.

Shore S.N., Kenyon S.J., Starrfield S. & Sonneborn G., 1996, *ApJ*, 456, 717.

Shafter A.W., 2002, in *Classical Nova Explosions*, eds. Hernanz M. & José J., NewYork: American Institute of Physics, p. 462.

Shull J. M. & van Steenberg M., 1982, *ApJS*, 48, 95.

Skopal A., Pribulla T., Buil C., Vittone A. & Errico L., 2009, *ASPC*, 401, 227.

Sneden C. & Lambert D. L., 1975, *MNRAS*, 170, 533.

Snijders M.A.J., Batt T.J., Seaton M.J., Blades J.C. & Morton D.C., 1984, *MNRAS*, 211, 7.

Snijders M. A. J., 1987, in *RS Ophiuchi(1985) and the recurrent nova phenomenon*, ed. Bode M. F., VNU Science press, Utrecht, p. 51.

Snijders M.A. J., Batt T. J., Roche P. F., Seaton M. J., Morton D. C., Spoelstra T. A. T. & Blades J. C., 1987, MNRAS, 228, 329.

Snijders M. A. J., 1990, *Lect. Notes Phys.*, 369, 188.

Sokoloski J.L., Luna G.J.M., Mukai K. & Kenyon S.J., 2006, Nature, 442, 276.

Spyromilio J., Meikle W. P. S., Learner R. C. M. & Allen D. A., 1988, *Nature*, 334, 327.

Starrfield S., Sparks W. M., & Truran J. W., 1986, *ApJ*, 303, L5.

Starrfield S., Gehrz R. D. & Truran J. W., in *Dust Formation & Nucleosynthesis in The Nova Outburst*, 1997, American Institute of Physics, vol. 402, p. 203.

Starrfield, S., Timmes, F.X., Hix, W.R. et al., 2004, ApJ, 612, L56.

Starrfield S., Iliadis C. & Hix W. R. in *Classical Novae*, Second Edition, 2008, eds. Bode M.F. & Evans A., Cambridge University Press, p. 96.

Stephenson F. R., & Green D. A., 2002, *Historical Supernovae and their Remnants*, Oxford: Clarendon Press.

Stickland D. J., Penn C. J., Seaton M. J., Snijders M.A. J. & Storey P. J., 1981, *MNRAS*, 197, 107.

Storey P. J. & Hummer D. G., 1995, MNRAS, 292, 41.

Swank J. H., 2007, *The Astronomer's Telegram*, 1011.

Vaytet N. M. H., O'Brien T. J. & Bode M. F., 2007, *ApJ*, 665, 654.

Venturini C., RudyR. J., LynchD. K., MazukS. & PuetterR.C., 2004, *AJ*, 128, 405.

Walker M. F., 1956, *ApJ*, 123, 68.

Wagner R. M. & Depoy D. L., 1996, *ApJ*, 467, 860.

Whitelock P. A., Carter B. S., Feast M. W., Glass I. S., Laney D., Menzies J. W., Walsh J. & Williams P. M., 1984, *MNRAS*, 211, 421.

Wichmann R., Krautter J., Kawara K., Williams R. E., 1990, *Astron. Gesellschaft Abstr. Ser.*, 5, 17.

Wichmann R., Krautter J., Kawara K. & Williams R. E., 1991, in *The infrared spectral region of stars*, Proceedings of the International Colloquium held in Montpellier, France 1990, eds. Jaschek C. & Andrillat Y., Cambridge University Press, p.353.

Williams R.E., Hey E.P., Sparks W.M., Starrfield S.G., Wyskoff S. & Truran J.W., 1985, *MNRAS*, 512, 753.

Williams R.E., 1992, AJ, 104, 725.

Williams R. E., 1985, in *Production and Distribution of CNO Elements*, ed. Danziger I. J., ESO, Garching, p. 225.

Wood-Vasey W.M. & Sokoloski J.L., 2006, ApJ, 645, L53.

Worters H L., Eyres S. P. S., Bromage G. E. & Osborne J. P., 2008, *MNRAS*, 379, 1557.

Warner B., 1995, *Cataclysmic variables*, Cambridge University Press.

Warner B., 2008, in *Classical Novae*, Second Edition, eds. Bode M.F. & Evans A., Cambridge University Press.

Yaron O., Prialnik D., Shara M. M. & Kovetz A., 2005, *ApJ*, 623, 398.